KU LEUVEN

FACULTEIT INGENIEURSWETENSCHAPPEN

Design and tuning of an elastic inflatable actuator with a non-linear response

Bert Van Raemdonck

Thesis voorgedragen tot het behalen van de graad van Master of Science in de ingenieurswetenschappen: werktuigkunde

Promotoren:

Prof. dr. ir. Dominiek Reynaerts
Dr. ir. Benjamin Gorissen

Assessoren:

Prof. dr. ir. Dirk Vandepitte
Dr. ir. Jun Qian

Begeleider:

Ir. Edoardo Milana

Academiejaar 2017 – 2018

Preface

This thesis manuscript is the result of a year full of work, frustrations but above all pleasure from my part and the invaluable support from many people. Firstly, I would like to thank my promotor prof. Dominiek Reynaerts for his fascinating lectures on pneumatics and precision mechanics which motivated me to choose this thesis in the first place. My co-promoter dr. Benjamin Gorissen only increased that motivation. His enthusiasm to explore new possibilities in the field of soft robotics and his open and helpful attitude made every meeting something to look forward to. My mentor Edoardo Milana was a big factor in that as well because of his useful tips and good humour. I also thank him for always being there to answer my questions, taking the time to show me how to model, make and measure soft actuators and offering detailed feedback on all my drafts. Moreover, I thank my promotor, co-promotor, mentor and assessors prof. Dirk Vandepitte and dr. Jun Qian as well as prof. Michaël De Volder for their attention, interaction and helpful comments in each presentation.

I owe my colleagues a word of gratitude as well. Andrea and every de facto member of the Soft Robotics group for their exciting research and attitude of sharing and building on each others ideas. They all make me look forward to working in the group in the years to come, which thanks to the incredible support from my co-promotor and the readiness of my promotor will become a reality. Also thanks to the staff of FabLab Leuven for the help in manufacturing the mould and for turning making anything at all into a pleasure. I thank my friends and in particular Ben for his concern and pep talks and for letting me interact with his cooperative robotic set-up to experience how hard robots start to tackle safe interaction with humans. Benjamin, Lien, Lisa and Wanne especially also reminded me that the whole world does not revolve around soft robotics, kindly protecting me from a tunnel vision.

Finally, this word of thanks would not be complete without mentioning my family to which I owe a lot. My sister Katleen, for her ever critical attitude towards my research and for her greatly appreciated willingness to take over tasks for which I did not have time due to my thesis. I hope that I can help her just as much when she starts working on her thesis soon. Mama, for her eagle eyes that have spotted mistakes in every report I have ever written but especially for her always looking out for me in times of need. Papa, for his expert remarks only someone not familiar with the field but with years of experience and full of good intentions can give. I will never forget how much you all blessed me with your patience and loving support.

Bert Van Raemdonck

Abstract

Elastic inflatable actuators (EIAs) are soft robotics structures which are safe in contact with delicate bodies and adapt their shape to the environment. This thesis introduces a new type of extending EIA which consists of a disc-spring inspired conical membrane made out of silicone rubber supported by a cylindrical wall. A unique feature of that so-called disc spring EIA is its highly non-linear pressure-volume characteristic featuring a local maximum and minimum in both pressure and volume. On gradually changing the pressure or volume, the membrane suddenly deforms significantly at those extrema due to a structural instability. Moreover, the local pressure minimum can occur at negative pressures such that the actuator can be bistable as well. Simulations and inflation experiments on moulded prototypes confirm all of those properties.

They also show that the positions of the extrema in the pressure-volume characteristic significantly depend on the thickness and initial angle of the conical membrane. This thesis describes a procedure to find the values for those two geometric parameters in function of the desired values for the extrema in either pressure or volume. It allows to easily design valveless systems of interconnected disc spring EIAs which perform sequences of motion which are different on inflation and deflation. The disc spring EIA therefore enables new soft, durable and compact applications which show complex behaviour without the need for software control.

Samenvatting

Elastische opblaasbare actuatoren (EIAs) zijn zacht robotische structuren die veilig zijn in contact met delicate voorwerpen en hun vorm aanpassen aan hun omgeving. Deze thesis stelt een nieuw soort EIA voor die in analogie met een schotelveer bestaat uit een kegelvormig siliconen membraan vastgemaakt aan een cilindrische ondersteunende wand. Die zogenoemde schotelveer EIA heeft een unieke niet-lineaire druk-volumekarakteristiek met een lokaal maximum en minimum in zowel druk als volume. Door de interne druk of het actuatorvolume geleidelijk te veranderen, vervormt het membraan plots op die punten omwille van een structurele instabiliteit. Bovendien kan de actuator bistabiel zijn omdat het drukminimum bij negatieve drukken voor kan komen. Simulaties en metingen tijdens het opblazen van gegoten prototypes bevestigen al die eigenschappen.

Ze tonen ook aan dat de posities van de extrema in de druk-volumekarakeristiek sterk afhankelijk zijn van de dikte en de initiële hoek van het kegelvormig membraan. Deze thesis beschrijft een procedure om de waarden voor die geometrische parameters te vinden in functie van de gewenste waarden voor de extrema in ofwel druk ofwel volume. Het is dan mogelijk om eenvoudig systemen van schotelveeractuatoren te ontwerpen die verschillende bewegingspatronen vertonen bij het opblazen en aflaten zonder kleppen te gebruiken. De schotelveer EIA kan dus leiden tot nieuwe zachte, duurzame en compacte toepassingen met complex gedrag zonder het gebruik van elektronische sturing.

Contents

List of Figures and Tables

List of Figures

List of Tables

List of Abbreviations and Symbols

Abbreviations

DAQ	data acquisition device
EIA	elastic inflatable actuator
FEM	finite element method
PMMA	polymethyl methacrylate

Symbols

a	a scalar
A_d	surface area of the conical disc spring membrane
A_t	surface area of the top cap
E	Young's modulus
f, g	a function
F_h	horizontal reaction force
F_v	vertical reaction force
G	shear modulus
H	initial cone height
H'	cone height after the application of pressure
h_w	wall height
K	bulk modulus
k_b	stiffness of the torsional spring representing local bending of the membrane
k_s	stiffness of the spring representing stretching of the circumferential membrane fibres
L_d	width of the conical disc spring membrane
L_{df}	lever arm of the force resulting from the pressure acting on the membrane
p	relative internal pressure

p_d	relative internal pressure of the disc spring EIA
$\bar{p}_{ps}$	average of the snap-through and snap-back relative internal pressure under pressure control
p_{psb}	relative internal pressure at pressure snap-back
p_{pst}	relative internal pressure at pressure snap-through
p_s	relative internal pressure of the source
r^2	coefficient of determination of a fitted equation
R_o	outer radius of the actuator
$R_{r,i}$	rounding radius of the inner corners
$R_{r,o}$	rounding radius of the outer corners
R_t	radius of the top cap
s	arc length
s_+, s_-	Mooney-Rivlin material model parameters
t	time
t_m	membrane thickness
t_w	wall thickness
U_{el}	stored elastic energy
V	internal volume
V_0	initial internal volume when the relative internal pressure is zero
V_d	internal volume of the disc spring EIA
V_s	internal volume of the source
$\bar{V}_{vs}$	average of the snap-through and snap-back internal volume under volume control
V_{vsb}	internal volume at volume snap-back
V_{vst}	internal volume at volume snap-through
W_{fl}	pressure-volume work by a fluid
y	vertical displacement
α	Rayleigh damping parameter
α_i	Ogden material model parameter
β	Rayleigh damping parameter
Δp_{ps}	difference between the snap-through and snap-back relative internal pressure under pressure control
ΔR	initial difference between the outer and inner radius of the disc spring membrane
$\Delta R'$	difference between the outer and inner radius of teh disc spring membrane after the application of pressure
ΔU_{psb}	Energy released by the actuator over a pressure snap-back transition
ΔU_{pst}	Energy released by the actuator over a pressure snap-through transition
ΔU_{vsb}	Energy released by the actuator over a volume snap-back transition
ΔU_{vst}	Energy released by the actuator over a volume snap-through transition

ΔV_{vs}	difference between the snap-through and snap-back internal volume under volume control
θ_m	initial membrane cone angle
θ'_m	membrane cone angle after the application of pressure
λ_i	principal strain component
μ_i	Ogden material model parameter
ν	Poisson ratio
ρ	material density
σ_{ii}	principal stress component

Chapter 1

Introduction

This thesis describes the design of an elastic inflatable actuator with a non-linear pressure-volume characteristic. It also discusses how to choose geometrical and material parameters of the actuator to influence key parameters of that characteristic. This section first provides background about the use of such actuators and the state of the art. Finally, it details the goal of the thesis and gives an outline for the rest of the manuscript.

1.1 State of the art

The vast majority of robots today consists of stiff parts with discrete joints providing a limited amount of controllable degrees of freedom. That structure allows for fast, accurate and repeatable movements with the application of considerable force. However, the stiffness of those robots also makes that they can inflict inadmissible damages to delicate bodies. Moreover, they struggle to adapt their shape to changing and unknown environments [1]. Thanks to sophisticated controllers processing many sensory inputs, stiff robots start to tackle those problems but those solutions are expensive and hard to miniaturize.

So-called soft robots do not suffer from those issues. They consist of more compliant parts and show more continuous deformation than stiff robots. Since they only have a limited amount of inputs to control the infinite degrees of freedom of that continuous deformation, soft robots are underactuated systems [2]. That means it is impossible to fully control the shape of a soft robot. On the other hand, there is no need for such control because the underactuation can lead to a form of hardware intelligence by which soft robots conform their shape to objects they touch [3]. Consequently, soft robots are useful in grasping objects with an unknown shape [4] or navigating unknown terrain and squeezing through openings [5]. Their compliance in combination with the lack of sharp edges also makes them unable to harm soft tissue [6]. Therefore, soft robots are suitable for applications that require intimate contact with humans like endoscopy [7] or assistance in rehabilitation [8]. Since those applications are possible without sensors or control, it is possible to make soft robots cheaper and smaller than their stiff counterparts.

Soft actuation technologies include among others electro-active polymers, shape memory alloys and elastic inflatable actuators (EIAs) [1]. Similarly to balloons, EIAs consist of a fluid-filled cavity enclosed by a flexible membrane. It is possible to control the flux of the fluid in and out of the cavity. The membrane then redirects the change in volume into a deformation of the actuator. Often, the membrane consists of a material with a high ultimate strain like silicone rubber to allow big deformations. In some EIAs, the membrane also contains inextensible fibres to make them stronger. Varying the membrane shape and composition results in actuators that can bend [9], twist [10], contract [11] etc. Figure 1.1 (a) and (b) show typical examples of such EIAs in their rest and actuated state.

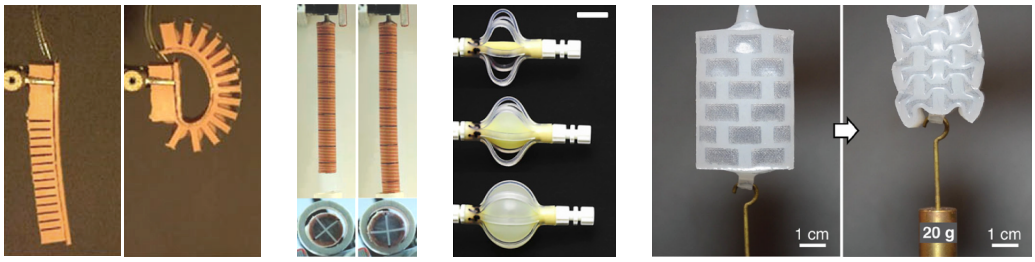

(a) (b) (c) (d)

Figure 1.1: Overview of EIAs presented in research literature in their rest and actuated states: (a) linear bending EIA [9], (b) linear twisting and extending EIA [10], (c) non-linear extending EIA [12] and (d) non-linear contracting EIA [13]

An advantage of EIAs over other actuation technologies is that they do not require electricity and are therefore safer in for example endoscopic applications. Additionally, they achieve high strokes and relatively high forces even below the millimetre scale [14] and are cheap to produce with moulding techniques. The main disadvantage of EIAs is their need for supply lines. They enforce a trade-off between the speed of actuation and the size of application, which limits the miniaturization possibilities of complex systems consisting of multiple EIAs [15]. Another disadvantage of EIAs is that they are generally hard to control because of the non-linear relationship between the input pressure and the deformation.

The non-linear input-output characteristic of EIAs originates in the non-linear stress-strain relation of the rubber-like membrane material. For particular EIAs like a common party balloon [16], that material property gives rise to a pressure-volume characteristic with a local maximum followed by a local minimum in pressure [17]. Actuators with such a characteristic show interesting properties which outweigh the disadvantages of the non-linear behaviour.

A first property is that when the pressure in those actuators passes the value of the local maximum, their volume suddenly increases [17]. Similarly, when the pressure is decreased again and drops below the value of the local minimum, their volume suddenly decreases. That snapping phenomenon opens up a path to faster actuation of EIAs. Conversely, it allows to reach the same speeds as in linear structures but

with a less powerful pressure supply or with thinner supply lines, resulting in smaller soft robots. Moreover, since a big change in volume[1] follows from a small change in pressure, sensitive actuators are a possibility.

A second property emerges when multiple EIAs with that characteristic share the same supply line. On increasing the pressure, the EIAs don't inflate simultaneously but show a sequence of inflation and deflation with fast transitions between some phases of the sequence. On decreasing the pressure again, a different sequence can occur. The particular sequence largely depends on the relative pressure values of the local maxima and minima of the different EIAs [12]. However, if those values are similar between the actuators, the dynamic effects of the connecting tubing dominate [7]. By exploiting those two effects, it is possible to design a system of EIAs with a single supply tube that performs an arbitrary sequence of motions. Therefore, non-linearities can be the key to compact systems with complex behaviour.

Additionally, in some of the steps in the sequence, the fluid required to quickly inflate an actuator comes from another actuator that simultaneously deflates [12]. The fluid then flows through a short piece of connecting tubing between the two actuators rather than through a long supply line. The former path generally has a lower resistance to flow than the latter, enabling faster actuation.

Despite the advantages of non-linear systems and research on them in fields such as metamaterials [18] or soft dielectric actuators [19], few examples of non-linear EIAs exist in literature. Some applications exploit the non-linearity of spherical balloons for sequencing [7] but their uniform expansion makes them into space-inefficient actuators. Overvelde et al. present extending actuators with latex tubes surrounded by a series of buckled braids, shown in figure 1.1 (c) [12]. Belding et al. study variations on the same concept which contract, bend and twist as well [20]. By varying the length of the tube and the braids, it is possible to tune the non-linear characteristics. However, neither study addresses the stability of the characteristics with the number of actuation cycles. Finally, Yang et al. present an actuator consisting of cells surrounded by elastic beams that buckle under application of negative pressure, pictured in figure 1.1 (d). That actuator shows less pronounced snapping [13] but the study does not determine or tune the pressure-volume characteristic.

Still, none of the discussed studies on non-linear actuators have led to an EIA which is both easy to tune, reliable on the long term and easy to miniaturize. Moreover, they do not provide straightforward methods to design the actuators in function of the desired values of the extrema of their pressure-volume characteristics. That means that no practical building blocks and design procedures are available to create complicated systems of EIAs at a small scale. This thesis attempts to fill in that gap.

[1] In common party balloons, representative values for the sudden increase or decrease in volume are a factors of 50 or 15, respectively [17]

1.2 Overview of the thesis

Concretely, the goal of this thesis is to design an EIA with a pressure-volume characteristic that shows a local maximum followed by a local minimum in pressure. Another goal is to describe a procedure on how to adapt geometrical and material parameters of the actuator in order to obtain design values for those pressure extrema. Preferably, those values should remain stable over a large number of actuation cycles. It is also desirable that the designed actuator is easy to miniaturize. A final objective is to redirect a change in internal volume efficiently into a useful deformation. An EIA that satisfies those criteria has the potential to become a building block in many practical applications.

Chapter 2 of this manuscript explores the different non-linear phenomena that can form the basis of such an EIA. In addition, it compares their usefulness and presents a design and model for an EIA that implements the most promising phenomena. Next, chapter 3 deals with the finite element simulation of the pressure-volume characteristic of that EIA. It first explains the different simulation techniques and then it discusses the features of the simulated characteristic. Chapter 4 presents the results of many of those simulations with varying material and geometric parameters. It describes the influence of those parameters on critical features of the pressure-volume characteristic and details a tuning procedure. To validate the conclusions from previous chapters in practice, chapter 5 discusses the characterization of prototypes of the designed EIA. After explaining the manufacturing process of those prototypes, it details the set-up used to measure the characteristics and examines the resulting data. Finally, chapter 6 repeats the most important conclusions of this thesis and makes suggestions for future research. Each chapter also includes a summary of the most important conclusions.

Chapter 2

Actuator design

Plenty of literature on non-linear phenomena not specific to the field of soft robotics is available. It therefore forms a source of inspiration for the design of non-linear EIAs. This chapter starts with an overview of known non-linear phenomena and discusses their potential for application in EIAs. It then introduces the disc spring EIA, which implements the most promising phenomena in a non-linear actuator. That introduction includes a motivation of the choice for the concept, a look at the design features and possible variations and finally the derivation of a qualitative analytical model for its behaviour.

2.1 Sources of non-linearities

The non-linearities of interest are non-monotonical relations between force and displacement, as only they can result in EIAs with the desired properties. For the purpose of designing EIAs, known sources of non-linearities fall into one of two categories with largely the same properties. Material non-linearities result from an interplay between a non-linear material characteristic and geometric tendencies and cease to exist if the material would be linear. Geometric non-linearities result from purely geometric tendencies and exist regardless of the material used in the structure.

2.1.1 Material non-linearities

The membranes of most EIAs consist of rubber-like materials which behave hyperelastically. They show a stress-strain characteristic which softens at low strains and stiffens at high strains but nonetheless stays monotonical [21]. In order to study how structures with non-monotonical non-linearities emerge from that characteristic, quantitative expressions for the material behaviour are indispensable. Those expressions follow from deriving the strain energy density function. Models like the ones by Mooney and Rivlin [22, 23], Ogden [24] and Gent [25] propose different forms for that function. Assuming a plain stress state in the membrane and incompressibility of the material, especially the Mooney-Rivlin model results in a compact stress-strain relationship:

$$\begin{aligned}\sigma_{11} &= \left(\lambda_1^2 - \frac{1}{\lambda_1^2\lambda_2^2}\right)\left(s_+ - s_-\lambda_2^2\right)\\ \sigma_{22} &= \left(\lambda_2^2 - \frac{1}{\lambda_1^2\lambda_2^2}\right)\left(s_+ - s_-\lambda_1^2\right),\end{aligned} \tag{2.1}$$

in which σ_{11} and σ_{22} are the principal stresses and λ_1 and λ_2 the corresponding principal strains. s_+ and s_- are material constants with approximate values of 300 kPa and -30 kPa respectively [17]. Those equations capture the softening of the stress-strain characteristic, but not the stiffening at high strains. However, they suffice to describe the non-linear behaviour of well-known structures. Moreover, the strains in practical EIAs should not become so high since they lead to faster degradation of the characteristic.

For simple EIAs it is possible to write two force equilibrium equations relating the internal pressure to the principal stresses in the membrane. Together with equations 2.1 and an expression for the internal volume in function of the principal strains, they form a system of five equations. Solving that system with the internal volume as independent variable results in the pressure-volume characteristic. Such calculations are possible for spherical balloons, cylindrical balloons [17] and cylindrical balloons with an inextensible fibre wound along their circumference. Appendix A discusses those calculations in more detail and figure 2.1 shows the resulting characteristics.

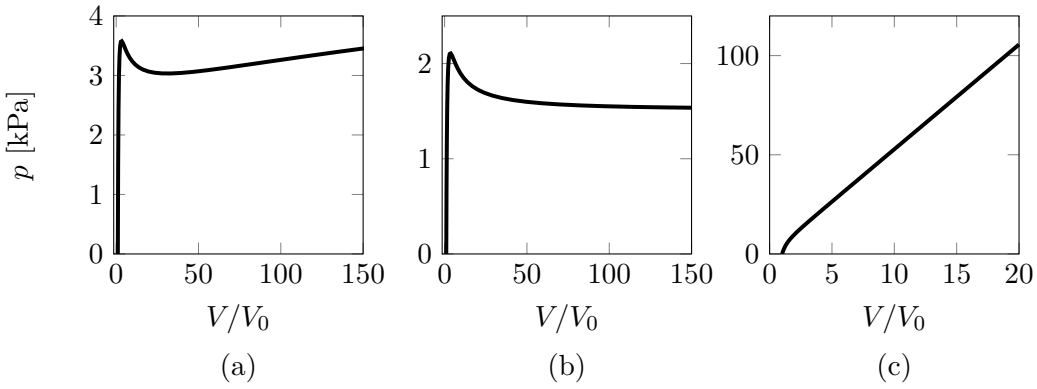

Figure 2.1: Pressure-volume characteristic of (a) a spherical balloon, (b) a cylindrical balloon and (c) a cylindrical balloon with inextensible circumferential fibres

Figure 2.1 (a) confirms that spherical balloons indeed have a local maximum followed by a local minimum in their pressure-volume characteristic. However, as noted before, spherical balloons are not practical EIAs. On inflation, they expand uniformly in all directions rather than in a single direction, which means they are not space efficient. Slender cylindrical balloons could be a more efficient alternative. In those structures, the radial strain is always higher than the axial strain [17] but the initial length is higher than the radius such that the axial deformation dominates. Figure 2.1 (b) however shows that cylindrical balloons do not show increase in

pressure for high volumes according to the Mooney-Rivlin model. Other models that capture the material behaviour more accurately do predict such an increase, but only because of strain stiffening close to the ultimate strain [26]. That means that a cylindrical balloon used in its non-linear range will quickly rupture.

Still, many EIAs in literature are in essence cylindrical balloons. Many of them include inextensible fibres wrapped around the circumference of the membrane to limit the radial expansion without hindering the axial expansion [4, 27, 28]. The inclusion of fibres also linearises the characteristic as shown in figure 2.1 (c). That makes such actuators useless for non-linear applications but increases their value in classical application. The reason is that higher pressures and hence higher forces are possible without causing extreme strains and that control becomes easier.

While none of the previously discussed balloons are practical non-linear EIAs by themselves, their combinations can be. An example is a cylindrical membrane surrounded by inextensible hoops with a gap between the membrane and the hoops. Before making contact with the hoops, the EIA behaves as a cylindrical balloon and afterwards as a fibre wound cylindrical balloon. If the contact occurs after the initial local pressure maximum, the EIA has a similar characteristic as a spherical balloon. Making the hoops from the same material as the membrane rather than from a second stiffer material allows for easier manufacturing at small scales. Figure 2.2 shows the operation of such an EIA and its pressure-volume characteristic as derived in appendix A. The characteristic shows the desired shape but the increase in volume on snapping is small and requires the hoops to be very thick and large.

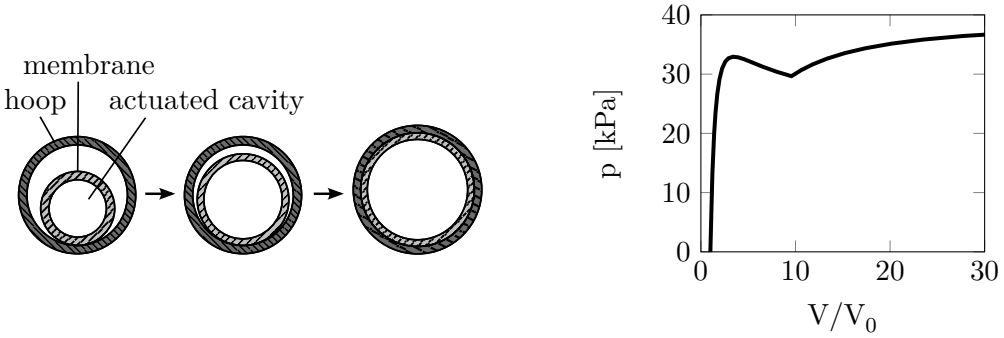

FIGURE 2.2: Schematic operation and pressure-volume characteristic of an EIA with disconnected hoops

The concept for another EIA results from studying the difference between the derivations of the characteristics of spherical and cylindrical balloons. The main difference is the force equilibrium. In a spherical balloon it reduces to $\sigma_{11} = \sigma_{22}$ and in a cylindrical balloon to $2 \cdot \sigma_{11} = \sigma_{22}$ with σ_{11} and σ_{22} respectively the axial and circumferential stress. As the factor in the last equation decreases to one, the slope of the resulting characteristic increases for high volumes. In a tubular EIA with a major circular segment as cross-sectional shape, $a \cdot \sigma_{11} = \sigma_{22}$, with $1 \leq a \leq 2$. Indeed, the circumferential stress σ_{22} in such an actuator is equal to the one in a

cylindrical balloon with the same radius and subject to the same pressure. However, a major circular segment has a higher ratio between area and circumference than a circle with the same radius. Since pressure works on the area and axial stress works on the circumference of the cross-section, the same pressure results in a higher axial stress σ_{11} than in an equivalent cylinder.

To realize such a cross-section in practice, the wall containing the chord that defines the major circular segment has to be stiff against bending. Otherwise, the cross-section quickly becomes roughly circular on inflation and the EIA would have the same characteristic as a cylindrical balloon. At the same time the axial stiffness of that wall should be as low as possible. Otherwise it would take most of the axial stress, decreasing σ_{11} and increasing the factor a in the membrane. A restricting wall consisting of stiff and compliant strips axially stacked onto each other satisfies those two requirements. To allow easy manufacturing at small scales, the stiff and compliant strips can consist of the same material as the membrane but have different thicknesses. Figure 2.3 shows the operation of such an EIA as well as its pressure-volume characteristic derived in appendix A. It illustrates that the characteristic only has a limited slope at high volumes because the cross section then becomes approximately circular. Consequently, the volume increase at snapping is enormous and the strains are high, leading to early failure. Moreover, the required aspect ratio of the stiff strips is high, which hinders manufacturing by moulding.

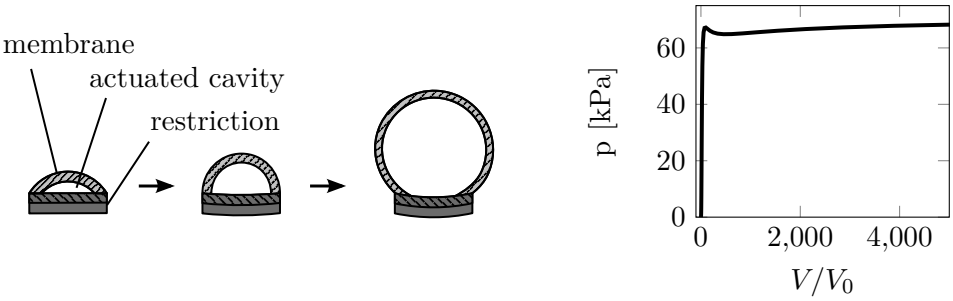

Figure 2.3: Schematic operation and pressure-volume characteristic of an EIA with a major circular segment as cross-section

Especially when the two previously discussed actuators incorporate stiffer materials, they implement the desired non-linearity in a compact design. Research also reveals many more material-induced non-linearities and ways to affect their behaviour [26, 29, 30], which could be an inspiration for better EIA designs. Hence it is possible to create practical non-linear EIAs relying on the non-linear behaviour of rubber. An interesting property of those actuators is that it is possible to reuse the same mould but with different non-linear materials to manufacture EIAs with varying characteristics. With the material as only variable, however, it is difficult to simultaneously tune both extrema of the pressure-volume characteristics as required for some sequencing applications. Another complication is that the non-linear behaviour of rubber depends on factors like the curing time and temperature, the previous loading history, the strain rate or the time between curing and operation

[31]. Therefore control of many parameters during manufacturing and operation is necessary for the EIA to behave as expected.

A final disadvantage of EIAs that owe their non-linear pressure-volume characteristic to a material non-linearity are the large strains involved. For example, the two previously shown non-linear EIA characteristics feature circumferential strains after snapping of respectively 2.5 and 5.5. Those values are below the ultimate strain of most silicone rubbers used for EIAs, but nonetheless they are higher than in most EIAs in literature. Consequently, the pressure-volume characteristics will vary more dramatically during the first inflation cycles due to the Mullins effect [32], further impeding accurate tuning. Finally, the higher strains lead to a lower fatigue life of the non-linear EIAs.

2.1.2 Geometric non-linearities

Many structures exist that feature a non-monotonical force-displacement relation despite consisting of a linear material. Rather, they owe the non-linearity to geometric tendencies. Well known examples include buckling shells, snapping surfaces and non-linear springs like disc springs. Many studies characterize their force-displacement relation but usually only for forces below the local maximum of that characteristic. The reason is that applying a force higher than that maximum leads to a snapping instability of the structure. The deformation then rapidly increases, passing through regions of high strain. In classical structures that strain is often higher than the ultimate strain of the linear material such that the structure fails.

If the structures consist out of materials with a high ultimate strain like rubber, however, snapping does not lead to failure. Many classical non-linear structures and phenomena classically associated with failure can therefore inspire non-linear EIAs. An important property of such EIAs is that the shape of their pressure-volume characteristic depends mostly on their geometric parameters. Those parameters are numerous and can affect the characteristic independently from one another. Hence, relatively straightforward tuning procedures can exist to simultaneously control the location of both extrema of the characteristic. It is also possible to manufacture multiple EIAs with different characteristics from the same batch of material. Consequently, unwanted variations in the material or the production process don't affect the relative values of the characteristics much.

A final advantage of EIAs with geometric non-linearities is that the involved strains can be low compared to EIAs with material non-linearities. As an illustration, the maximum strain in snapping disc springs is in the order of only a couple of percent [33]. That is possible because they do not inherently need high strains for the non-linear behaviour to occur as in EIAs with material non-linearity. Consequently, they can be more robust and can have higher fatigue lives. In conclusion, geometric non-linearities allow the design of EIAs with predictable, controllable and reliable pressure-volume characteristics. That is why they serve as the inspiration for the non-linear EIA discussed in this thesis.

2.2 Disc spring elastic inflatable actuator

2.2.1 Conceptual operation

In classical mechanics, disc springs or Belleville springs are metal or composite sheets in the form of the surface of a truncated circular cone. When it deforms axially, it first flattens and then becomes a cone again but in the inverted direction. In certain disc springs, the corresponding axial load first increases, then decreases and finally increases again [33]. An EIA with a conically shaped rubber membrane with supporting walls to define an actuated cavity can therefore have a non-linear pressure-volume characteristic. Figure 2.4 schematically shows the deformation of such an actuator.

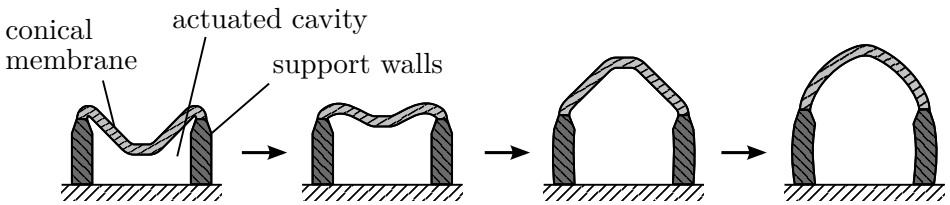

Figure 2.4: Schematic operation of a disc spring EIA

The figure also shows some effects by which the behaviour of a disc spring EIA will differ from a classical disc spring. Firstly, the cone angle of the disc spring EIA will generally be higher in order to maximize the stroke of the actuator. Moreover, in an ideal disc spring the inner and outer edges are free to move radially, but in the EIA they have to connect to other material to close the fluid cavity. Due to those two factors the compressive radial stresses will be higher than in a similar classical disc spring as the membrane flattens. Those stresses can lead to the membrane buckling at some pressure instead of deforming as a more rigid disc spring, which adds another non-linear effect to the characteristic. The connections between the membrane and the rest of the EIA also act as a spring in bending. Their reaction will increase roughly linearly with the instantaneous cone angle, partly linearising the characteristic again. The support walls will also stretch, especially at high cavity pressures when the conical membrane will start to behave more as a balloon. Finally, the EIA consists of non-linear silicone rubber which will affect the characteristic mostly in stages with high strains. Those stages in particular are the one where the conical membrane becomes nearly flat and the one where it balloons.

Despite all of those effects, a disc spring EIA will most probably have a non-linear characteristic. Indeed, a structure very similar to it and which exhibits non-linear behaviour exists outside of the academic context. The structure in question is the eye socket featured in certain hollow squishy toys [34, 35]. On pressing those toys, their internal pressure rises and the eyes jump out with an audible “pop”, indicating the presence of a snap-through phenomenon. Researchers also report snapping of a silicone rubber shell under pressure variations in a medical context [36]. Those examples illustrate that the proposed disc spring EIA can indeed have the desired

characteristic. A major advantage of the concept is that snapping occurs at relatively low strains. Moreover, a unique feature is that it can be bistable if the minimum in the pressure-volume characteristic has a negative value for pressure. The EIA also has a simple shape and can consist out of a single material, facilitating manufacturing. Finally, with a sufficiently thick support wall the radial expansion of the actuator is minimal. The actuator has a low aspect ratio compared to conventional EIAs however, which potentially hinders integration in some applications.

2.2.2 Detailed design

Figure 2.5 shows the concrete EIA design studied in this thesis and defines the different components and the main geometric parameters. The conical membrane implements the disc spring and buckling phenomena so has the most pronounced effect on the non-linearity of the pressure-volume characteristic. The shape and dimensions of the other components depend more on the particular boundary conditions of an application rather than on the requirements for the characteristic. For example, the shape of the support wall can vary to work with a particular clamping system. Other applications do not feature a top cap to connect the disc spring EIA to another EIA placed on top of it. The hinges adapt their shape to the components they connect to form a smooth transition. Their corners are rounded to minimize the stresses especially in the internal corners.

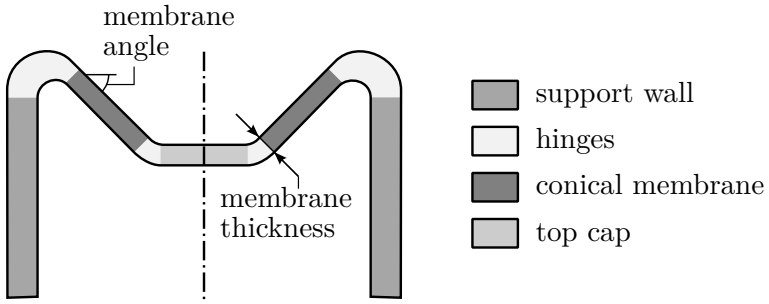

FIGURE 2.5: Schematic overview of the components and main geometric parameters of the disc spring EIA

If the top cap of the EIA shown in figure 2.5 performs the main interaction with the environment, it acts as an extending actuator. However, if that interaction mainly takes place on a point on the conical membrane, the EIA also acts as a bending actuator. Another way to use the disc spring EIA to produce a bending motion is to place the top cap at an angle in the rest state, making the conical membrane asymmetrical. Figure 2.6 (a) shows such a design. The advantage of that implementation is that the connection to the environment and the associated load sits in the middle of the membrane, so the stress distribution is more uniform. The disc spring EIA can also produce a twisting motion if an inextensible fibre or thick silicone ridge rests on top of the conical membrane in a spiral shape. Figure 2.6 (b) illustrates that concept. As the membrane inverts, each point on its top surface

moves radially outwards, especially in thick membranes. Because the spiralling structure is more or less inextensible, the increase of the radius of the spiral forces it to uncurl which twists the membrane especially near the top cap.

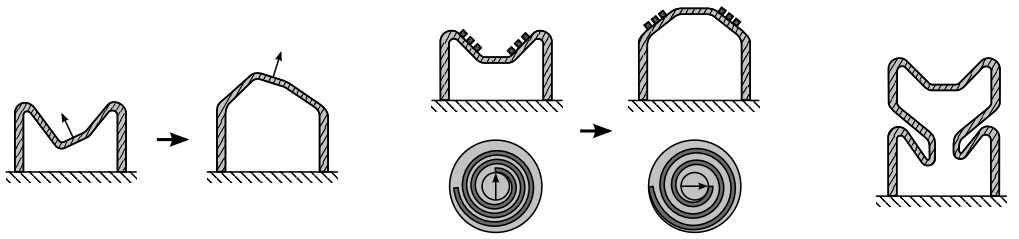

(a) (b) (c)

Figure 2.6: Design variations on the disc spring EIA: (a) bending actuator, (b) twisting actuator, (c) series configuration of a bending and extending actuator

All those variations of the disc spring EIA have the same fundamental non-linear behaviour as the extending actuator in figure 2.5. Hence, the analysis of the characteristic of the extending disc spring EIA and the procedure to tune it as presented in this thesis also applies to them. The disc spring concept therefore leads to a family of building blocks for non-linear applications. It is possible to connect those building blocks in parallel or in series. In parallel configurations separate actuators have supply lines which connect to each other. Series configurations consist of a stack of EIAs with holes in their membranes to connect their cavities together as in figure 2.6 (c). In the series configurations, the deformation of each EIA unit affects the motion of the ones above it, which is useful in applications such as artificial cilia. A disadvantage of disc spring EIA in such a configuration is that the cavity then has many overhangs. That hinders conventional moulding of the structure, but it is possible to use sacrificial mould parts or direct 3D-printing.

2.2.3 Simplified analytical model

In order to gain insight into how different parameters affect the behaviour of the presented disc spring EIA, it is instructive to derive an analytical model for it. That model should capture the main features of the characteristic while being easy to interpret. Simplifying the actuator to a rigid disc spring representing the conical membrane achieves that goal. Several models in literature describe such a structure but none capture the big deformation, the pressure load case and the constraints by the top cap and the hinges. Therefore, figure 2.7 (a) introduces a lumped parameter model tailored to the disc spring EIA.

The proposed model consists of two links representing the top cap and the conical disc spring membrane. It assumes that the top cap fixes the radius R_t of the inner edge of the membrane while the outer hinge has no effect on the translation of the outer edge. A point force perpendicular to each link and acting at the centroid of the represented area simulates the loading by the internal pressure in the actuator. The

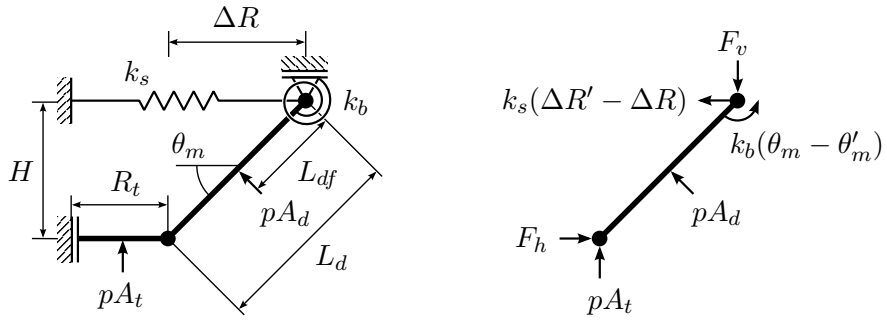

FIGURE 2.7: (a) Lumped parameter model for the disc spring EIA with (b) the free body diagram for the membrane

pressure causes the top cap of the disc spring EIA to rise, initially decreasing the cone height H' and the cone angle θ'_m. Consequently, the radius of each circular fibre in the membrane increases leading to a profile of circumferential stress. Under the assumption that the section of the membrane remains straight and that the material behaves linearly, the shape of that profile is constant. It is therefore possible to model the effect of stretching the circumferential fibres into a single linear spring with stiffness k_s. It is proportional to the stiffness of the disc spring section to uniaxial tension $EL_d t_m$ with E the Young's modulus and t_m the membrane thickness.

As the top cap rises, the disc spring membrane initially becomes flat and then inverts. That corresponds to the curvature in the plane normal to the radial fibre at each point approaching zero before changing sign. The result is a bending moment which is roughly directly proportional to the difference between the membrane angle in the deformed and initial state. In the model, a torsional spring with stiffness k_b proportional to the bending stiffness of the membrane section $EL_d t_m^3$ represents that moment. Additionally, it allows to incorporate the bending moment generated by the hinges of the disc spring EIA.

Thanks to the two springs, it is possible to obtain a simplified expression for the pressure load needed to sustain a certain deformation of the disc spring. The first step is to create the free body diagram of the link representing the conical membrane as in figure 2.7 (b). The horizontal force equilibrium and the moment equilibrium around the outer hinge then are

$$\begin{cases} F_h - pA_d \sin(\theta'_m) - k_s(\Delta R' - \Delta R) = 0 \\ F_h H' - pA_t \Delta R' - pA_d L_{df} + k_b(\theta_m - \theta'_m) = 0 \end{cases} \tag{2.2}$$

Since $\Delta R' = \sqrt{L_d^2 - H'^2}$ and $\theta'_m = \text{asin}(\frac{H'}{L_d})$, the pressure is

$$p = \frac{k_s H' \left(\sqrt{L_d^2 - H'^2} - \Delta R\right) - k_b \left(\text{asin}\left(\frac{H'}{L_d}\right) - \theta_m\right)}{A_t \sqrt{L_d^2 - H'^2} + A_d \left(L_{df} - \frac{H'^2}{L_d}\right)}, \tag{2.3}$$

with all values, apart from p and H', constant for a certain disc spring EIA. Figure 2.8 plots the result of equation 2.3 for representative values of those constants.

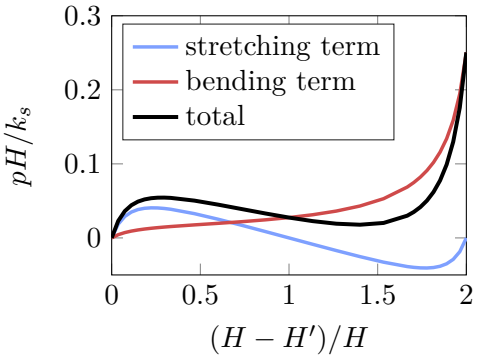

Figure 2.8: Pressure-displacement characteristic for a representative disc spring according to the analytical model

The resulting characteristic features the desired non-linearity with a local maximum followed by a local minimum. They appear because of the non-monotonical term with k_s in the equation, representing the stretching of the circumferential fibres. The other term with the bending stiffness k_b increases monotonically with the displacement of the top cap. Since the former term is uneven around $H' = 0$, k_s affects the difference between the extreme pressures but not their average. Increasing k_b on the other hand increases the average of the two but decreases their difference until they become equal and disappear. As $k_s \propto t_m$ and $k_b \propto t_m^3$, a disc spring EIA with a higher membrane thickness has a steeper and less non-linear characteristic. Both stiffnesses are proportional to E and L_d, so changing the material modulus and the size of the membrane only scales the characteristic.

Summary

EIAs can feature a non-linear pressure-volume characteristic either because of a material non-linearity or because of a geometric non-linearity. Of those two, structures with a geometric non-linearity generally experience lower strains, enable simpler tuning procedures and have more reproducible characteristics. Therefore, the next chapters of this thesis study an actuator with a geometric non-linearity, namely the disc spring EIA. It is a simple structure with a conical membrane resembling a classical disc spring. The non-linear force-displacement characteristic of disc springs and a potential buckling of the membrane lead to the non-linear pressure-volume characteristic of the EIA. The prevalence of the non-linearity depends on the membrane thickness according to an analytical model. Advantages of the specific design of the disc spring EIA are that it is simple in shape, compact with little radial expansion and potentially bistable. Finally, extending, bending and twisting variations with the same properties exist, forming building blocks for complex systems.

Chapter 3

Simulation of the general actuator behaviour

The finite element method (FEM) allows to simulate the general behaviour of the presented disc spring EIA accurately. This chapter first discusses the set-up for the different types of FEM analyses in this thesis. That discussion includes the settings common to all simulations and the settings and utility of both static and dynamic simulations. Afterwards it presents and discusses the results of those analyses for a single representative disc spring EIA. The most important result is its static pressure-volume characteristic which has a unique shape that enables new applications. It also forms the basis for an analysis of the stability of the actuator in several situations and of the energies released and velocities attained during unstable transitions.

3.1 Finite elements simulation set-up

In the field of soft robotics, the standard FEM environment is Dassault System's Abaqus software because of its non-linear capabilities. The simulations presented in this thesis therefore use that software. This section specifically discusses the settings in Abaqus used to simulate the disc spring EIA but many ideas also apply to other software packages and other EIAs.

3.1.1 General set-up

All discussed FEM simulations in this thesis use an axisymmetric model of the disc spring EIA with a section as in figure 3.1. Table 3.1 lists the default values for the parameters of that model. Unless specified otherwise, each FEM simulation in this thesis implements those values. Since the model is axisymmetric, it requires fewer elements than a three dimensional simulation for the same accuracy. An axisymmetric model therefore enables faster, lighter and more accurate simulations. However, it does not allow to study non-axisymmetric deformation modes which occur in practical disc spring EIAs due to imperfections. The assumption is that those modes do not significantly affect the pressure-volume characteristic.

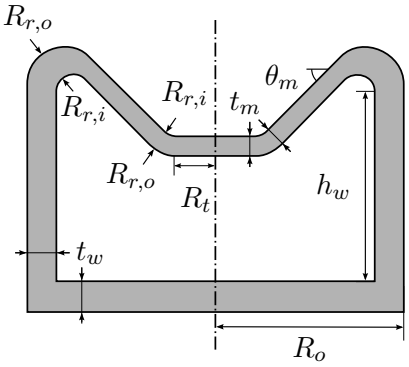

Figure 3.1: Schematic overview of the components and main geometric parameters of the disc spring EIA

Table 3.1: Values of geometric and material parameters of the standard disc spring EIA FEM model

Parameter	h_w	R_o	$R_{r,i}$	$R_{r,o}$	R_t	t_m	t_w	θ_m
Value	10	10	1	2	2	1	1.5	45
Unit	mm	mm	mm	mm	mm	mm	mm	°
Parameter	μ_1	α_1	K	ν	ρ	α	β	
Value	75449	5.863	10^9	0.4999	1070	0.008	0.008	
Unit	Pa	-	Pa	-	kg/m^3	1/s	s	

A mesh of axisymmetric CAX4RH and CAX3H elements generated by Abaqus discretizes the disc spring EIA section. A mesh refinement study indicates that decreasing the element seed size past 0.2 mm changes the values of the pressure-volume characteristic by less than 2 % of their range. Unmodelled effects in real EIAs probably result in higher variations of the characteristic, so an element size of 0.2 mm gives acceptable results in a sufficiently short time. Most of those unmodelled effects relate to the material behaviour of the used silicone rubber. The reason is that modelling for example the viscoelastic or creep behaviour of rubber or the Mullins effect requires many parameters which are not documented for many materials. The discussed simulations therefore use an Ogden material model with parameters listed in table 3.1 as an approximation of Dragon Skin™ 10 silicone [37, 38]. Since the material is nearly incompressible, the elements are of the hybrid type.

Defining a hydraulic fluid cavity interaction allows to measure and drive the internal volume and pressure of the EIA during deformation. That definition requires a continuous surface with endpoints on the symmetry axis to bound the cavity. Such a surface only exists if a wall of material closes off the bottom of the cavity of the disc spring EIA, as shown on figure 3.2. All elements on the fluid cavity surface need to be of the same type, so the bottom wall consists out of the same material and elements as the rest of the section. A cavity point on the symmetry axis indicating the interior side of the surface completes the fluid cavity definition. It stores the

information on the cavity volume and pressure in the variables CVOL and PCAV, respectively. The displacement data of the EIA comes from the membrane apex.

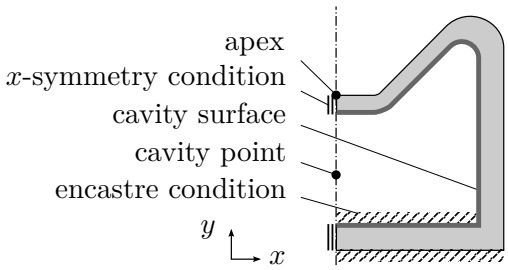

FIGURE 3.2: Schematic model of the FEM set-up for the disc spring EIA

Each simulation features two types of geometric boundary conditions as shown in figure 3.2. The first boundary condition is an x-symmetry condition on the edges of the section on the symmetry axis. It prevents translation along the x-axis and rotation in the xy-plane to preserve continuity of the axisymmetric model. The second boundary condition is an encastre condition on the horizontal edges of the bottom wall. It prevents any translation or rotation such that the bottom wall is approximately rigid and does not affect the pressure-volume characteristic.

3.1.2 Static simulations

A static simulation finds equilibrium solutions even if they are not dynamically stable. That means that a static simulation of a non-linear EIA does not for example show a rapid increase in volume when the pressure reaches a critical value. Instead, the volume increases and the pressure decreases by a small amount past that point. Consequently, it allows to calculate the full pressure-volume characteristic. That fundamental static characteristic is useful to predict the behaviour of the EIA in interaction with structures with diverse pressure-volume characteristics.

In conventional static solution methods, one variable is an independent driver with a value which varies monotonically between steps. However, in the static pressure-volume characteristic either variable can vary non-monotonically. On reaching an extremum of the driver, the classical solution methods fail to converge because the solution becomes infinitely sensitive to an increment in that variable. In the arc length method on the other hand, the value for the driver is an additional unknown in each step. That method looks for solutions for the next iteration in a circle of values for the dependent as well as the driving variables around the previous equilibrium [39]. In that way both pressure and volume can vary non-monotonically and determination of the full static characteristic is possible.

Static simulations of the disc spring EIA in Abaqus therefore use a “Static (Riks)” step, which implements the arc length method. The driver for the simulation is a boundary condition defining the fluid cavity pressure at which the simulation ends. Enabling the “Nlgeom” option in the step settings ensures that the simulation takes non-linear geometric effects due to the big deformations into account. Finally, the

incrementation method is automatic but with a low maximum increment. Otherwise, the simulation does not take enough steps to capture the full characteristic in sufficient detail.

3.1.3 Dynamic simulations

The disadvantage of the static simulation is that it does not mimic the real behaviour of the disc spring EIA with dynamic instabilities. Most importantly, it does not capture the velocity or power of snapping phenomena. Additionally, static simulations do not yield the deformations and stresses involved in snapping. Those data are important for later optimization of the disc spring EIA design to maximize snapping speed or to minimize stresses. Performing a dynamic simulation on top of a static simulation therefore has added value. Moreover, comparing the results of the dynamic and static simulations allows to validate the arc length method.

The disadvantage of studying the dynamic behaviour of an EIA is that it depends on the application. One important application dependent factor that influences that behaviour is the pressure-volume characteristic of the source. As shown in section 3.2.2, the relative values of the slopes of the source and the EIA characteristics determine which states of the EIA are stable [17]. An illustration is a spherical party balloon with a characteristic as shown in figure 2.1 (a). It snaps under pressure control but not under volume control, so its dynamic behaviour varies drastically depending on the source. Other application dependent factors influencing the dynamic behaviour of the EIA are the inertia and viscosity of the actuating fluid and the fluidic resistance of the connecting tubing. In conclusion, results of a dynamic simulation are not fundamental to the EIA itself. Consequently, dynamic simulations feature less prominently in this thesis.

Dynamic simulations of the disc spring EIA in Abaqus use a “Dynamic, Implicit” step with non-linear geometry. The advantage of using an implicit over an explicit method is the better stability during snapping and the possible subsequent oscillations. In addition, the application type of the step is “Moderate dissipation” to dampen those oscillations as much as possible. In reality damping comes from both the viscosity of the actuating fluid and the material damping. The simulation also includes that last effect in the material definition of the rubber. The exact values for the Rayleigh damping coefficients α and β of the used material are not available in literature, however. Therefore, the simulation uses the lowest values that still remove most oscillations, leading to the values in table 3.1.

The time period of the step is in the order of multiple seconds. That minimizes the damping and inertial effects in the dynamically stable regions of the characteristic. To get sufficient time resolution during snapping, the time step size needs to be small but that needlessly slows down the simulation in stable regions. Therefore, the simulation uses non-uniformly spaced time points for which the solver calculates the results. The approximate bounds for the time intervals with higher and lower spacing follow from a coarse simulation with uniformly spaced sample points.

This thesis presents two types of dynamic simulations. The first type implements pressure control by putting a boundary condition on the fluid cavity pressure. The

second type implements volume control by defining a volume flux to the fluid cavity with the "Fluid flux" keyword in the input file of the simulation. In both types of simulations, the driving variables have a time-varying amplitude which starts at zero, increases to a maximal value and then decreases again to simulate both inflation and deflation. The amplitudes are such that the change of either pressure or volume mostly happens at a constant rate. At the start and end of both the increasing and decreasing phase, however, a rounding factor ensures that the amplitude changes gradually. That minimizes the acceleration and jerk of the amplitude of the driving variable so it induces minimal oscillations.

3.2 Simulated behaviour of a disc spring actuator

The methods described above allow to confirm the non-linearity of the pressure-volume characteristic of the disc spring EIA before manufacturing one. The simulations in this section all implement the default values for the parameters from table 3.1.

3.2.1 Static pressure-volume characteristic

Figure 3.3 shows the pressure-volume characteristic of a disc spring EIA resulting from a static simulation. The characteristic has the desired non-linearity that leads to snapping behaviour and sequencing in practical applications. The non-linearity is more involved than in the characteristics of the spherical balloon and the other structures discussed in section 2.1.1, however. Not only do up to five equilibrium volumes correspond to a single pressure in the disc spring characteristic, but multiple equilibrium pressures can also correspond to the same volume. It is the first example of such a pressure-volume characteristic in EIA research literature.

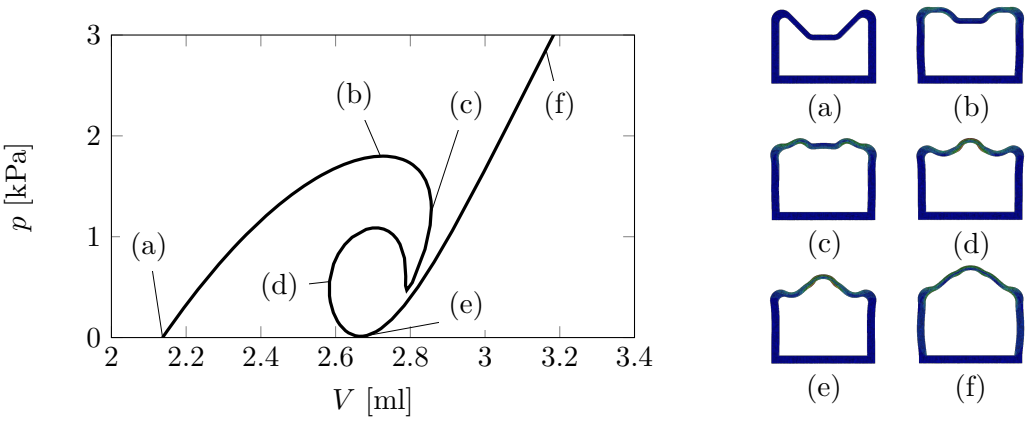

FIGURE 3.3: Static pressure-volume characteristic and corresponding deformation of a disc spring EIA

A study of the deformation of the disc spring EIA corresponding to various points on the pressure-volume characteristic indicates what effects form the basis of its

complex shape. States (a) and (b) in figure 3.3 show that initially the membrane deforms largely as a rigid disc spring, which explains the peak in pressure at (b). Past state (b) the membrane bends more and more under compressive radial stresses. That causes its behaviour to diverge from that of a rigid disc spring. Instead, the bent membrane then approximately behaves as a connection of two concentric disc springs, as modelled in appendix B. At point (c) only the outermost disc spring is inverted. Next, the internal pressure causes the innermost one to invert. After inversion, a disc spring has a higher strain energy than before, however. Therefore, if the outermost disc spring then inverts back, the total strain energy increases less than in the case where it stays inverted. In the light of that observation, the simulated transition between state (c) and (d) in which the slope of both the inner and outer portion of the membrane changes sign is plausible. Since that transition consists of the inversion of two rigid disc springs, the pressure once more changes non-monotonically. Meanwhile, the height of the hinges stays roughly constant, so the inversion leads to a decrease in volume. Another factor contributing to that decrease is the support wall because it stretches linearly with pressure, which drops between (c) and (d). That effect is modest, however, since the wall is relatively thick. Past state (d), the membrane straightens out, causing its behaviour to converge again to that of a single rigid disc spring. That explains the appearance of a final extremum in pressure at point (e). Between points (e) and (f) the deformation as a disc spring ends as the internal pressure causes the membrane to stretch more like a spherical balloon. The strains remain limited, such that at state (f) the actuator behaves roughly linearly.

One of the effects of the described behaviour is that the pressure-volume characteristic of the disc spring EIA has extrema in volume at point (c) and (d). At those points, the slope of the characteristic becomes infinite. That means that the disc spring EIA has states which are unstable under volume control as well as under pressure control. On gradually increasing the volume of the actuator with, for example, a syringe and an incompressible fluid, the shape of the membrane and the internal pressure suddenly change at point (c). The same happens at point (d) on decreasing the volume. Those snapping transitions happen at constant internal volume, while under pressure control snapping leads to a volume flux through the supply line. The snapping phenomena under volume control therefore open up a way for faster actuation in applications where the supply lines need to be thin or long.

More generally, the infinite slope of the pressure-volume characteristic at points (c) and (d) means that the corresponding states are inherently unstable. The next section shows that regardless of the characteristic of the source, the EIA will snap at those points. That means that it is impossible to cross them quasi-statically to reach the second set of pressure extrema. The points between (c) and (d) are not inherently unstable, however. If the actuator therefore reaches such a point due to a dynamic phenomenon, it can remain there. Assuming that such a phenomenon is controllable, it is possible to configure the snapping behaviour of the disc spring EIA by putting its state either between (a) and (b) or (c) and (d). On increasing the pressure, the actuator then snaps at different pressures. Another way in which the disc spring EIA can lead to soft programmable structures is through its potential bi-stability.

The low value for the pressure at point (e) suggests that with other dimensions the actuator has multiple possible equilibrium volumes at zero pressure. That means that the disc spring EIA can remember its state such that under pressure control it will either snap or not depending on whether the initial state is at point (a) or near (e). In conclusion, the unique pressure-volume characteristic of the disc spring EIA enables the design of elastic inflatable structures with novel complex behaviour.

3.2.2 Dynamic stability

It is possible to predict the dynamic behaviour of a disc spring EIA from its static pressure-volume characteristic $p_d(V_d)$ and the characteristic $p_s(V_s)$ of the source that drives it. Such an analysis starts by expressing p_s in function of V_d. If an incompressible fluid fills the entire system, that transformation consists of substituting V_s with $V_{tot} - V_d$. A static equilibrium implies the absence of a fluid flux or a pressure gradient in the system such that $p_d(V_d) = p_s(V_{tot} - V_d)$. Graphically, the equilibrium configurations therefore correspond to the points where the disc spring EIA and mirrored and translated source characteristics intersect.

The stability of those configurations follows from applying an infinitesimal disturbance in the volume of the disc spring EIA δV_d. That results in the following pressures in the system:

$$\begin{aligned} \text{in the disc spring EIA: } & p_d(V_d + \delta V_d) = p_d(V_d) + \frac{dp_d(V_d)}{dV_d}\delta V_d \\ \text{in the source: } & p_s(V_{tot} - (V_d + \delta V_d)) = p_s(V_{tot} - V_d) + \frac{dp_s(V_{tot} - V_d)}{dV_d}\delta V_d \\ & = p_d(V_d) - \frac{dp_s(V_s)}{dV_s}\delta V_d. \end{aligned} \tag{3.1}$$

If $\delta V_d > 0$ and $dp_d(V_d)/dV_d > -dp_s(V_s)/dV_s$, then $p_d(V_d+\delta V_d) > p_s(V_{tot}-(V_d+\delta V_d))$. That pressure gradient causes a volume flux out of the disc spring. That flux opposes the initial increase in volume δV_d and therefore restores the previous equilibrium configuration. If, on the other hand, $dp_d(V_d)/dV_d < -dp_s(V_s)/dV_s$, the resulting pressure gradient causes a volume flux into the disc spring. That reinforces the disturbance δV_d, eventually leading to a finite change of the volume and of the difference between p_d and p_s. Consequently, the disc spring EIA and the source are no longer in static equilibrium and the system gains kinetic energy in a snapping transition. If finally $dp_d(V_d)/dV_d = -dp_s(V_s)/dV_s$, an infinitesimal disturbance δV_d results in the system attaining a new equilibrium close to the previous one. That means that there is no opposition to new disturbances such that they can accumulate to bring the system into an unstable state. The above study remains valid for a negative δV_d as well. Therefore, the condition for stability of a disc spring EIA connected to an arbitrary source [17] is:

$$\frac{dp_d(V_d)}{dV_d} > -\frac{dp_s(V_s)}{dV_s} \quad \text{or} \quad \frac{dp_d(V_d)}{dV_d} > \frac{dp_s(V_{tot} - V_d)}{dV_d}. \tag{3.2}$$

That expression confirms that the local maxima in volume in the pressure-volume characteristic of the disc spring EIA are inherently unstable. As the state of the EIA

evolves in a stable manner either from (b) to (c) or from (e) to (d) in figure 3.3, $dp_d(V_d)/dV_d$ approaches $-\infty$. That makes the satisfaction of equation 3.2 impossible.

It is possible to interpret the stability criterion on a graph of $p_d(V_d)$ and $p_s(V_{tot} - V_d)$. The stable configurations correspond to the (p, V) points where both curves intersect and the slope of p_d is more positive than the one of p_s. That means that snapping occurs when at the point representing the current state the curves become tangent to one another. The state then dynamically transitions to another point of intersection between the two curves where the slope of p_d is more positive than the one of p_s. That analysis holds true for an arbitrary source characteristic, even one corresponding to another disc spring actuator.

Two of the most common source characteristics are the ones corresponding to a pressure controller and a volume controller. An ideal pressure controller maintains the same pressure despite variations in volume such that $dp_s(V_s)/dV_s = 0$ everywhere. That means that snapping occurs when at the intersection of p_d and p_s the EIA characteristic has zero slope, which corresponds to a local maximum or minimum in pressure. The state then snaps to another intersection of p_d and p_s at a different volume but at the same pressure. On inflation starting from zero pressure, the disc spring EIA therefore snaps from the first local maximum in pressure to a higher volume. On deflating the disc spring EIA again, it snaps from the first local minimum it encounters to a lower volume. This thesis refers to those two snapping transitions as pressure snap-through and pressure snap-back respectively.[1] A dynamic simulation implementing a pressure control source confirms that those transitions occur as described above. The result is visible in figure 3.4 (a).

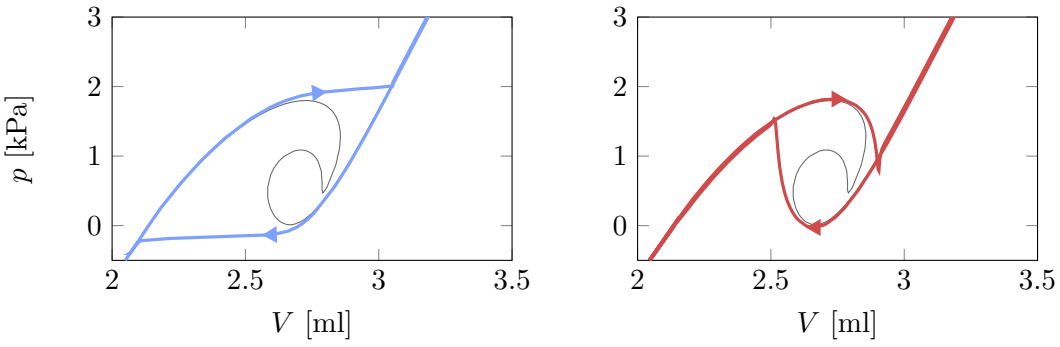

Figure 3.4: Dynamic pressure-volume characteristics of the disc spring EIA with (a) pressure control and (b) volume control compared to the static characteristic

Figure 3.4 (b) shows the result of a dynamic simulation implementing volume control. An ideal volume controller maintains the same volume regardless of the pressure so $dp_s(V_s)/dV_s = -\infty$ everywhere. In practice that slope has a finite

[1] In literature snap-through refers to a snapping transition under pressure or load control and snap-back to one under volume or displacement control. No terminology exists to denote the direction of the transition. This redefinition allows to more clearly treat all possible snapping transitions.

negative value because of the compressibility of every fluid which causes a small reduction in volume on an increase in pressure. Still, snapping only occurs when in a state the disc spring EIA characteristic locally has a nearly infinite slope. That corresponds to a local maximum or minimum in volume. On inflation starting from zero pressure, volume snap-through occurs at the first local maximum in volume to a lower pressure. On deflating again, volume snap-back occurs at the first encountered local minimum in volume to a higher pressure. The simulation in figure 3.4 (b) confirms that snapping occurs at those points and shows that the volume stays roughly constant during the transition.

The correspondence between the theory and the simulation results in figure 3.4 is not perfect, however. Firstly, the dynamic characteristic separates from the static characteristic before reaching the local extrema. The reason is that in the simulations the driving variable changes linearly with time. That means that when its values comes close to the corresponding extremum, a small increment corresponds to a large change in the non-controlled variable and the deformation of the membrane. The velocity of the membrane therefore increases, amplifying inertial and damping forces and removing the situation from a quasi-static inflation. At pressure snap-back for instance, those forces oppose the membrane deformation such that the actual snapping transition requires a lower pressure to start. The second difference between the dynamic simulation and the predicted snapping behaviour is that neither pressure nor volume stays constant during snapping. The most likely reason is that the snapping transition does not happen instantaneously. Therefore, the source characteristic changes noticeably during snapping. In practice, the overshoot and hysteresis around the static characteristic are probably also higher than in the presented simulations.

3.2.3 Snapping energies

During a snapping transition, an exchange takes place between the elastic and kinetic energy of the disc spring EIA and the pressure-volume work of the fluid filling it. A measure for both the change in the elastic energy and the work by the fluid follows from the static pressure-volume characteristics of the disc spring EIA and the source. Those characteristics therefore allow to investigate the energy released during snapping. That in turn gives an indication of the relative speeds during snapping transitions without needing an application-specific dynamic simulation.

The elastic energy stored in the disc spring EIA follows from an analysis of a quasi-static inflation or deflation with an incompressible fluid. In that case, the conservation of energy dictates that all pressure-volume work goes into changing the elastic energy. It therefore corresponds to the signed area under the static pressure-volume characteristic of the disc spring EIA between the current state and a reference state. In that characteristic, pressure is not a unique function of volume, however, so it is impossible to calculate the area by directly evaluating $\int p_d dV_d$. On the other hand, both p_d and V_d are a unique function of the arc length. Therefore, the elastic energy stored in the disc spring EIA at a state corresponding to arc length s' is:

$$U_{el} = \int_0^{s'} p_d(s) \frac{dV_d(s)}{ds} ds. \tag{3.3}$$

In that equation, $s = 0$ at the initial state corresponding to $p_d = 0$ and $V_d = V_0$ which serves as the zero reference for the energy calculations. Figure 3.5 shows the result of evaluating the equation for the static characteristic shown in figure 3.3. The graph also contains the points defining four snapping transitions. That shows that snapping under volume control starts at a state corresponding to a local extremum in the stored elastic energy. That is consistent with the result from section 3.2.2 that those states lie on a local volume extremum in the pressure-volume characteristic, such that $dV_d(s)/ds$ changes sign there.

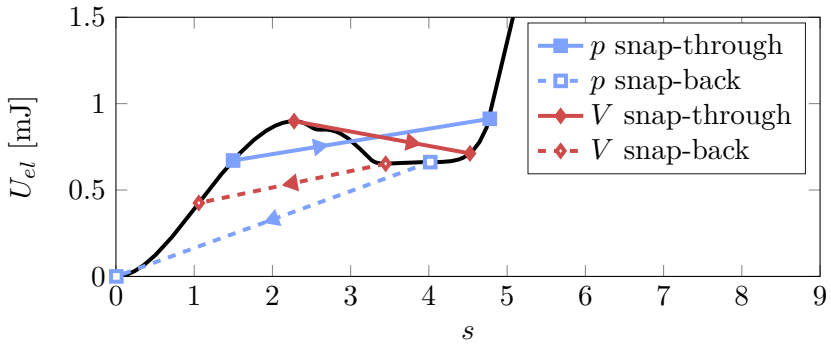

Figure 3.5: Stored elastic energy in the disc spring EIA and how it changes during four snapping transitions

The work by the fluid in the EIA during snapping corresponds to the area under the pressure-volume path of that transition. In an ideal instantaneous transition, that path is a straight line between the two relevant points where the static disc spring and source characteristic intersect. That means that the work by the fluid

$$W_{fl} = \frac{p_{d,end} + p_{d,start}}{2} \left(V_{d,end} - V_{d,start}\right), \tag{3.4}$$

with *start* and *end* referring to the start and end point of the studied snapping transition. In practice, however, that equation does not hold because the snapping path is not a straight line. Many factors like the flow resistance of the tubing that connects the disc spring EIA to the source influence its shape instead. For example, the flow resistance causes a drop in the pressure of the disc spring EIA due to a volume flux into the actuator. That means that during pressure snap-through, $p_d < p_s$ while $p_{d,start} = p_{d,end} = p_s$. Equation 3.4 then overestimates the fluidic work . Still, that equation is easy to interpret and accurate enough to qualitatively compare different snapping transitions.

Combining the results from equation 3.3 and 3.4 then gives the amount of energy released from the disc spring EIA during a snapping transition as

$$\Delta U = \frac{p_{d,end} + p_{d,start}}{2} \left(V_{d,end} - V_{d,start}\right) - \int_{s_{start}}^{s_{end}} p_d(s) \frac{dV_d(s)}{ds} ds. \tag{3.5}$$

Graphically, that expression corresponds to the area between the line segment connecting the start and end point of the snapping transition and the static pressure-volume characteristic.[2] Figure 3.6 shows that area for snap-through and snap-back of the disc spring EIA both under pressure and volume control. The areas corresponding to pressure snap-through and snap-back fully contain the areas corresponding to respectively volume snap-through and snap-back. That means that under pressure control the released energy during snapping is inherently higher than under volume control. The same is not necessarily true for the kinetic energy of the membrane. As mentioned previously, snapping under pressure implies a volume flux through the connecting tubing which causes viscous dissipation, lowering the kinetic energy.

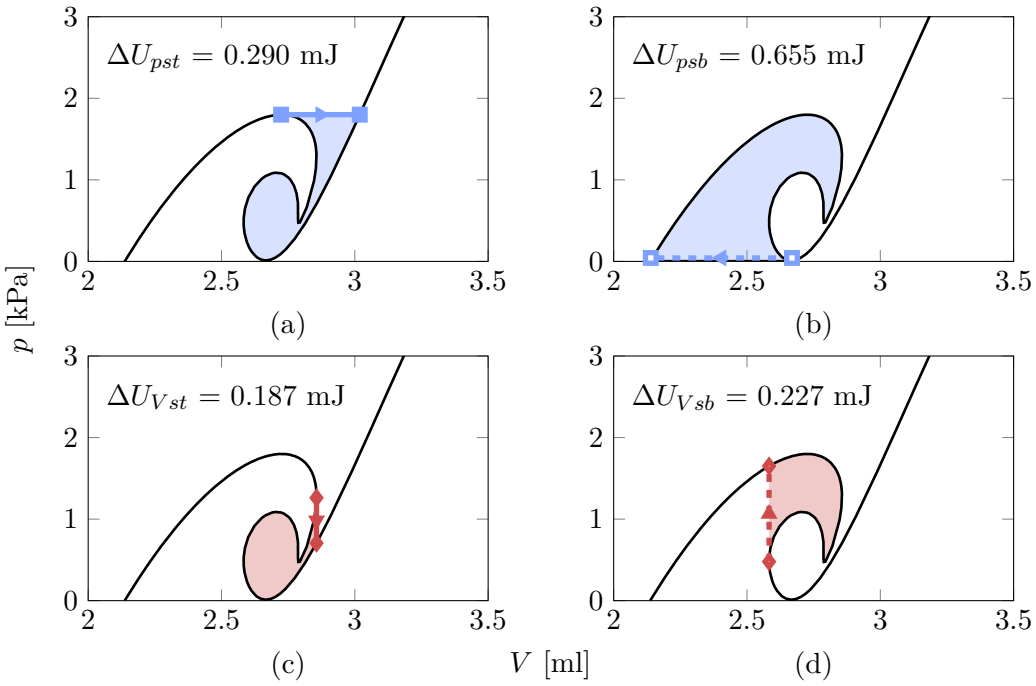

FIGURE 3.6: Snapping energies expressed as areas on the pressure-volume characteristic of a disc spring EIA for (a) pressure snap-through, (b) pressure snap-back, (c) volume snap-through and (d) volume snap-back

In the dynamic simulations presented in this thesis, the fluid filling the actuator cavity is inviscid. Consequently, the snapping energies from figure 3.6 are a good measure for the kinetic energy of the membrane during the corresponding transitions. That energy is approximately proportional to the squared vertical velocity of the apex of the membrane. Figure 3.7 shows the vertical displacement and velocity of the apex of the disc spring EIA for the same dynamic simulations as in figure 3.4. The markers in figure 3.7 (b) correspond to the square roots of the snapping energies

[2] In case the pressure-volume characteristic intersects itself however, some cut-off areas either count double or as negative area.

of figure 3.6, uniformly scaled to fit the simulated peak velocities. The relative values of both quantities agree well, with deviations probably due to the fact that not all points on the membrane deform proportionally with the apex.

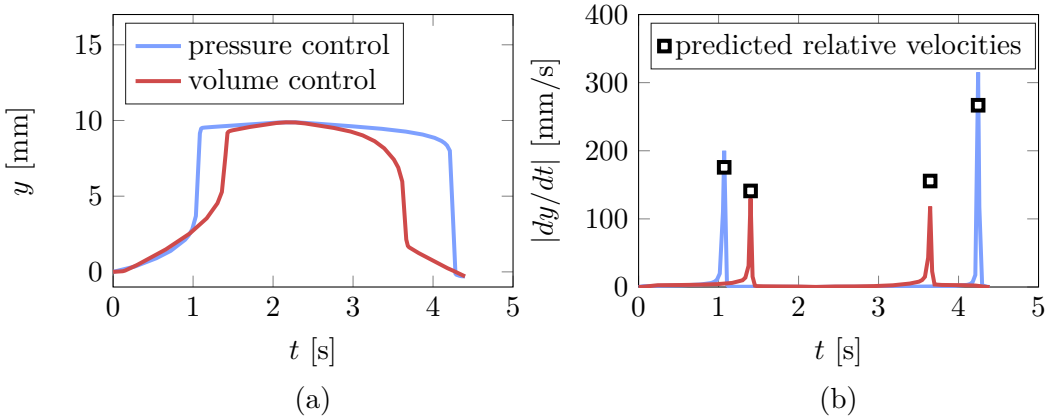

Figure 3.7: Vertical (a) displacement and (b) velocity of the apex of the disc spring EIA in dynamic simulations with pressure and volume control

Finally, the maximal principal Cauchy strain in the simulation is 0.284 and occurs at the inner hinge during pressure snap-back. It is an order of magnitude lower than in EIAs relying on material non-linearities in section 2.1.1. The reason is that the disc spring EIA has a higher ratio between the energy released on snapping and the total elastic energy at that point. Consequently, for the same released energy it has a lower average stress, strain and final volume than actuators with material non-linearities made of the same material.

Summary

The analytical model of the disc spring EIA presented in section 2.2.3 only describes its behaviour qualitatively. A more accurate description follows from a FEM analysis in Abaqus with an axisymmetric model featuring a fluid cavity interaction. In a static simulation, the results are fundamental to the actuator and independent of other parameters in an application. The simulated static pressure-volume characteristic of the disc spring EIA is non-linear. Moreover, it is the first one reported in literature to feature more than two extrema in pressure as well as extrema in volume. That unique characteristic potentially enables faster actuation in small applications and programming of the snapping behaviour by means of a dynamic inflation-deflation sequence. The static pressure-volume characteristic also allows to predict the dynamic behaviour of the disc spring EIA connected to a source with an arbitrary characteristic. In particular, the points at which the actuators snaps are those where both characteristics are tangent to each other. Additionally, the energy released during those transitions is related to the area between both characteristics. Those results agree with those of two representative dynamic simulations.

Chapter 4

Parameter study

In many applications it is necessary to tune the disc spring EIA to obtain a desired behaviour. Relations between the parameters defining the actuator geometry and various performance metrics assist in a fast and accurate tuning procedure. This chapter first discusses which parameters are most appropriate to tune the actuator behaviour and how their values vary in the presented parameter study. Then it presents how points where snapping occurs under pressure and volume control depend on those parameters. Those relations lead to a procedure to quickly find an estimate for the geometric parameters that yield a disc spring EIA that snaps at the desired points. A next section shows how the energy released during the subsequent snapping transitions depends on the geometric parameters as well. That results in a procedure to find the actuator that releases maximal energy at a set snap-through volume.

4.1 Parameter study methodology

In principle, all geometric variables listed in table 3.1 affect the static pressure-volume characteristic of the disc spring EIA. The most suitable parameters for tuning are those that have a significant effect on the characteristic and are independent of application dependent boundary conditions. The rounding radii of the hinges do not qualify because their influence is negligible. The parameters defining the geometry of the support wall on the other hand can appreciably change the characteristic. That wall stretches roughly linearly with the pressure in the cavity, so it influences the volumes at which the extrema of the characteristic occur. Changing its stiffness is therefore a straightforward way to tune the snapping points under volume control without affecting the snapping points under pressure control much. However, the behaviour of the support wall depends on the boundary conditions of the application. In particular, it often interfaces with a clamping system which imposes a certain geometry and changes its deformable length.

The only remaining parameters then are those describing the conical membrane. Of those parameters, the membrane thickness and angle depend the least on requirements other than those on the pressure-volume characteristic. Moreover, they are suitable tuning parameters because all extrema are highly sensitive to them.

Initial simulations with a disc spring EIA in figure 4.1 show that increasing the membrane thickness or decreasing the membrane angle linearises the response. That is consistent with the qualitative conclusions drawn from the analytical disc spring model in section 2.2.3. Past certain values, first the extrema in volume and then those in pressure disappear so no snapping occurs. Decreasing the membrane thickness or increasing the membrane angle causes the characteristic to curl up and eventually to intersect itself. Its shape then starts to become so involved that the simulation requires a very dense mesh and an unreasonable amount of time to reach the linear region at high volumes. For a disc spring EIA with a membrane angle of 45°, the relevant range for the membrane thickness goes from 0.5 mm to 2 mm. On changing the membrane angle for a disc spring EIA with a membrane thickness of 1 mm, the relevant range lies between 20° and 55°. Those values therefore form the boundaries for the parameter study presented in this chapter. The membrane thickness and angle of the various disc spring EIAs in the presented parameter study change with increments of 0.1 mm and 5°, respectively.

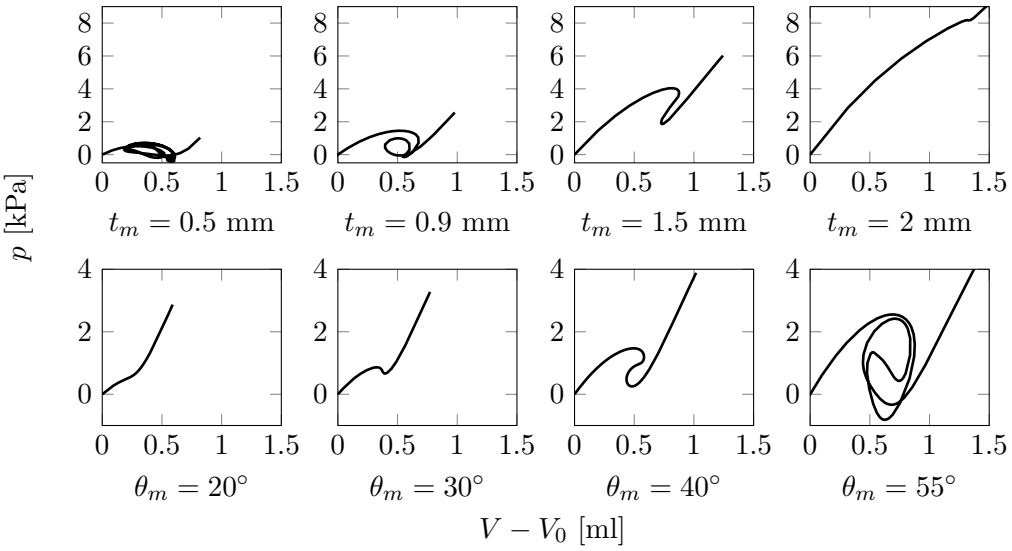

Figure 4.1: Evolution of the pressure-volume characteristic of a disc spring EIA with varying membrane thickness or angle

Apart from geometric parameters, material parameters influence the static pressure-volume characteristic as well. Changing the material mainly results in a more or less uniform scaling of that characteristic along the pressure axis. That means that the values for the volume at the various extrema largely remain unchanged. The reason is that due to the generally small strains in the disc spring EIA a constant shear modulus G and Poisson's ratio ν suffice to describe the behaviour of its material. The pressure-volume characteristic of such an actuator with a certain shape qualitatively follows from $f(p, V, V_0, G, \nu) = 0$, with f an unknown function. A dimensional analysis allows to reduce that expression to $g(p/G, V/V_0, \nu) = 0$. Most rubbers are nearly incompressible so they have a similar Poisson ratio of about 0.5.

The only significant effect on the pressure-volume characteristic resulting from a change in material therefore goes through p/G, which corresponds to scaling the pressure axis. The dimensionless pressure-volume characteristics in figure 4.2 confirm that. Deviations only occur because the modulus changes for increasing strains due to the non-linearity of the material. Since the overall effect of tuning the material is straightforward, it does not feature as a separate tuning parameter in this chapter. Instead, all presented variables are dimensionless to make them independent of the used material and dimensional scale.

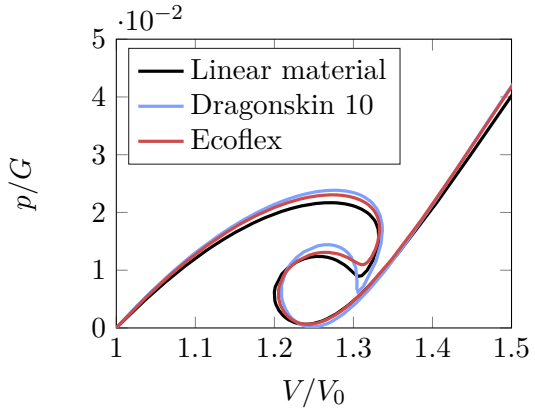

Linear material:
$E = 20$ MPa, $\nu = 0.45$
$\Rightarrow G = E/(2(1+\nu)) = 6.9$ MPa
Dragonskin™ 10 [38]:
$\mu_1 = 75.4$ kPa, $\alpha_1 = 5.86$
$\Rightarrow G = \sum \mu_i$[40] $= 75.4$ kPa
Ecoflex™ 00-30 [41]:
$\mu_1 = 1.9$ kPa, $\alpha_1 = -3.85$,
$\mu_2 = 22.2$ kPa, $\alpha_2 = 0.66$,
$\mu_3 = 3.6$ kPa, $\alpha_3 = 4.2$
$\Rightarrow G = \sum \mu_i = 27.7$ kPa

FIGURE 4.2: Dimensionless pressure-volume characteristic of the disc spring EIA for varying materials

4.2 Parameter dependence of the snapping pressures and volumes

4.2.1 Simulated results

As mentioned in section 3.2.2, many EIA applications use a source with pressure control or volume control. Snapping then occurs on reaching the first and last locally extreme pressure or volume in the actuator characteristic respectively. The relative magnitude of those extrema between multiple EIAs also determines their sequence of inflation and deflation when they connect to a common supply line. Finally, the sign of the pressure at pressure snap-back determines whether the actuator can be bistable or not. The first and last extrema in both pressure and volume therefore are important design parameters for the disc spring EIA.

Instead of investigating those extreme values separately, it is more intuitive to consider their average and difference. The average $\bar{p}_{ps}$ of the first and last extremum in pressure is a measure for the average stress during snapping under pressure control. The difference Δp_{ps} between the pressures roughly is proportional to the energy released during those transitions. Similarly, $\bar{V}_{vs}$ and ΔV_{vs} of the first and last extremum in volume relate to the average strain and released energy during snapping under volume control respectively. Another important advantage of considering

the transformed variables is that they allow to decouple the effects of changing the membrane angle and thickness. For example, inspection of figure 4.1 shows that the extrema in pressure significantly depend on both geometric parameters. $\bar{p}_{ps}$, on the other hand, stays approximately constant in the presented characteristics for different membrane angles. That means that it is possible to vary the membrane angle to obtain a desired Δp_{ps} without changing $\bar{p}_{ps}$ for a certain membrane thickness much. That decoupling simplifies the tuning procedure.

Figure 4.3 features the dimensionless plots showing the relation between the membrane thickness and angle on one hand and $\bar{p}_{ps}$ and Δp_{ps} on the other hand. Figure 4.4 shows similar plots for $\bar{V}_{vs}$ and ΔV_{vs}. The plot of $\bar{p}_{ps}$ confirms that it is nearly independent of the membrane angle as the contours belonging to different angles nearly coincide. That is not the case for $\bar{V}_{vs}$ but the flat profile and even spacing of the contours suggests an approximately linear dependence on both the membrane thickness and angle. Δp_{ps} and ΔV_{vs} are more complicated functions of the parameters. They depend monotonically on the membrane angle but show maxima and inflection points for different values of the membrane thickness.

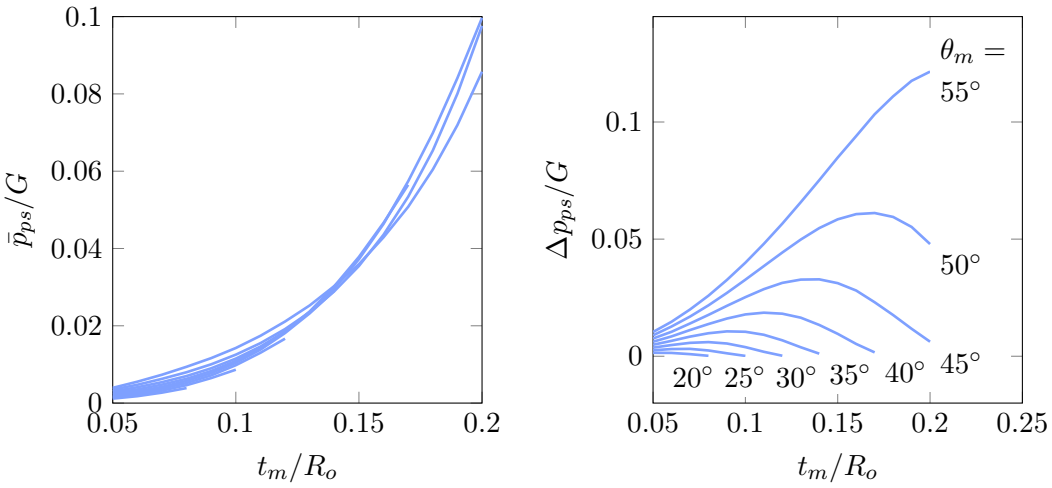

Figure 4.3: Dependence of the snapping pressures of the disc spring EIA on the membrane thickness and angle

In order to interpolate and extrapolate the simulated data, it is useful to fit an analytical equation to each of the shown surfaces in function of the membrane thickness and angle. The smallest order polynomial that captures the main features of each surface without over fitting the data has the form

$$\begin{aligned} a_{00} + a_{10}\,\theta_m + a_{01}\,\frac{t_m}{R_o} + a_{20}\,\theta_m^2 + a_{11}\,\theta_m\,\frac{t_m}{R_o} + a_{02}\left(\frac{t_m}{R_o}\right)^2 + \dots \\ \dots + a_{21}\,\theta_m^2\,\frac{t_m}{R_o} + a_{12}\,\theta_m\left(\frac{t_m}{R_o}\right)^2 + a_{03}\left(\frac{t_m}{R_o}\right)^3. \end{aligned} \tag{4.1}$$

Assuming a value for θ_m in degrees, fitting such equations to the simulated values for $\bar{p}_{ps}$, Δp_{ps}, $\bar{V}_{vs}$ and ΔV_{vs} in Matlab results in the coefficients in table 4.1. That

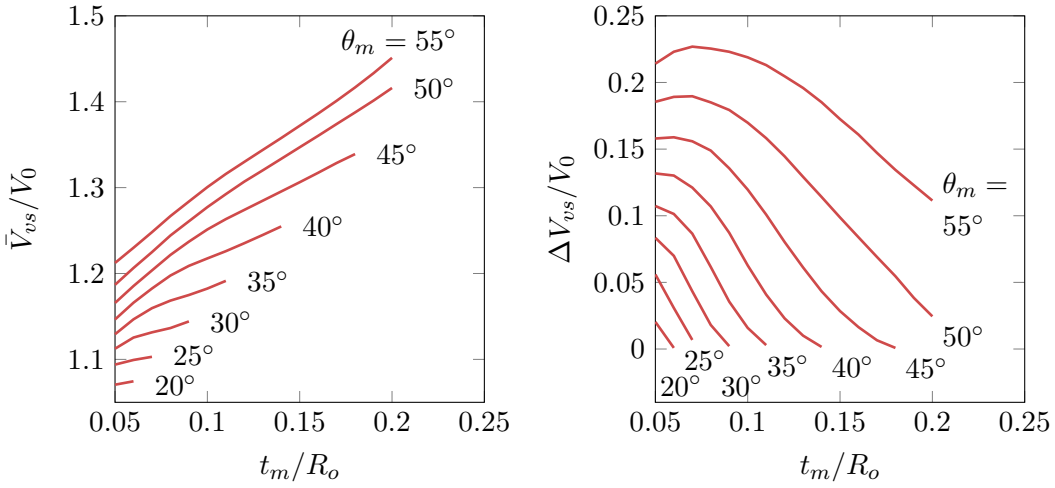

FIGURE 4.4: Dependence of the snapping volumes of the disc spring EIA on the membrane thickness and angle

table also contains the coefficient of determination r^2. Its value is close to one for every surface, indicating good agreement between the data and the corresponding fitted model. r^2 is smallest for Δp_{ps} which results in the model yielding lower values than the simulations especially for thin and shallow membranes.

TABLE 4.1: Coefficients of the polynomial models fitted to the simulated snapping points of the disc spring EIA

Coefficient	a_{00}	a_{10}	a_{01}	a_{20}	a_{11}
Value for $\bar{p}_{ps}$	0.02165	$-1.033 \cdot 10^{-3}$	-0.3436	$4.949 \cdot 10^{-6}$	0.02189
Value for Δp_{ps}	-0.1108	$5.024 \cdot 10^{-3}$	2.141	$-4.583 \cdot 10^{-5}$	-0.09445
Value for $\bar{V}_{vs}$	1.123	$-6.736 \cdot 10^{-3}$	-1.249	$1.058 \cdot 10^{-3}$	0.1891
Value for ΔV_{vs}	0.01882	$8.081 \cdot 10^{-3}$	-2.881	$-1.273 \cdot 10^{-4}$	0.0236

Coefficient	a_{02}	a_{21}	a_{12}	a_{03}	r^2
Value for $\bar{p}_{ps}$	-1.207	$-3.586 \cdot 10^{-5}$	-0.1076	30.39	0.9989
Value for Δp_{ps}	-6.214	$6.688 \cdot 10^{-4}$	0.4056	-43.79	0.9934
Value for $\bar{V}_{vs}$	-21.67	$-1.924 \cdot 10^{-3}$	0.1401	34.13	0.9997
Value for ΔV_{vs}	-1.351	$1.904 \cdot 10^{-3}$	-0.6029	72.13	0.9967

The fitted models allow to extrapolate Δp_{ps} and ΔV_{vs} in order to investigate for which combinations of geometric parameters they become zero. That creates boundaries in the parameter space which separate disc spring EIAs with and without snapping behaviour under pressure or volume control. Figure 4.5 (a) shows those boundaries. The dashed line is not consistent with the simulated data and only appears because the model for Δp_{ps} is unreliable for small membrane angles and thicknesses. The solid lines on the other hand agree well with the simulations but still

misclassify some data points by a small margin. In practice however, few applications require disc spring EIAs close to that boundary since the displacement and energy released during their snapping transitions are small.

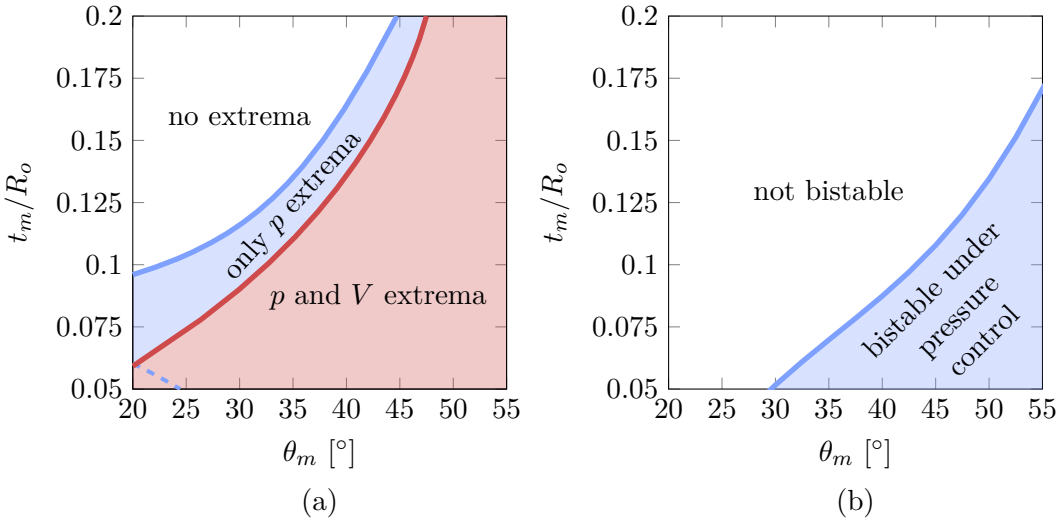

Figure 4.5: Phase diagram for (a) the existence of extrema in the pressure-volume characteristic of the disc spring EIA and (b) bistability under pressure control in function of the membrane angle and thickness

Another potential use for the fitted models for $\bar{p}_{ps}$ and Δp_{ps} is to investigate which disc spring EIAs are bistable under pressure control. Bistability is possible when the pressure at pressure snap-back is negative or when $\bar{p}_{ps} - \Delta p_{ps}/2 < 0$. The fitted models to those two quantities allow to obtain an analytical expression for the boundary of bistable disc spring EIAs in parameter space. However, the inaccuracy of the model for Δp_{ps} again leads to a result that does not comply well with the simulations for small membrane angles and thicknesses. The boundary shown in figure 4.5 (b) therefore follows from bicubic interpolation of the simulated snap-back pressures instead.

4.2.2 Tuning procedure

For many applications like sequencing it is necessary to design EIAs with predefined values for both $\bar{p}_{ps}$ and Δp_{ps} or for both $\bar{V}_{vs}$ and ΔV_{vs}. It is not obvious, however, how to select the membrane thickness and angle from figure 4.3 or 4.4 that result in a disc spring EIA with those properties. The reason is that especially for the snapping volumes a change in membrane thickness for a fixed angle and vice versa causes a large variance in both snapping points. A linear coordinate transform can reduce that variance and hence simplify the tuning procedure. Such an operation involves expressing the snapping points in function of two orthogonal linear combinations of the geometric parameters $x = \theta_m + a \cdot t_m/R_o$ and $y = -a \cdot \theta_m + t_m/R_o$. That corresponds to horizontally scaling and rotating the surfaces with θ_m and t_m as

horizontal coordinates and the snapping points as vertical coordinates. Since the surface describing the parameter dependence of $\bar{V}_{vs}$ is nearly planar, for some a the projection of that surface on the $(x, \bar{V}_{vs})$-plane resembles a single straight line. Similarly, another a leads to the different curves for $\bar{p}_{ps}$ in figure 4.3 coinciding more with a single cubic curve. That means that a change in y does not cause significant variations in those average values such that x and y are partly decoupled.

The optimal a follows from an iterative search algorithm implemented in Matlab. As input it takes either the simulated data for $\bar{p}_{ps}$ or $\bar{V}_{vs}$ and the corresponding values for θ_m and t_m. First, it normalizes both geometric parameters to range from zero to one. Then, it proposes multiple values for a that correspond to uniformly spaced rotations between $-90°$ and $90°$. Each a leads to a set of x-coordinates for all data points. The algorithm then uses those coordinates to fit a one-dimensional model which is cubic for $\bar{p}_{ps}(x)$ and linear for $\bar{V}_{vs}(x)$ and records the coefficient of determination. Finally, the two proposed a's next to the one that results in the maximal r^2 form the boundaries for a new range of proposed coefficients in the next iteration. That process continues until the divisions reach a desired resolution.

Figures 4.6 and 4.7 show the pressure and volume snapping points after such an optimal coordinate transform as well as the corresponding a's. The plots of $\bar{p}_{ps}(x)$ and $\bar{V}_{vs}(x)$ show the curves fitted to the x-projected data points. The coefficients of determination for those fits are 0.9925 and 0.9908 respectively. The plots of $\Delta p_{ps}(y)$ and $\Delta V_{vs}(y)$ contain various contours corresponding to constant values of x. They result from evaluating the fitted models for Δp_{ps} and ΔV_{vs} with coefficients as in table 4.1. Some combinations of x and y on the plots do not lead to a membrane thickness and angle within the range of the simulations and hence follow from extrapolation. They appear as dotted lines on the plots, while solid lines represent the interpolated values. The latter are more likely to correctly predict the behaviour of the disc spring EIA in reality.

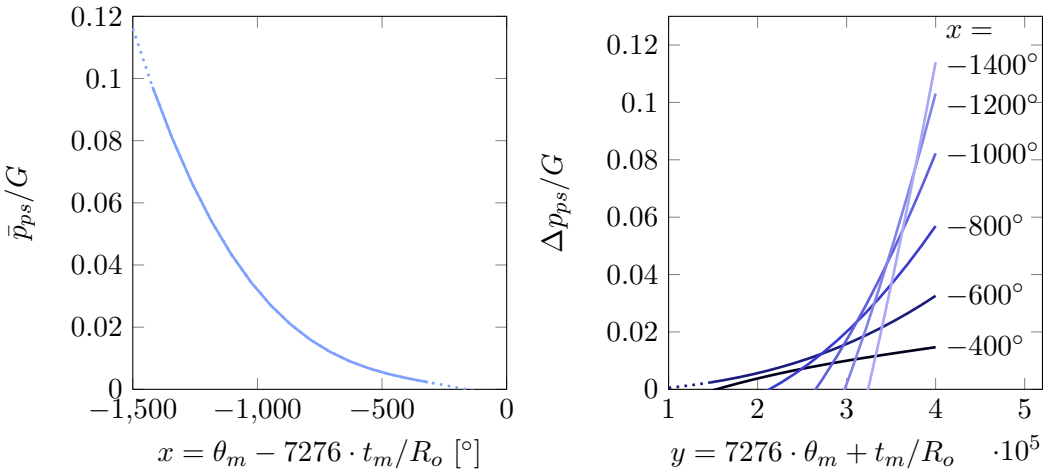

FIGURE 4.6: Dependence of the snapping pressures of the disc spring EIA on maximally decoupled orthogonal parameters

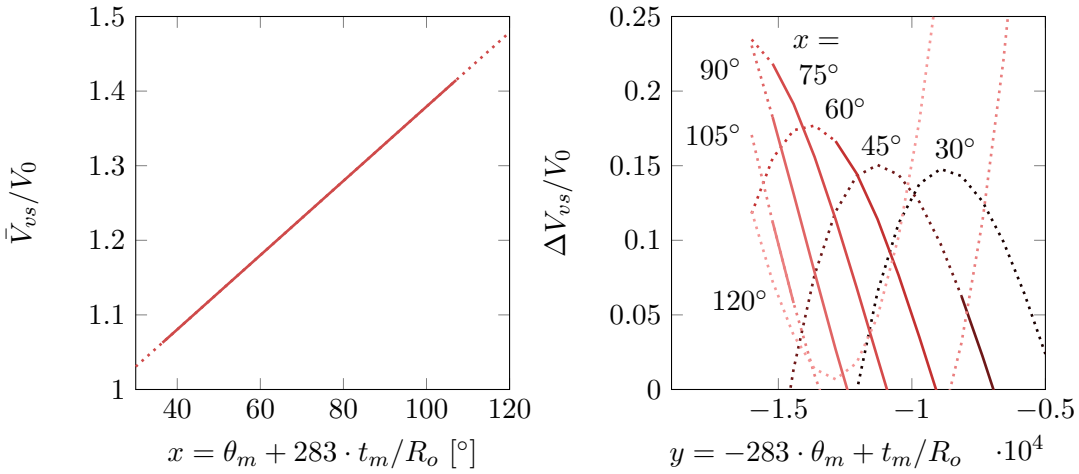

Figure 4.7: Dependence of the snapping volumes of the disc spring EIA on maximally decoupled orthogonal parameters

Figure 4.6 enables the following procedure to tune a disc spring EIA with a set snap-through and snap-back pressure under pressure control:

Input Desired pressure on pressure snap-through and snap-back: p_{pst}, p_{psb}
Output θ_m and t_m for a disc spring EIA that realizes those pressures
Procedure

1. Calculate $\bar{p}_{ps} = (p_{pst} + p_{psb})/2$ and $\Delta p_{ps} = p_{pst} - p_{psb}$ and divide those values by the shear modulus G of the used material.
2. From the left plot in figure 4.6, find the x-value that results in the desired $\bar{p}_{ps}/G$.
3. From the right plot in figure 4.6, find the y-value that results in the desired $\Delta p_{ps}/G$ in combination with the x-value found in the previous step.
4. Calculate the required membrane thickness and angle as

$$\theta_m = \frac{x - ay}{a^2 + 1} \text{ and } t_m = R_o \frac{ax + y}{a^2 + 1} \text{ with } a = -7276 \text{ and } \theta_m \text{ in degrees}$$

The procedure to tune the actuator to reach a given snap-through and snap-back volume under volume control is fully analogous. The differences are a division by V_0 instead of G, that the required plots feature in figure 4.7 and that $a = 283$.

4.3 Parameter dependence of the snapping energies

4.3.1 Simulated results

Section 3.2.3 demonstrates that snapping energies derived from the static pressure-volume characteristic correlate to the velocity of snapping transitions. Qualitatively,

the difference between the deformation of the disc spring EIA before and after such a transition is proportional to the integral of that velocity. The snapping energies therefore encode important information on the dynamic behaviour of the disc spring EIA which merits a parameter study. Figures 4.8 and 4.9 show the simulated energies for snap-through and snap-back transitions under pressure and volume control. Together they define an interval in which the corresponding energies for a disc spring EIA connected to any source with non-negative stiffness dp_s/dV_s lie.

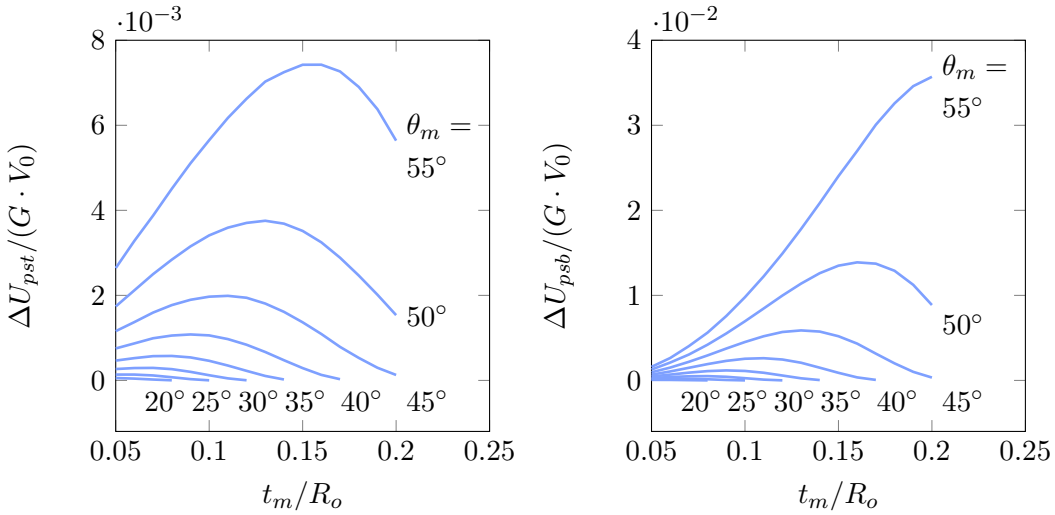

FIGURE 4.8: Dependence of the snapping energies of the disc spring EIA under pressure control on the membrane thickness and angle

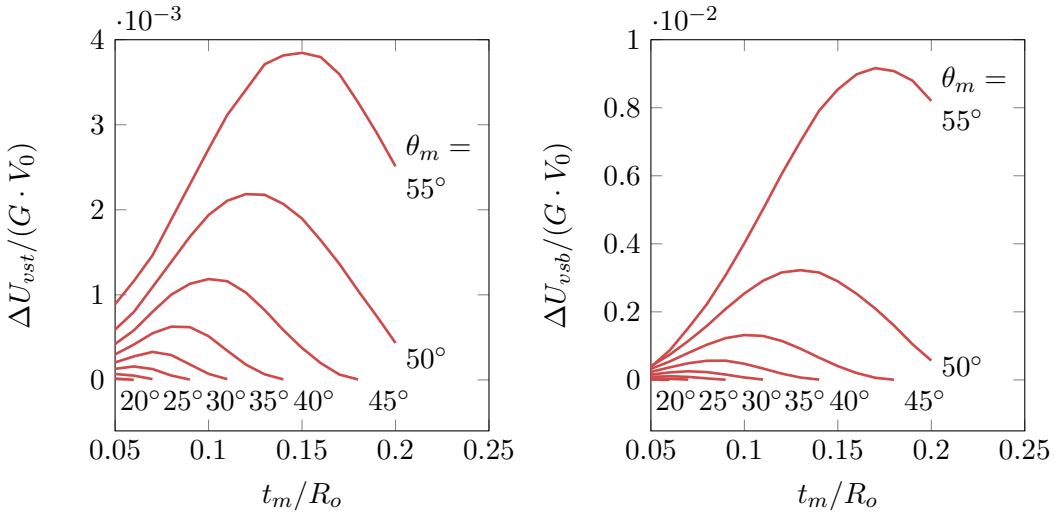

FIGURE 4.9: Dependence of the snapping energies of the disc spring EIA under volume control on the membrane thickness and angle

The presented snapping energies correspond to the areas shaded in figure 3.6. The areas for pressure snap-through and snap-back are proportional to Δp_{ps} if their shapes stay roughly constant for varying membrane angles and thicknesses. Under that assumption the plots for ΔU_{pst}, ΔU_{psb} and Δp_{ps} have a similar shape, which figure 4.8 confirms. An analogous reasoning predicts that ΔU_{vst}, ΔU_{vsb} and ΔV_{vs} are proportional to each other. However, figure 4.9 contradicts the prediction. The reason is that the edges of the corresponding areas partly lie on the inner loop of the pressure-volume characteristic. As discussed in section 3.2.1, that loop mostly results from the buckling behaviour of the membrane which significantly depends on the geometric parameters. In figure 4.1 the shape of that segment indeed changes so it does not scale with ΔV_{vs} as assumed. The areas for ΔU_{pst} and especially ΔU_{psb}, on the other hand, have a segment outside of that loop. Its shape varies less such that Δp_{ps} is a good predictor for the snapping energies under pressure control.

4.3.2 Tuning procedure

The absolute value of the snapping energy is rarely a parameter that drives the design of a disc spring EIA. Instead, in many applications it is useful to maximize the energy released during a snapping transition at a set pressure or volume. That allows to minimize the size of a disc spring EIA which attains a certain velocity or displacement during such a transition. According to the simulated data in figures 4.8 and 4.9, all snapping energies increase monotonically with the membrane angle. They evolve non-monotonically with the membrane thickness, however, reaching a maximum at a particular value for each simulated angle. It is therefore possible that the disc spring EIA with maximal snapping energy at a set snapping point lies within the bounds of the simulated parameter space.

To find that optimal actuator, it is necessary to first see which sets of geometric parameters lead to that particular snapping point. For the pressure on pressure snap-through, they lie on the contours $t_m = f(\theta_m, p_{pst})$ of $p_{pst}(\theta_m, t_m)$. An analytical expression for the latter function follows from combining the previously fitted models as $p_{pst} = \bar{p}_{ps} + \Delta p_{ps}/2$. Then it is possible to find the snapping energy for all actuators with the same snap-through pressure by evaluating a fitted polynomial model for $\Delta U_{pst}(\theta_m, t_m)$ at $t_m = f(\theta_m, p_{pst})$. The membrane angle for which $\Delta U_{pst}(\theta_m, f(\theta_m, p_{pst}))$ becomes maximal is the optimal one for a p_{pst}.

A similar procedure yields the optimal membrane angle and thickness for the other snapping transitions under pressure and volume control. Of the studied snapping energies, $\Delta U_{pst}(\theta_m, f(\theta_m, p_{pst}))$, $\Delta U_{psb}(\theta_m, f(\theta_m, p_{psb}))$ and $\Delta U_{vsb}(\theta_m, f(\theta_m, V_{vsb}))$ do not show a maximum at any set snapping point. Instead, they increase monotonically with the membrane angle over the simulated range. The optimal value for the angle therefore is a compromise between the released energy and the strain during a snapping transition. $\Delta U_{vst}(\theta_m, f(\theta_m, V_{vst}))$ on the other hand does show a maximum in membrane angle for any snap-through volume. The evolution of the optimal angle and matching thickness features in figure 4.10.

That figure enables the following tuning procedure:

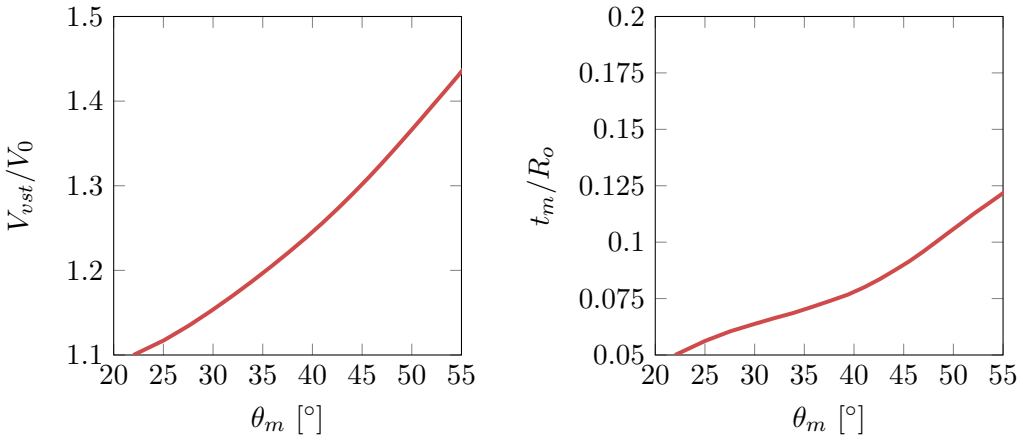

FIGURE 4.10: Relation between the volume at which volume snap-through starts and the geometric parameters that maximize the snapping energy at that point

Input	Desired volume on volume snap-through: V_{vst}
Output	θ_m and t_m for the disc spring EIA snapping at the desired volume that releases maximal energy during that transition

Procedure

1. Divide V_{vst} by the internal volume V_0 of the disc spring EIA at zero pressure.
2. From the left plot in figure 4.10, find the value for θ_m that results in the desired V_{vst}/V_0.
3. From the right plot in figure 4.10, find the value for t_m/R_o that corresponds to the obtained value for θ_m.

Summary

Section 3.2 shows how the static pressure volume characteristic of the disc spring EIA determines its behaviour in a variety of applications. By studying the influence of material and geometric parameters on that characteristic, it is therefore possible to design actuators fit for a particular goal. The only effect of changing the material is that the pressure values of the characteristic scale roughly uniformly with the shear modulus. The most suitable geometric tuning parameters are the membrane angle and thickness. They depend minimally on application specific boundary conditions and affect the characteristic significantly. Both decreasing the membrane angle and increasing the thickness linearises the characteristic such that extrema in pressure and volume can disappear. Either parameter affects all those points simultaneously. For well chosen linear combinations of the two geometric parameters on one hand and the snapping pressures and volumes on the other hand, a partial decoupling occurs. One of the performance parameters then depends on only one input parameter which simplifies tuning of an actuator to reach set snapping points. Finally, all

energies released on snapping increase with the membrane angle and show maxima for certain membrane thicknesses. As a result a pair of geometric parameters exists that maximizes the energy of a volume snap-through transition which starts at a set volume.

Chapter 5

Manufacturing and experimental characterization

In order to confirm the simulated characteristics of the disc spring EIA, it is necessary to manufacture a prototype and perform experiments on it. The first section of this chapter describes the hardware and methods used to create such prototypes. The second section deals with the experimental measurement of the dynamic pressure-volume characteristic of several produced actuators. After detailing the experimental set-up, it presents the measured characteristics and compares them to the simulated ones.

5.1 Manufacturing of the disc spring actuator

The most common methods to produce EIAs at the centimetre scale are additive manufacturing and rubber moulding [15]. No examples exist of non-linear EIAs resulting from an additive manufacturing process with a rubber-like material. One potential reason is that the bond between layers of the material is too weak to sustain the high strains required for significant material non-linearity to arise. The strains in the disc spring EIA can remain small, however, so additive manufacturing can be a viable option for its production. Still, rubber moulding results in a higher material quality with fewer imperfections. It also enables faster, less expensive and more reproducible production with a greater variety in possible materials for the actuator. Therefore, the disc spring EIA prototypes analysed in this study follow from a rubber moulding process. The main disadvantage of that method is the complexity of the mould for structures with large overhangs. That is not a problem for a single actuator, but for stacks like in figure 2.6 (c) additive manufacturing is probably the better option.

5.1.1 Mould design

Figure 5.1 gives an overview of the different parts and features of the mould used to manufacture the disc spring EIAs in this study. Appendix C.1 contains all of

their dimensions. The male and female mould part are the most critical components because they define the geometry of the produced actuator. After putting them together, the cavity between the two parts has roughly the same shape as the simulated actuator with dimensions as in table 3.1. The main difference is that the moulded EIA has a ridge running around its circumference. That ridge allows secure clamping of the actuator to the supply line as described in section 5.2.1.

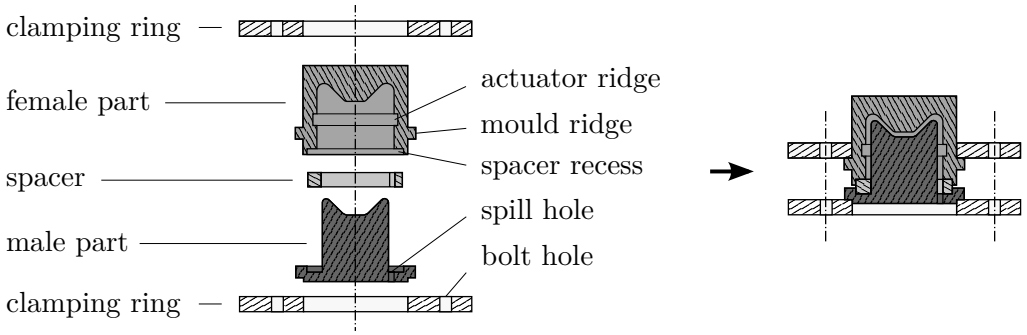

Figure 5.1: Schematic cross-section of the mould used to manufacture the disc spring EIA

The separation line of the mould is near the bottom of the cavity to prevent flashing on any of the deforming parts of the produced actuators. Near that line, both the male and female part have a recessed area to accommodate a spacer ring. By making spacers of multiple heights, it is possible to manufacture disc spring EIAs with different membrane thicknesses from the same male and female mould part. Changing the height of the spacer varies the thickness of the conical membrane and the top cap by different amounts while in the simulations they are always equal. According to additional simulations, however, that slight difference in geometry does not affect the stable segments of the pressure-volume characteristics significantly.

On closing the mould, the spacer aligns the axes of all components. A set of keys on the male part also fits into slots in the spacer and the female part to prevent rotation around the main axis. Finally, two clamping rings loosely slide over the exterior of the male and female part and catch behind ridges on both halves. Each ring has four holes for bolts that compress the mould axially. To allow air and excess material to escape from the cavity during that compression, the male part features a spill hole which aligns with a channel in the spacer.

The male and female mould parts as well as the spacers used in this study are 3D-printed parts. They consist out of layers of Vero PureWhite™ material [42] shaped by a stereolithographic process on an Objet30 Prime™ machine [43]. Since it prints with a layer height of only 28 μm, the mould surfaces are smooth and precisely dimensioned. Residual support material sticking to the surfaces defining the mould cavity could deteriorate the smoothness and accuracy of the moulded actuators. To avoid any support material on those surfaces, the orientation of the male and female parts during printing is such that spacer recesses face upwards. Finally, the clamping rings have a two-dimensional shape and do not require high precision, so laser cutting

PMMA material suffices to produce them. Figure 5.2 shows the printed mould parts, the total mould assembly and a manufactured disc spring EIA analysed in this study.

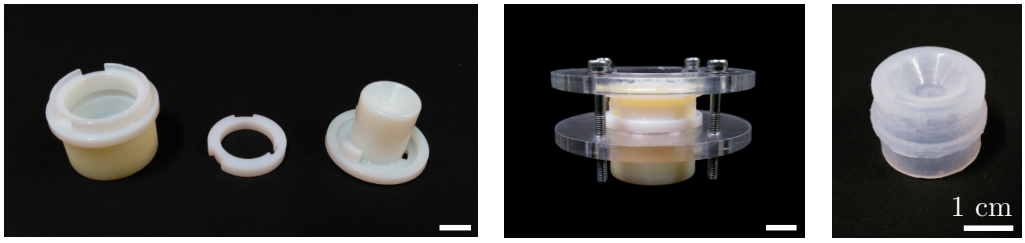

(a) (b) (c)

FIGURE 5.2: (a) Individual printed mould parts and (b) assembled mould to manufacture (c) the disc spring EIA prototype

5.1.2 Manufacturing procedure

The first step in manufacturing a disc spring EIA with the presented mould is the preparation of the material and the mould. The studied actuators consist of Dragonskin™ 30 silicone which has a long working time and is relatively stiff.[1] The product comes packaged as two components. A mixture of both components in a one to one weight ratio with a total weight of 10 g yields enough material to create a disc spring EIA with $R_o = 10$ mm. To evacuate most air bubbles from the mixture, it is desirable to first stir it vigorously for one minute and then place it in a vacuum pump for three minutes. The material has a working time of 45 minutes [37], so it is possible to continue degassing for a longer time if bubbles keep rising from the mixture. Preparation of the 3D-printed mould parts can happen in the meantime. That involves cleaning them with ethanol to remove any contamination which could inhibit the curing of the silicone and sliding the correct spacer over the male part.

The next step is to pour the silicone into the mould. To fill the cavity of the female mould part, it is best to keep it at an angle and slowly pour into the mouth of the cavity. That way, the silicone level gradually rises in the region defining the outer hinge of the disc spring EIA which prevents air bubbles from getting trapped there. For a membrane thickness of up to 2.5 mm, the proximal face of the groove corresponding to the actuator ridge acts as a fill line. It is desirable to fill the conical cup of the male mould part with silicone as well. Otherwise a pocket of air can get trapped in that cup when inserting the male part into the female one. The act of pouring the material can also introduce air bubbles. Therefore, the two mould parts filled with silicone need another three minute long degassing treatment in the vacuum pump.

[1] Values for the parameters of a hyperelastic model for Dragonskin™ 30 are not available in literature which is why the simulations use a model for Dragonskin™ 10. The assumption is that for the same strains, the stresses in both materials differ by a constant scale factor.

The mould is then ready for the assembly step. It starts with quickly flipping the male mould part with the spacer and inserting it into the cavity of the female part with the keys aligned. Keeping the male part at an angle and tilting it in place once the cup is fully surrounded by the mixture allows air to escape from between the two silicone masses. Next, it is possible to install the clamping rings, tighten the bolts and clean up the excess silicone which subsequently spills from the mould. The clamping rings allow to orient the axis of the mould at an angle of about 40° with the horizontal plane. With the spill hole at the highest point, any air bubble loosened during the curing process can then escape. Dragonskin™ 30 takes sixteen hours to cure at room temperature [37]. To speed up the manufacturing process in this study, the disc spring EIAs cures in an oven at 75°C for thirty minutes.

The final manufacturing step is to demould the cured disc spring EIA. Cutting away any excess silicone before taking the male and female half apart decreases the force required for the separation. After disassembling the mould, the produced actuator is likely stuck in the female part. The piece of silicone cured in the spill hole forms a tab which allows to separate the support wall of the EIA from the cavity surface. That reveals the actuator ridge which reinforces the support wall and therefore is a suitable place to grab with blunt tweezers to pull the actuator from the mould. Cutting away the tab of silicone from the spill hole with a scalpel then finishes the disc spring EIA prototype. Since that tab sits near the bottom of the support wall, an imprecise cut does not weaken the actuator or affect its behaviour.

5.2 Experimental characterization of the disc spring actuator

As illustrated in section 3.2, the static pressure-volume characteristic of the disc spring EIA allows to predict its behaviour in numerous applications. Experimental validation of the simulated characteristic would therefore confirm most conclusion drawn previously. However, section 3.2.2 shows that it is impossible to measure the characteristic in its entirety because the actuator always snaps before reaching the inner loop. Actuating the EIA with a volume controlled source maximizes the fraction of the characteristic that is stable. Consequently, an experiment which measures the pressure in a disc spring EIA connected to such a source gives the most information on the characteristic.

5.2.1 Experimental design

Figure 5.3 shows a diagram of the hardware used to measure the pressure-volume characteristic of the disc spring EIA. A 60 ml syringe pump with a stepper motor drives the inflation and deflation of the actuator. If no elasticity is present between the pump and the EIA, the former acts as a controller which imposes a known change in internal volume on the latter. To remove most of the elasticity, a procedure exists to fill the entire system with a practically incompressible fluid like water. The first step consists of configuring the T-valves to connect the syringe pump exclusively

to the reservoir to suck in water. Inevitably, that also introduces some air into the pump. Removal of the air happens by holding the nozzle of the syringe upwards and decreasing the internal volume until all bubbles surface in the reservoir. In the next step, the T-valves isolate the syringe pump and connect the clamped disc spring EIA, the reservoir and the deairing syringe together. The position of the latter needs to be higher than the other components. Its plunger has to sit at the maximal insertion depth and like the EIA supply tube has to face up. By repeatedly raising and lowering the plunger of the deairing syringe without pushing air into the system, it collects the air and fills the other components with water.

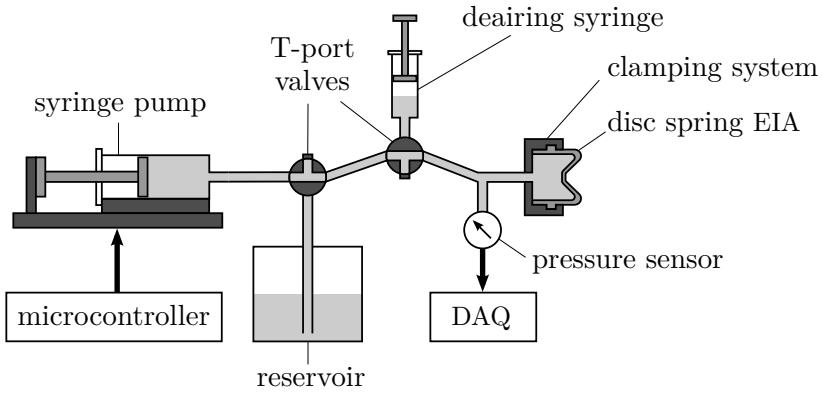

FIGURE 5.3: Schematic overview of the experimental set-up to measure the pressure-volume characteristic of a disc spring EIA

Another condition to ensure volume control of the disc spring EIA is the absence of leaks. Therefore it is necessary to connect the actuator firmly to the supply tube with the clamping system shown in figure 5.4. The base plate of the clamping system features a protrusion with a central opening to tightly plug the supply tube into. The support wall of the disc spring EIA loosely fits over that protrusion in order not to create additional tensile stresses which could affect the characteristic. To seal the connection, a slightly under dimensioned assembly of two jaw plates and a compression ring radially press the wall and the protrusion together. Finally, a locking plate bolted to the base plate traps the actuator ridge such that the EIA can not move axially. Appendix C.2 contains the dimensions of each of those parts.

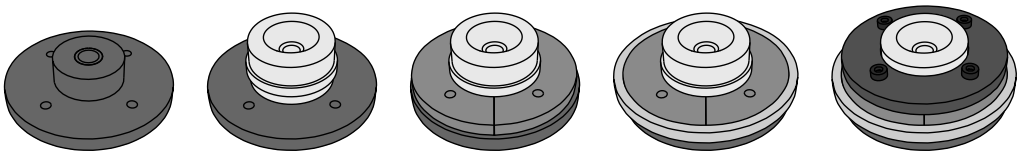

FIGURE 5.4: Stages of assembly of the clamping system: (a) base plate, (b) disc spring EIA, (c) jaw plates, (d) compression ring, (e) locking plate and bolts

After securing the disc spring EIA and deairing the entire set-up, the measurement of the pressure-volume characteristic of the disc spring EIA can begin. First, the T-port valves need to connect all components to the reservoir in order to equalize the pressure in the system. Next, it is necessary to configure them to connect the syringe pump with the actuator and isolate the other components. An Arduino Uno microcontroller board can then drive the stepper motor of the syringe pump resulting in a constant flow rate of about 0.085 ml/s. A larger rate increases the influence of dynamic effects on the measured characteristic while a lower rate leads to significant noisy vibrations in the motor. To measure as much of the characteristic as possible, each experiment consists out of both inflating and deflating the EIA. During that process, a Keller PR-21S pressure transducer located close to the actuator measures its internal pressure. At a 10 V DC supply voltage, the sensor produces an output between 0 V and 5 V for gauge pressures between 0 bar and 2.5 bar [44]. A National Instruments data acquisition device captures that output and sends it to a LabVIEW™ program for inspection and storage.

The result of each experiment is a list of pressure values in function of time. Because those values are significantly lower than the maximal sensor operating pressure, the signal to noise ratio is limited. It is possible to increase that ratio by measuring each actuator repeatedly and averaging the resulting pressure data. The results are optimal if each of the averaged values represents the same point on the pressure-volume characteristic. However, the microcontroller does not communicate with the data acquisition device so the precise volume at each point is unknown. A convolution procedure allows to align corresponding data points instead. The first step is to manually select a distinctive slice of the inflation and deflation pressure data from a single experiment with for example a local maximum. Then, convolution of that slice with the data from other experiments happens, with normalization of each data set to compensate for sensor drift. The offset for which the convolution becomes maximal then allows to align the pressure data for averaging.

Since the averaged signal contains less noise, determination of the four time points defining the start and end of the inflation and deflation phase can be more accurate. Additionally, in both phases the magnitude of the volume change is known and equal so they take the same amount of time. That means that it is only necessary to manually find the three time points corresponding to the most abrupt changes in the slope of the pressure signal. The fourth one then follows by equating the durations of both phases. Those time points isolate the data corresponding to changing volumes. As the total change in volume is known and the volume flow rate is constant, it is possible to linearly transform the time axes into volume axes. The result is an experimental pressure-volume characteristic for inflation and deflation under volume control.

5.2.2 Measured pressure-volume characteristic of a disc spring actuator

Figure 5.5 presents the experimental dynamic pressure-volume characteristics for disc spring EIAs with membrane thicknesses of 0.65 mm, 1.00 mm, 1.35 mm and

1.71 mm. In addition, it plots vertically scaled versions of corresponding simulated static characteristics. The uniform scale factor is 3.91 to compensate for the difference in 100 % modulus of the Dragonskin™ 10 in the simulation and the Dragonskin™ 30 in the prototypes [37]. Comparison of the two graphs for each actuator shows that they share several important features. Firstly, the experiments confirm that in practice the disc spring EIA can have the desired non-linear characteristic with a local maximum and minimum in pressure. Since the minimal pressure is negative for the actuator with a 0.65 mm thick membrane, it is bistable as well. Furthermore, the discontinuities in measurements with the two thinnest membranes prove that snapping under volume control is possible. For increasing thicknesses, first those discontinuities and then the extrema disappear while the general pressure level increases. All those observations are consistent with the most important qualitative findings of the previous chapters. That means that the disc spring EIA is indeed a practical non-linear actuator.

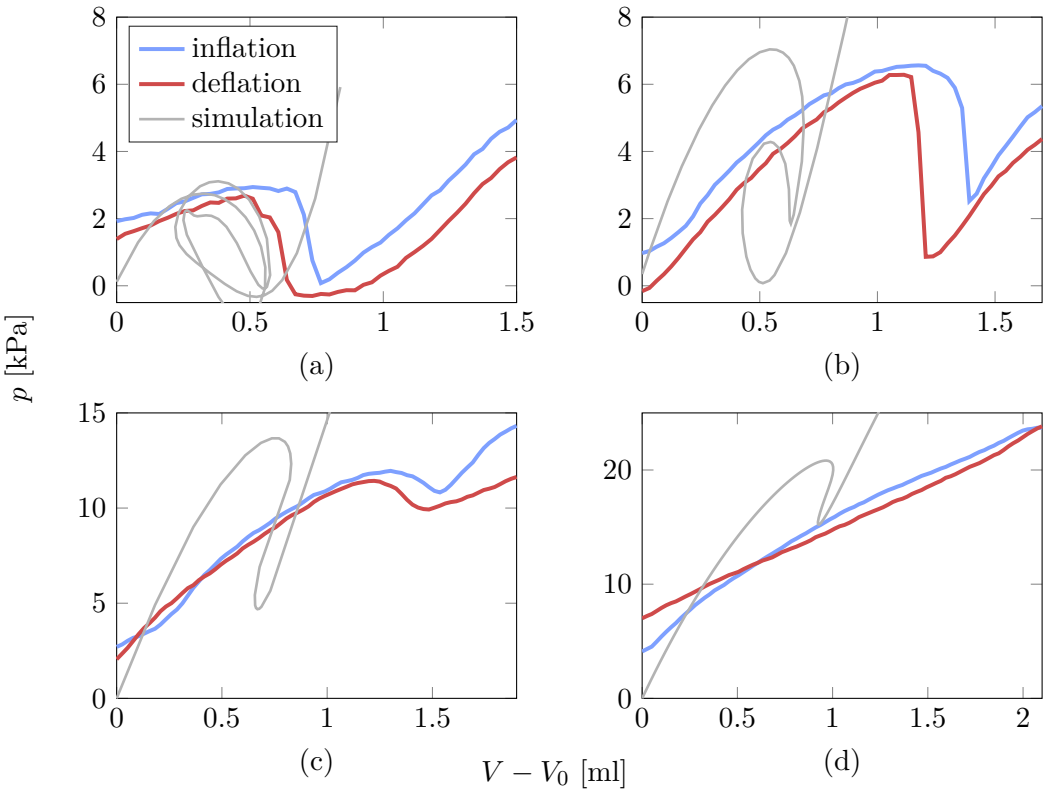

FIGURE 5.5: Measured pressure-volume characteristic on inflation and deflation compared to simulations for disc spring EIAs with membrane thicknesses of (a) 0.65 mm, (b) 1.00 mm, (c) 1.35 mm, (d) 1.71 mm

Despite important similarities, the qualitative agreement between the experiments and the corresponding simulations is not perfect. A first difference occurs for the disc spring EIAs with membrane thicknesses of 0.65 mm and 1.00 mm. The simulated

pressure-volume characteristics do not show sharp corners in the relevant range. In experiments with volume control, the slope of the pressure signal should therefore gradually become steeper on nearing the snapping points where it is vertical. However, in most of the actual measurements the discontinuities occur before those points and the slope changes suddenly. The reason is probably that due to the increasing compressive radial stresses the membrane reaches a bifurcation point where its shape can be axisymmetric or not. Since the non-axisymmetric mode of deformation is unstable, the disc spring membrane suddenly inverts. In the inverted state the tensile radial stresses in the membrane restore the axisymmetry so the measurements follow the simulations once more. It is possible to verify that explanation in a future study by using a three-dimensional FEM model.

Another qualitative difference between the simulations and measurements occurs for the disc spring EIAs with membrane thicknesses of 1.35 mm and 1.71 mm. While the simulations predict that those actuators snap under volume control, the measurements do not show the corresponding discontinuities. It is possible that snapping does occur in reality but that the pressure difference and kinetic energy released during the transition are small. The measured change in pressure is then limited in magnitude and spread out over time, so it does not appear as a clear discontinuity. The simulated characteristics partially support that explanation as they predict a weak volume snap-through transition. On the other hand, they indicate a stronger volume snap-back transition occurring at lower pressures especially for the 1.35 mm thick membrane. In practice, however, the membrane likely deforms non-axisymmetrically before building up sufficient strain energy for such a pronounced transition.

Apart from the general shape of the experimental characteristics, the simulations predict the numerical values of the pressures well. The main differences are probably due to the slight mismatch between the simulated and manufactured geometry as explained in section 5.1.1. Another factor can be the clamping system which restricts the support wall. Finally, dynamic effects like viscoelasticity of the silicone and viscosity of the water cause the pressure to be lower on deflation than on inflation. Incorporating those three effects into future simulations by altering the geometry, boundary conditions and material model respectively can lead to more accurate results.

While the pressures agree well between theory and practice, the volumes do not. The volumes at which pressure extrema occur in the measurements exceed the corresponding values in the simulations by a factor of almost two. The most likely cause is leakage of water from the experimental set-up. That means that a change in volume in the syringe pump is bigger than the corresponding change in actuator volume. Since the horizontal axis of the experimental characteristics represents the pump displacement, the actual actuator volume is lower than in the plots. The presence of a small puddle of water underneath the connection of the pressure sensor after the experiments confirms that leakage is a factor.

Studying the difference between consecutive measurements of the same actuator indicates a leak as well. Figure 5.6 shows those data for the inflation and deflation phase of a 1.35 mm thick membrane, with the local extrema horizontally aligned with the convolution procedure. The stroke of the syringe pump is the same in each

experiment but the pressure at the end of both phases decreases after each cycle. Still, the measured height of the extrema does not change between experiments, so the characteristic is unaltered by for example the Mullins effect. The only explanation for the decreasing final pressure is therefore that the final actuator volume decreases after each cycle due to a leak. Because the volume lost through a leak is proportional to the pressure in the system, a higher final pressure in one experiment leads to it dropping more in the next one. That is consistent with the measurements.

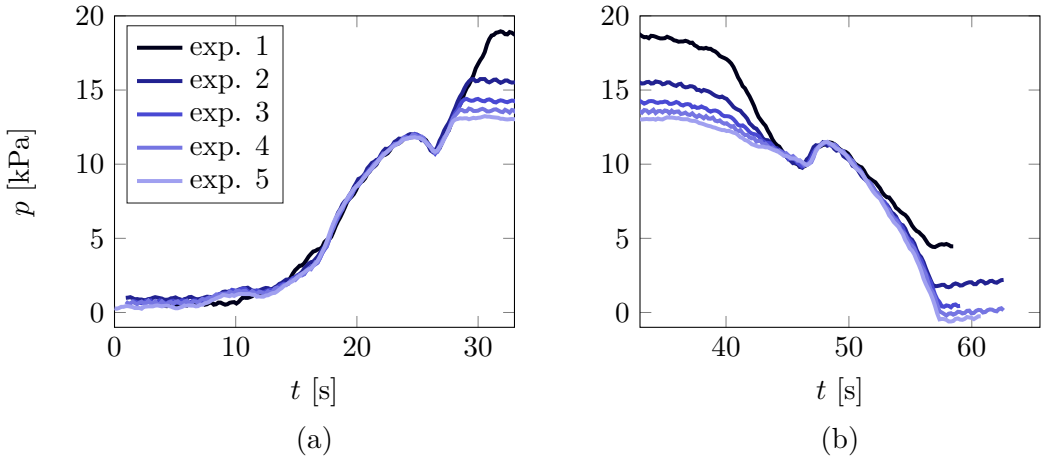

FIGURE 5.6: Pressure signals measured during the (a) inflation and (b) deflation phase in subsequent experiments with a disc spring EIA with a membrane thickness of 1.35 mm

Figure 5.6 also shows that in a region at the start of the inflation and deflation phases the slope of the signal gradually increases to match the simulation. Those transitions complicate finding the exact starting point of each phase which affects the precision of the volume axis of the experimental characteristics. Since the effect is present in the first experiment before the occurrence of high pressures as well, leakage does not explain it. Instead, it is possible that slack in the syringe pump causes a time-varying flux after reversing the direction of motion of the plunger. The effect can be substantial because the syringe has a significant radius of 14.5 mm so a limited displacement of about 3 mm suffices to inflate the actuator. Reversing the motion of the plunger before each phase and using a thinner syringe probably reduce the difference between the measurements and the simulations.

Summary

The simulations in chapters 3 and 4 suggest that the disc spring EIA has a non-linear and easily tuned characteristic which enables novel applications. In order to verify the conclusions from those chapters, it is necessary to manufacture prototypes of the actuator and measure their characteristics. The prototypes result from a rubber moulding process with degassing steps to avoid the presence of air bubbles which

weaken the membrane and affect its characteristic. The mould itself consists out of several 3D-printed parts including a small spacer to adjust the membrane thickness of the prototypes. The experimental pressure-volume characteristic of those actuators under volume control gives the maximal amount of information on their general behaviour. It follows from filling the EIA with a known amount of water using a syringe pump while a sensor records the pressure. The results agree well with the simulations. They confirm that disc spring EIAs with thin membranes can snap both under pressure and volume control. However, snapping occurs earlier than expected because the membrane suddenly deforms non-axisymmetrically. The slope of the characteristics and the volumes at which their extrema occur also do not match with the simulations. The reason is probably that water leaks from the set-up, leading to an overestimation of the actuator volume in the experiment. Redoing the experiment with fewer leaks and performing the simulations with a three dimensional model will likely increase the agreement between theory and practice. Still, the experiments already corroborate many of the previous conclusions on the behaviour of the disc spring actuator proving that it is a practical non-linear EIA.

Chapter 6

Conclusion

Elastic inflatable actuators are soft structures which are safe in contact with delicate objects, adapt their shape to the environment and can be small and disposable. If their pressure-volume characteristic moreover features a local maximum and minimum, they show rapid snapping and complex interaction with other EIAs. This study introduces an actuator with those properties. The disc spring EIA consists of a silicone rubber membrane in the shape of a truncated cone supported by a cylindrical wall. On inflating the cavity enclosed by those components, the apex of the actuator rises such that the membrane first flattens and then inverts. Its deformation resembles that of a classical disc spring, a well-studied structure with a non-monotonical force-displacement characteristic for particular dimensions. Analogously, the pressure-volume characteristic of the disc spring EIA can feature the desired local maximum and minimum in pressure. The minimal pressure can be negative which causes the actuator to be bistable under pressure control.

As the conical membrane flattens under inflation, the compressive radial stress increases which can lead to it buckling. In addition to extrema in pressure, the pressure-volume characteristic then shows extrema in volume. That means that the disc spring actuator is the first known EIA which can snap under volume control on reaching those points. Since no fluid flows through the supply line in such a transition, rapid actuation is possible in applications with long and thin supply lines. The buckling of the membrane can also lead to the occurrence of additional pressure maxima and minima in the pressure-volume characteristic. Apart from the first and last extrema along the curve, those points are not reachable in a quasi-static manner. If further research reveals a dynamic way to reach the additional extrema, however, on-line configuration of the snapping behaviour of the EIA becomes possible.

Only disc spring EIAs with steep and thin membranes show multiple extrema in pressure, extrema in volume and bistability. Decreasing the membrane cone angle linearises the characteristic by lowering the maxima and raising the minima until they coincide and disappear. Increasing the membrane thickness raises both the maxima and the minima, but the latter by a higher amount. Finally, changing the stiffness of the material uniformly scales the pressure values of the characteristic while changing the overall size scales the volume values. It is therefore possible

to design disc spring EIAs with arbitrary positions of the first and last extrema in pressure or volume. This study presents a procedure to find the membrane angle and thickness in function of the desired values of those extrema based on finite elements simulations. That allows to easily design systems of interacting disc spring EIAs with complex behaviour.

Because the disc spring EIA has a non-linear characteristic which is easy to tune, it satisfies the goal of the thesis to develop a practical non-linear EIA for use in complex applications. Apart from the unique features of the characteristic, it has several advantages over existing solutions. Firstly, the strain of the membrane is an order of magnitude lower than in most known non-linear EIAs. That means that the characteristic degrades less with time so it is suitable for applications that need to run continuously and reliably. Despite the low strains, the energy released on a snapping transition of a disc spring EIA can be significant. Consequently, the size of the actuator after snapping stays small compared to other non-linear EIAs made of the same material which release the same amount of energy. Another advantage is that the radial expansion of the actuator during inflation is limited. It can therefore perform fast motion and apply high impact forces in a compact system. Finally, the disc spring EIA is a monolithic structure with a simple shape which enables easy manufacturing through moulding even at the millimetre scale.

The full three-dimensional shape of the actuator potentially hinders further miniaturization with lithography and etching processes, however. Further research is in order to design a 2.5D equivalent structure or to exploit the anisotropy or isotropy of etching processes to manufacture conical or hemispherical membranes. Another potential disadvantage of the disc spring EIA is the fact that its stroke is proportional to its radius. Consequently, it is unsuitable for slender applications like fingers in a gripper. It is possible to transfer the motion of the disc spring actuator to a tall structure through a soft transmission mechanism like cables but that complicates the system. In flat applications such as valves, on the other hand, the low aspect ratio of the disc spring EIA allows compact integration.

Directions for further research

Experiments with the disc spring EIA show that it snaps before reaching an extremum in the characteristic, invalidating the results of the parameter study to some degree. The experimental data are compromised because of a leak in the set-up, so a new measurement campaign is necessary. The leak is unlikely to be the cause of the early snapping, however. Instead, the deformation of the membrane suggests that as the compressive stress increases, a bifurcation occurs which favours an asymmetric shape. Since the simulations use an axisymmetric model in order to limit the duration of the parameter study, they fail to capture that effect. Further simulations with a three-dimensional finite elements model can represent the observed motion to more accurately predict the behaviour of the actuator. They can also give insight into how to introduce an asymmetric element in the design to tune the points of volume snapping without affecting the points of pressure snapping.

Another way to tune the characteristic is to vary the shape of the membrane. This study only considers designs with a conical membrane but for example hemispherical or toroidal shapes are possible as well. They can lead to actuators with lower strains, higher snapping energies and characteristics with more or less involved shapes. Further research into the influence of different membrane shapes therefore allows to optimize actuator design. Moreover, it is possible to introduce an asymmetric section or a spiralling ridge in the membrane to produce bending or twisting motion on inflation. This study briefly touches on those concepts but further development can lead to a range of building blocks with the same advantages as the presented extending EIA. It can then also investigate complex but compact systems consisting of stacks of those building blocks or rings of concentric membranes with different deformations.

Finally, it is interesting to explore different applications made possible by the unique features of the disc spring EIA. For example, the bistability of the membrane can result in a soft valve that only requires energy on switching. Such a valve experiences significant hysteresis due to the difference between the snap-through and snap-back pressure. That allows the valve to continuously switch its own supply line to generate an oscillating pressure signal from a constant input pressure. A potential application for such a system is to drive an array of soft artificial cilia to advance fluids at small scales. By connecting a disc spring valve to each cilium or cluster of cilia, they can beat at different phases even though the entire system features a single external supply line. A recent paper by Rothemund et al. presents a similar valve developed independent of and simultaneous with this thesis. It confirms that the generation of oscillating pressure is possible with the described structure [45]. Their structure does not work with incompressible fluids, however, while the disc spring EIA does because of the extrema in volume in its characteristic.

The paper also discusses the use of the valve to actuate an actuator on sensing contact with an object. It does not consider a simpler structure without a valve that accomplishes the same task. Such a structure consists of a linear soft actuator connected to a disc spring EIA preloaded to a fraction below its snapping pressure. Contact with the environment causes an increase in the pressure such that the disc spring snaps and suddenly actuates the linear EIA by changing its volume. If the deformation of latter actuator breaks the contact, the contact force always stays limited. The described structure can hence implement a type of obstacle avoidance in a robust way, which is useful in for example endoscopic applications.

A final unique feature of the disc spring EIA is the high amount of released snapping energy relative to its size. It can therefore produce high peak actuation speeds and impact forces even at small scales and under volume control. Potential applications include jumping, puncturing of vessels or rapid flushing of clogged canals. In conclusion, despite its simple shape the disc spring EIA enables a variety of novel applications with added value for society.

Appendices

Appendix A

Analytical models for EIAs featuring material non-linearity

The pressure-volume characteristics of the EIAs with material non-linearities presented in section 2.1.1 result from analytical models. The procedure to obtain those models follows the one proposed by Müller and Strehlow [17]. The first step in that procedure is to assume that the membrane consists of rubber that adheres to the incompressible Mooney-Rivlin material model[1] [22, 23]:

$$\begin{aligned} \sigma_{11} &= \left(\lambda_1^2 - \frac{1}{\lambda_1^2\lambda_2^2}\right)\left(s_+ - s_-\lambda_2^2\right) \\ \sigma_{22} &= \left(\lambda_2^2 - \frac{1}{\lambda_1^2\lambda_2^2}\right)\left(s_+ - s_-\lambda_1^2\right). \end{aligned} \tag{A.1}$$

In that equation, σ_{11} and σ_{22} are the principal stresses in the plane of the membrane and λ_1 and λ_2 are the corresponding principal strains. s_+ and s_- are material parameters with a value of 300 kPa and -30 kPa [17] in each structure analysed in the following sections. The next step is to write the equilibrium between those stresses and the relative internal pressure in the EIA. An additional equation gives the volume of the structure in function of the principal strains. Eliminating the stresses and strains from all those equations results in an expression for the pressure in function of the volume.

A.1 Spherical EIA

The pressure-volume characteristic of a spherical balloon or EIA has been derived many times in literature. The method by Müller and Strehlow leads to the following expression [17]:

$$p = 2\frac{t_{m,0}}{R_0}\left(\frac{1}{\lambda_1} - \frac{1}{\lambda_1^7}\right)\left(s_+ - s_-\lambda_1^2\right), \tag{A.2}$$

[1] repeated from equation 2.1

with $t_{m,0}$ the initial membrane thickness t_m and R_0 the initial membrane radius R at zero relative internal pressure. The characteristic in figure 2.1 (a) results from that equation with $R_0 = 23$ mm, $t_{m,0} = 0.18$ mm and $\frac{V}{V_0} = \lambda_1^3$.

A.2 Cylindrical EIA

Müller and Strehlow obtain the following expression for the pressure-volume characteristic of a cylindrical balloon [17]:

$$p = 2\frac{t_{m,0}}{R_0}\left(\frac{\lambda_1}{\lambda_2^2} - \frac{1}{\lambda_1^3\lambda_2^4}\right)\left(s_+ - s_-\lambda_2^2\right), \tag{A.3}$$

with λ_1 the axial and λ_2 the radial strain of the balloon. They relate as

$$\lambda_1 = \sqrt{\frac{1}{2}\frac{S\lambda_2^2 - \frac{1}{\lambda_2^2}}{2S + \lambda_2^2} + \sqrt{\left(\frac{1}{2}\frac{S\lambda_2^2 - \frac{1}{\lambda_2^2}}{2S + \lambda_2^2}\right)^2 + \frac{S\frac{1}{\lambda_2^2} + 2}{2S + \lambda_2^2}}}, \tag{A.4}$$

in which $S = -\frac{s_+}{s_-}$ is a material constant. For the characteristic in figure 2.1 (b), $R_0 = 1$ mm and $t_{m,0} = 8$ μm. It results from calculating first λ_2 and then p for several values of λ_1. The relative volume for each value is $\frac{V}{V_0} = \lambda_1\lambda_2^2$.

A.3 Cylindrical EIA wrapped with inextensible fibres

Many EIAs studied in literature resemble cylindrical balloons with inextensible fibres wound along their circumference. However, no models for such structures which take the non-linearity of the material into account are available in literature. The method by Müller and Strehlow allows to create such a model instead.

Since the circumferential fibres prevent the EIA from stretching radially, the tangential strain $\lambda_2 = 1$ for any pressure. That means that the axial stress

$$\sigma_{11} = \left(\lambda_1^2 - \frac{1}{\lambda_1^2}\right)(s_+ - s_-). \tag{A.5}$$

That stress also features in the axial equilibrium of a circular section of the balloon

$$p\pi R^2 = 2\pi R t_m \sigma_{11} \Leftrightarrow p = 2\frac{t_m}{R}\sigma_{11} \tag{A.6}$$

The radius of the section $R = R_0$ because $\lambda_2 = 1$. The membrane thickness t_m follows from the assumption that the membrane material is incompressible so

$$2\pi RLt_m = 2\pi R_0 L_0 t_{m,0} \Leftrightarrow t_m = \frac{R_0}{R}\frac{L_0}{L}t_{m,0} = \frac{t_{m,0}}{\lambda_2\lambda_1} = \frac{t_{m,0}}{\lambda_1}, \tag{A.7}$$

with L the length of the actuator λ_1 the axial strain. Substituting equations A.5 and A.7 into A.6 yields the same equation as A.3 but with $\lambda_2 = 1$

$$p = 2\frac{t_{m,0}}{R_0}\left(\lambda_1 - \frac{1}{\lambda_1^3}\right)(s_+ - s_-). \tag{A.8}$$

If $R_0 = 1$ mm and $t_{m,0} = 8$ μm, evaluating that equation leads to the pressure-volume characteristic in figure 2.1 (c) where $\frac{V}{V_0} = \lambda_1$.

A.4 Cylindrical EIA with disconnected hoops

A way to create a slender EIA with a pressure-volume characteristic which shows both a maximum and minimum is to place inextensible hoops around a cylindrical membrane. The radius of the hoops R_h is larger than the initial radius of the membrane R_0. That means that as long as the radius of the membrane $R < R_h$, the EIA behaves as a cylindrical balloon including the pressure peak. When the membrane contacts the hoops, $R = R_h$ and the EIA behaves as a cylindrical EIA wrapped with inextensible fibres with a monotonically increasing characteristic. Since $\lambda_2 = R_h/R_0$ instead of one, that characteristic is not the same as A.8 but follows from a similar derivation. The total characteristic therefore is

$$\begin{cases} p = 2\frac{t_{m,0}}{R_0}\left(\frac{\lambda_1}{\lambda_2^2} - \frac{1}{\lambda_1^3\lambda_2^4}\right)\left(s_+ - s_-\lambda_2^2\right) & \lambda_2 < \frac{R_h}{R_0} \\ p = 2\frac{t_{m,0}}{R_h}\left(\lambda_1 - \frac{R_0^2}{\lambda_1^3 R_h^2}\right)\left(s_+ - s_-\frac{R_h^2}{R_0^2}\right) & \lambda_2 = \frac{R_h}{R_0} \end{cases} \tag{A.9}$$

with the relation between λ_1 and λ_2 when $\lambda_2 < R_h/R_0$ given by equation A.4.

For small-scale applications, it is difficult to assemble the EIA with the inextensible hoops. If the hoops consist out of the same rubber material as the membrane, however, it is possible to mould the entire EIA as a single piece. That change in material only affects the characteristic after the membrane and the hoops make contact.

Under the assumption that the gap between consecutive hoops is small, the membrane does not bulge in that gap. Therefore, the tangential strain of the membrane $\lambda_{2,m}$ is uniform throughout the actuator. Another assumption is that no relative motion occurs at the interface between the membrane and the hoops, so the hoops share the axial load with the membrane. Since the thickness of the hoops is an order of magnitude larger than the membrane thickness, the only factor influencing the axial hoop strain $\lambda_{1,h}$ is the Poisson contraction. The resulting change in length of the hoops is equal to the change in length of the part of the membrane in contact with the hoop. That results in a different axial strain $\lambda_{1,c}$in those parts of the membrane than in the unconstrained sections so they have different thicknesses. Figure A.1 shows the model resulting from those assumptions.

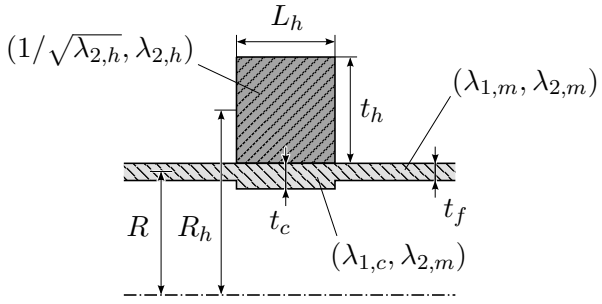

FIGURE A.1: Diagram of the model for the cylindrical EIA with disconnected hoops with the dimensions and axial and tangential strains of each section

The axial and tangential stress in the unconstrained sections of the membrane and the tangential stress in the constrained sections and the hoops then become respectively

$$\sigma_{11,m} = \left(\lambda_{1,m}^2 - \frac{1}{\lambda_{1,m}^2\lambda_{2,m}^2}\right)(s_+ - s_-\lambda_{2,m}^2) \tag{A.10}$$

$$\sigma_{22,m} = \left(\lambda_{2,m}^2 - \frac{1}{\lambda_{1,m}^2\lambda_{2,m}^2}\right)(s_+ - s_-\lambda_{1,m}^2) \tag{A.11}$$

$$\sigma_{22,c} = \left(\lambda_{2,m}^2 - \frac{1}{\lambda_{1,c}^2\lambda_{2,m}^2}\right)(s_+ - s_-\lambda_{1,c}^2) \tag{A.12}$$

$$\sigma_{22,h} = \left(\lambda_{2,h}^2 - \frac{1}{\lambda_{2,h}^2}\right)(s_+ - s_-). \tag{A.13}$$

In those equations, $\lambda_{2,m}$ is the independent variable on which the other strains depend. The axial strain of the sections of the membrane in contact with the hoops $\lambda_{1,c} = \lambda_{1,h}\bar{\lambda}_{1,c}$, with $\bar{\lambda}_{1,c}$ the axial strain in the membrane at the moment of contact with the hoops. $\bar{\lambda}_{1,c}$ is a constant which follows from from evaluating equation A.4 at $\lambda_2 = \frac{R_h - t_{h,0}/2}{R_0}$. The tangential strain of the hoops $\lambda_{2,h}$, on the other hand, follows from numerically solving

$$\lambda_{2,h} = \frac{R_h}{R_{h,0}} = \frac{R + \frac{t_h}{2}}{R_{h,0}} = \frac{\lambda_{2,m}R_0 + \frac{t_{h,0}}{2\sqrt{\lambda_{2,h}}}}{R_{h,0}}. \tag{A.14}$$

Finally, it is possible to find $\lambda_{1,m}$ in function of $\lambda_{2,m}$ by writing the axial and radial force equilibrium of the actuator and eliminating the pressure p from them:

$$\begin{cases} \pi R^2 p = 2\pi R t_m \sigma_{11,m} \\ 2RLp = 2(L_m t_m \sigma_{22,m} + NL_h t_c \sigma_{22,c} + NL_h t_h \sigma_{22,h}) \end{cases} \tag{A.15}$$

$$\Leftrightarrow 2t_m L\sigma_{11,m} - L_m t_m \sigma_{22,m} - NL_h t_c \sigma_{22,c} - NL_h t_h \sigma_{22,h} = 0, \tag{A.16}$$

with $t_m = \frac{t_{m,0}}{\lambda_{1,m}\lambda_{2,m}}$, $t_c = \frac{t_{m,0}}{\lambda_{1,c}\lambda_{2,m}}$ and $t_h = \frac{t_{h,0}}{\sqrt{\lambda_{2,h}}}$ because of the assumed incompressibility of the used material. N is the number of hoops with width $L_h = \frac{L_{h,0}}{\sqrt{\lambda_{2,h}}}$ and L_m is the length of the unconstrained membrane, equal to

$$L_m = (\lambda_{1,c}L_0 - NL_h)\frac{\lambda_{1,m}}{\lambda_{1,c}}. \tag{A.17}$$

The total length of the inflated EIA then is $L = L_m + NL_h$.

With those equations, it is possible to calculate the pressure-volume characteristic of the cylindrical EIA with disconnected hoops numerically. The first step is to evaluate equations A.4 and A.3 for $1 < \lambda_2 < \frac{R_{h,0} - t_{h,0}/2}{R_0}$. The next step is to numerically solve equation A.16 in function of $\lambda_{1,m}$ for each sample of $\lambda_{2,m} \geq \frac{R_{h,0} - t_{h,0}/2}{R_0}$. With the values of $\lambda_{1,m}$ and $\lambda_{2,m}$ known, the relative volume of the

actuator $\frac{V}{V_0} = \lambda_{1,m}\lambda_{2,m}^2$ and the pressure follows from evaluating either equation in A.15. If $L_0 = 30$ mm, $R_0 = 4$ mm, $t_{m,0} = 0.5$ mm, $NL_{h,0} = 4.5$ mm, $R_{h,0} = 20$ mm and $t_{h,0} = 20$ mm, that procedure leads to the characteristic plotted in figure 2.2.

Figure A.2 shows that characteristic for several values of the initial radius of the hoop $R_{h,0}$. It indicates that $R_{h,0}$ should be large enough to preserve the local maximum in pressure before the membrane contacts the hoops and small enough to limit the strain in the membrane after snapping. Finally, the figure reveals that $R_{h,0}$ is a parameter which enables a straightforward tuning procedure because it affects the local minimum but not the local maximum in pressure.

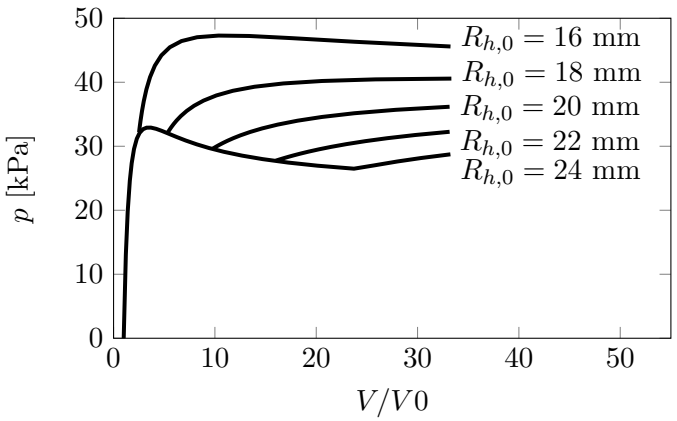

FIGURE A.2: Evolution of the pressure-volume characteristic of a cylindrical EIA with disconnected hoops with initial radii of the hoops

A.5 Tubular EIA with a circular segment as cross-section

Another design for a slender EIA is a tubular one with a circular segment for the cross-section perpendicular to the main axis. The flat wall corresponding to the chord that defines the segment has to be stiff against bending. Otherwise, the application of pressure causes it to bend so the cross-section becomes circular. The EIA would then behave similar to a cylindrical one without a local minimum in the pressure-volume characteristic. At the same time, the flat wall has to be compliant in the axial direction. Otherwise, the axial strain is one which leads to a similar derivation of the characteristic as in the case of a cylindrical EIA wrapped with inextensible fibres in section A.3. The result then is a monotonically increasing characteristic.

A wall consisting out of alternately stiff and compliant tangential strips satisfies the requirements on the stiffness. Such a wall is stiff against bending in the plane perpendicular to the main tube axis because the strips are loaded in parallel such that their stiffnesses add up. For stretching in the axial direction on the other hand, the strips are loaded in series so their compliances add up. The difference in stiffness

between the two types of strips can result from either a difference in material or a difference in thickness. This section models the latter implementation with tall and short strips because it is easier to manufacture at small scales.

The model assumes that the thickness of the tall tangential strips is high enough to prevent any bending of the flat wall. That also means that their axial stiffness is an order of magnitude higher than those of the short strips, so the only factor that affects their axial strain is the Poisson contraction. If the gap between consecutive tall strips moreover is limited, the short strips deform as flat rectangles. As a result, the tangential strain $\lambda_{2,s}$ is uniform throughout the flat wall. Finally, in general the axial force on the cap of the actuator resulting from the pressure does not coincide with the neutral axis. That leads to the actuator bending, so the axial strain varies throughout the membrane. However, the assumption is that bending is minimal because the asymmetry is limited so the axial strain of the membrane $\lambda_{1,m}$ is uniform. Figure A.3 shows the model that adheres to those assumptions.

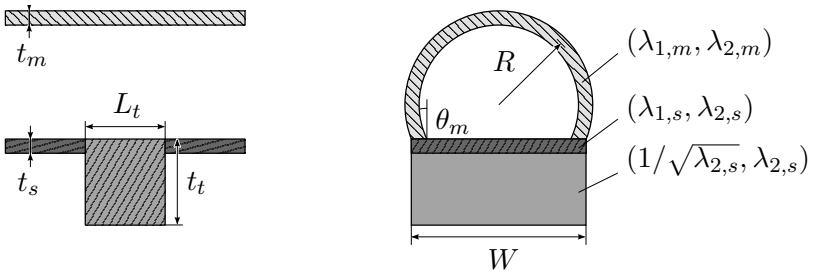

Figure A.3: Diagram of the (a) axial and (b) radial cross-section of the model for the tubular EIA with a circular segment as cross-section with the dimensions and axial and tangential strains of each section

The simplified expressions for the axial and tangential stress in the membrane and the short strips and the tangential stress in the tall strips then are:

$$\sigma_{11,m} = \left(\lambda_{1,m}^2 - \frac{1}{\lambda_{1,m}^2 \lambda_{2,m}^2}\right)(s_+ - s_- \lambda_{2,m}^2) \tag{A.18}$$

$$\sigma_{22,m} = \left(\lambda_{2,m}^2 - \frac{1}{\lambda_{1,m}^2 \lambda_{2,m}^2}\right)(s_+ - s_- \lambda_{1,m}^2) \tag{A.19}$$

$$\sigma_{11,s} = \left(\lambda_{1,s}^2 - \frac{1}{\lambda_{1,s}^2 \lambda_{2,s}^2}\right)(s_+ - s_- \lambda_{2,s}^2) \tag{A.20}$$

$$\sigma_{22,s} = \left(\lambda_{2,s}^2 - \frac{1}{\lambda_{1,s}^2 \lambda_{2,s}^2}\right)(s_+ - s_- \lambda_{1,s}^2) \tag{A.21}$$

$$\sigma_{22,t} = \left(\lambda_{2,s}^2 - \frac{1}{\lambda_{2,s}}\right)\left(s_+ - s_- \frac{1}{\lambda_{2,s}}\right). \tag{A.22}$$

A first relation between the four unknown strains in those expressions follows from the axial equilibrium of the actuator and the tangential equilibrium of the membrane

cut at the connection with the flat wall:

$$\begin{cases} Ap = Ct_m\sigma_{11,m} + Wt_s\sigma_{11,s} \\ WLp = 2t_m\sigma_{22,m}\cos(\theta_m) \end{cases} \tag{A.23}$$

$$\Leftrightarrow WL(C\sigma_{11,m} + Wt_s\sigma_{11,s}) - 2At_m\sigma_{22,m}\cos(\theta_m) = 0, \tag{A.24}$$

with $t_m = \frac{t_{m,0}}{\lambda_{1,m}\lambda_{2,m}}$ and $t_s = \frac{t_{s,0}}{\lambda_{1,s}\lambda_{2,s}}$. $W = \lambda_{2,s}W_0$ is the width of the flat wall and $L = \lambda_{1,m}L_0$ is the total length of the actuator. The area of the major circular segment A is

$$\begin{aligned} A &= \pi R^2\frac{\pi + 2\theta_m}{2\pi} + \frac{WR\sin(\theta_m)}{2} = \left(\frac{W}{2\cos(\theta_m)}\right)^2\frac{\pi + 2\theta_m}{2} + \frac{W^2\sin(\theta_m)}{4\cos(\theta_m)} \\ &= \frac{\lambda_{2,s}^2W_0^2}{4}\left(\frac{\pi + 2\theta_m}{2\cos^2(\theta_m)} + \tan(\theta_m)\right), \end{aligned} \tag{A.25}$$

with θ_m the angle between the base of the membrane and the flat wall, which is positive if the cross-section is a major circular segment and negative if it is a minor circular segment. Finally, $C = \lambda_{2,m}C_0$ is the arc length of the membrane. It is also possible to write the arc length in function of the membrane angle:

$$C = R(\pi + 2\theta_m) = \frac{W}{2\cos(\theta_m)}(\pi + 2\theta_m) = \frac{\lambda_{2,s}W_0}{2\cos(\theta_m)}(\pi + 2\theta_m), \tag{A.26}$$

resulting in the following relation between $\lambda_{2,m}$, $\lambda_{2,s}$ and θ_m:

$$\lambda_{2,m} = \frac{C}{C_0} = \frac{\frac{\lambda_{2,s}W_0}{2\cos(\theta_m)}(\pi + 2\theta_m)}{\frac{W_0}{2\cos(\theta_{m,0})}(\pi + 2\theta_{m,0})} = \lambda_{2,s}\frac{\cos(\theta_{m,0})(\pi + 2\theta_m)}{\cos(\theta_m)(\pi + 2\theta_{m,0})} \tag{A.27}$$

Writing the tangential equilibrium of a section of the flat wall allows to obtain another relation between the unknown strains:

$$Lt_m\sigma_{22,m}\sin(\theta_m) = NL_tt_t\sigma_{22,t} + L_st_s\sigma_{22,s}, \tag{A.28}$$

with N the number of tall strips, $L_t = \frac{L_{t,0}}{\sqrt{\lambda_{2,s}}}$ the length of a single tall strip and $L_s = L - NL_t$ the length of all short strips combined. The final relation between the strains follows from writing that condition on the length of the strips in function of the axial strains:

$$\lambda_{1,s}L_{s,0} = \lambda_{1,m}L_0 - N\frac{L_{t,0}}{\sqrt{\lambda_{2,s}}} \Leftrightarrow \lambda_{1,s} = \frac{\lambda_{1,m}L_0 - N\frac{L_{t,0}}{\sqrt{\lambda_{2,s}}}}{L_0 - NL_{t,0}} \tag{A.29}$$

In conclusion, three relations A.24, A.28 and A.29 describe the relations between the four unknown strains $\lambda_{1,m}$, $\lambda_{2,m}$, $\lambda_{1,s}$ and $\lambda_{2,s}$. All other variables follow from those strains. It is therefore possible to calculate the analytical pressure-volume characteristic for the tubular EIA with a circular segment as cross-section. A procedure to calculate it numerically starts with imposing a value for the axial strain

of the membrane $\lambda_{1,m}$. The next step is to write equations A.24, A.28 and A.29 in function of $\lambda_{1,s}$, $\lambda_{2,s}$ and θ_m only. Choosing θ_m over $\lambda_{2,m}$ as fundamental unknown variable simplifies the solution procedure as it eliminated the need to numerically solve equation A.27 for θ_m. Solving the system of the three equations numerically then results in a value for each variable. Substituting those values in either equation of A.23 yields the pressure in the actuator, while the volume $\frac{V}{V_0} = \lambda_{1,m}\frac{A}{A_0}$ with A as in equation A.25. If $L_0 = 30$ mm, $t_{m,0} = 0.5$ mm, $W = 8$ mm, $t_{s,0} = 0.3$ mm, $t_{t,0} = 30$ mm, $NL_{t,0} = 15$ mm and $\theta_{m,0} = -72°$, the resulting pressure-volume characteristic is equal to the one shown in figure 2.3.

Figure A.4 shows the dependence of that characteristic on the initial membrane angle. For $\theta_{m,0} < 0$, the slope of the characteristic does not become significantly positive past the local pressure maximum. The reason probably is that the arc length C of the membrane becomes significantly larger than the width W of the actuator in the neighbourhood of that maximum. The cross-section of the actuator then is approximately circular, so the characteristic resembles that of a cylindrical EIA.

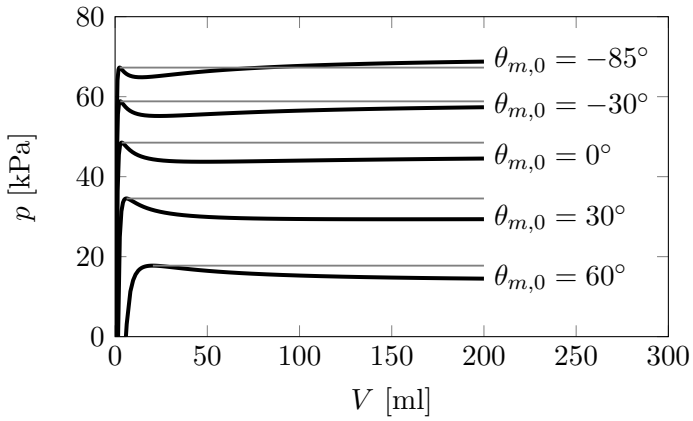

Figure A.4: Evolution of the pressure-volume characteristic of a tubular EIA with a circular segment as cross-section with varying initial membrane angles

For highly negative initial membrane angles, the initial shape of the cross-section is a minor circular segment. Due to inflation it becomes a major circular segment past a certain volume which causes the positive slope of the characteristic for higher volumes. At extremely high volumes, the cross-section again becomes nearly circular so the pressure reaches a plateau. That plateau can either lie below or above the pressure of the first local pressure maximum depending on the geometry. In the latter case, the EIA shows a snapping transition between two finite volumes on pressure control. Still, the tangential membrane strain after pressure snap-through in most cases is beyond the ultimate strain of the material so snapping leads to failure. For example, the presented actuator with $\theta_{m,0} = -85°$ experiences a tangential strain of over 12 past snap-through, while few rubbers reach an ultimate strain of more than 10 [37]. The proposed design therefore is unlikely to constitute a practical non-linear EIA.

Appendix B

Analytical model for a buckling disc spring

Section 2.2.3 presents a lumped analytical model for the disc spring EIA. Its purpose is not to predict the numerical values of the static pressure-volume characteristic accurately but to understand what effects cause its general shape. The model shows that the combination of stretching and bending of the circumferential fibres of the membrane explains the presence of a single maximum and minimum in pressure. It does not capture or rationalize the full characteristic, however, which can have extrema in volume and more than two extrema in pressure. A discussion in section 3.2.1 proposes that those additional extrema originate in the buckling of the membrane, which causes it to behave as two concentric connected disc springs. The analytical model presented in this appendix builds on that suggestion to model the shape of the pressure-volume characteristic more accurately.

Figure B.1 (a) shows a lumped parameter model which consists out of two connected models for a rigid disc spring. One link represents the top cap while two links represent the inner and outer portion of the membrane. Two linear springs with stiffnesses $k_{s,i}$ and $k_{s,o}$ represent the stretching effect, while the torsional stiffnesses $k_{b,i}$ and $k_{b,o}$ represent the bending effect in the inner and outer portion respectively. The stretching effect in the latter is generally less pronounced than in the former. The reason is that the same radial displacement yields a lower strain because the initial radius is higher. Consequently, $k_{s,i} > k_{s,o}$ if both portions have a similar geometry and the radial stiffness of the outer hinge in limited. A middle hinge connects the two links of the model. It features a torsional spring as well to represent the stiffness of the membrane against bending in the plane containing the radial and axial directions. Since it also partially represents bending of the circumferential material fibres in both the outer and inner disc spring, it is not obvious how the stiffnesses of the different torsional springs relate to each other. Finally, point forces represent the result of the pressure load on each link.

Figure B.1 (b) shows the free body diagram of the two links representing the portions of the membrane. It does not include the reaction forces in the inner and outer hinge in order not to overload the figure. The free body diagram allows to

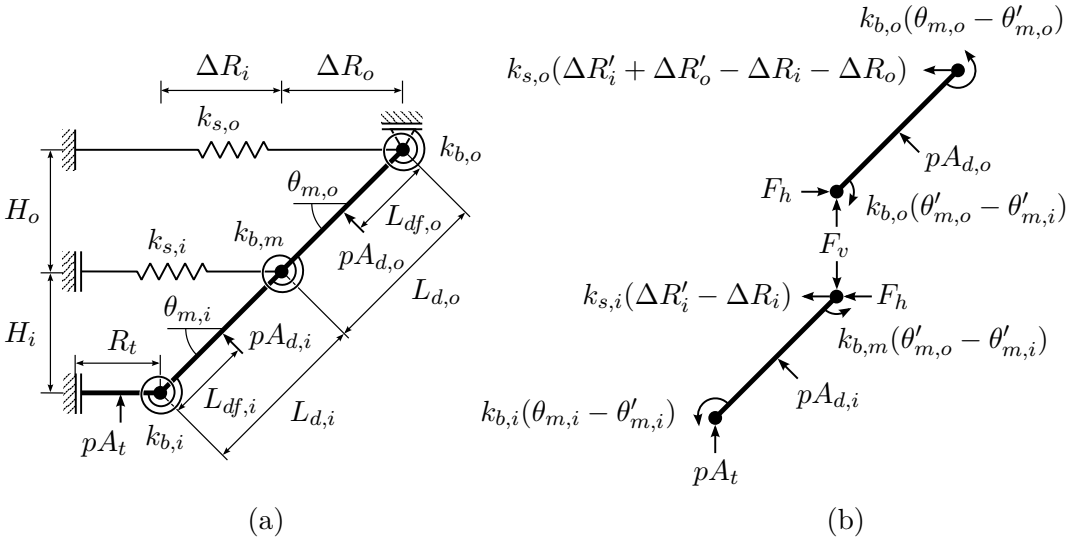

Figure B.1: (a) Lumped parameter model for a buckling disc spring EIA with (b) the free body diagram for the links representing the membrane

write the horizontal equilibrium of the inner link and its moment equilibrium around the inner hinge as well as the vertical equilibrium of the outer link and its moment equilibrium around the outer hinge:

$$\begin{cases} pA_t + pA_{d,i}\cos(\theta'_{m,i}) - F_v = 0 \\ k_{b,i}(\theta_{m,i} - \theta'_{m,i}) + pA_{d,i}L_{df,i} + k_{s,i}(\Delta R'_i - \Delta R_i)H'_i - F_v\Delta R'_i + \dots \\ \qquad \dots + F_h H'_i + k_{b,m}(\theta'_{m,o} - \theta'_{m,i}) = 0 \\ F_h - pA_{d,o}\sin(\theta'_{m,o}) - k_{s,o}(\Delta R'_i + \Delta R'_o - \Delta R_i - \Delta R_o) = 0 \\ F_h H'_o - F_v\Delta R'_o - k_{b,i}(\theta'_{m,o} - \theta'_{m,i}) - pA_{d,o}L_{df,o} + k_{b,o}(\theta_{m,o} - \theta'_{m,o}) = 0, \end{cases} \tag{B.1}$$

with $\Delta R'_i = \sqrt{L_{d,i}^2 - H_i'^2}$, $\theta'_{m,i} = \operatorname{atan}(H'_i/\Delta R'_i)$, $\Delta R'_o = \sqrt{L_{d,o}^2 - H_o'^2}$ and $\theta'_{m,o} = \operatorname{atan}(H'_o/\Delta R'_o)$. The four unknowns in that system of four equations are the membrane angles $\theta'_{m,i}$ and $\theta'_{m,o}$ and the forces in the middle hinge F_h and F_v. It is possible to solve the system numerically for different imposed values for the pressure p. The displacement of the top cap is then $y = H_i + H_o - L_{d,i}\sin(\theta'_{m,i}) - L_{d,o}\sin(\theta'_{m,o})$. Additional geometric relations allow to find the volume under the different links. However, such a calculation is inaccurate because the model does not consider the deformation of the support wall or the bending of the top cap. The volume moreover is roughly proportional to y, so a pressure-displacement plot contains all of the relevant information.

If $L_{d,i} = L_{d,o} = 10$ mm, $L_{df,i} = L_{df,o} = L_{d,i}/2$, $\theta_{m,i} = \theta_{m,o} = 45°$, $k_{s,i} = 20$ N/mm, $k_{s,o} = 12$ N/mm, $k_{b,i} = 1.3$ N/mm, $k_{b,m} = 1.95$ N/mm, $k_{b,o} = 3.25$ N/mm, $A_t = 20$ mm^2, $A_{d,i} = 100$ mm^2 and $A_{d,o} = 300$ mm^2, the model results in the characteristic in figure B.2. That characteristic has multiple extrema in pressure as well

as extrema in volume and a general shape similar to the simulated static pressure-volume characteristic shown in figure 2.8. The deformation of the model also agrees well with the deformation of the disc spring EIA in the FEM simulation. The lumped model therefore confirms that the membranes behaves as two connected disc springs under high compressive strains.

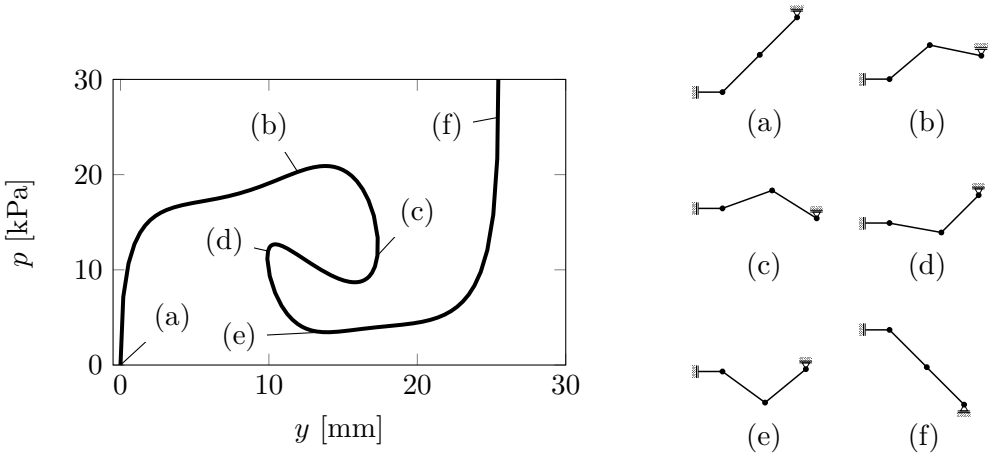

FIGURE B.2: Static pressure-displacement characteristic and corresponding deformation of an analytical model of a buckling disc spring

The correspondence between the results of the lumped model and the FEM simulation is not perfect, however. Firstly, the analytical characteristic shows additional inflection points between points (a) and (b) on one hand and (e) and (f) on the other hand. They both correspond to inversion of the outer disc spring. The reason that those inflection points do not appear in the FEM simulations is that at those points the membrane performs a kind of rolling motion. Instead of the entire outer portion of the disc spring inverting at once, the inversion starts at one end and evolves towards the other end. Since the inversion is stretched out, it does not cause a distinct inflection point and decreases the initial slope of the characteristic. A possible way to include that effect in the lumped model is to change the relative length of the links in function of the membrane angles, but the exact relation is unclear.

The second limitation of the analytical model is that it predicts a characteristic that rises asymptotically for high pressures. The most likely explanation is that the links are rigid while in reality both the conical membrane and the support wall can stretch. Their elasticity causes a change in the volume roughly proportional to the internal pressure in the actuator which affects the slope throughout the characteristic. Replacing the rigid links by linear springs and attaching a vertical linear spring to the outer hinge allows to incorporate those effects to make the lumped model more accurate. Still, the simplified model shown in figure B.1 suffices to explain where the unique features of the pressure-volume characteristic of the disc spring EIA originate.

Appendix C

Technical drawings of the disc spring EIA mould and clamp

C.1 Technical drawings of the disc spring EIA mould parts

Section 5.1.1 introduces the mould used to manufacture the disc spring EIA prototypes measured in this study. The following pages contain the technical drawings for the parts constituting that mould:

- page 68: male mould part
- page 69: mould spacer
- page 70: female mould part
- page 71: mould clamping ring

The bolts used to press those parts together are standard M3 $\times$ 35 bolts fitted with corresponding washers and nuts.

The presented mould spacer leads to a disc spring EIA with a membrane thickness of 0.65 mm. Mould spacers with the same profile and thicknesses of 3.5 mm, 4.0 mm and 4.5 mm allow to manufacture the other prototypes used in the experimental study with a membrane thickness of 1.0 mm, 1.35 mm and 1.71 mm respectively. The manufactured actuator with a membrane thickness of 1.0 mm has the same geometry as the simulated model apart from the actuator ridge. In the other actuators, the membrane thickness and the thickness of the top cap are different from each other while in the simulated model they are equal.

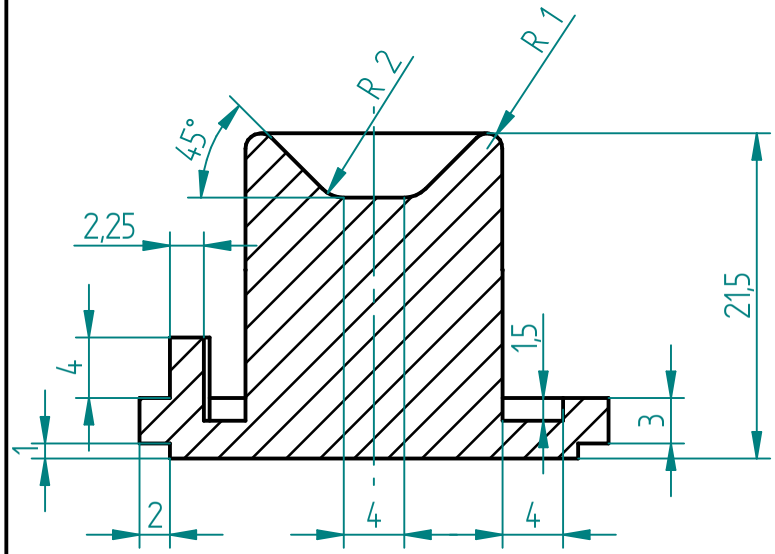

SECTION A–A

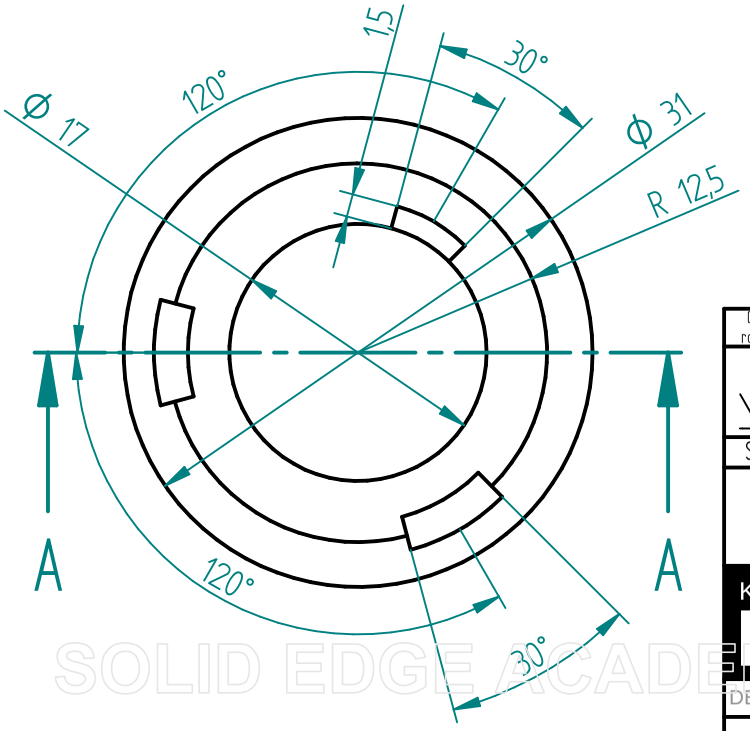

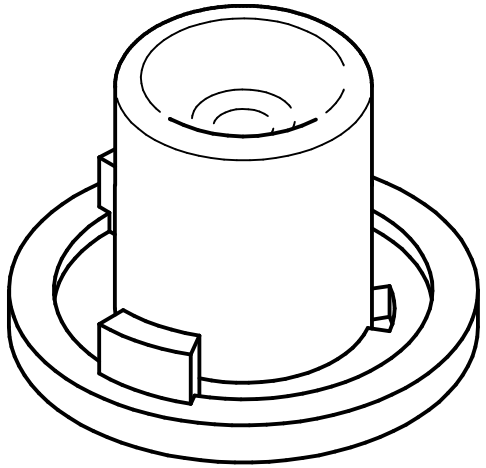

General roughness	General tolerance	Material:	Drawing No.
	+0.1 mm −0.1 mm +0.1° −0.1°	Vero PureWhite	1
Scale	Projection	Machine:	File No. / Amount
2:1		Objet30 Prime	1 / 1

KATHOLIEKE UNIVERSITEIT LEUVEN
DEPARTEMENT WERKTUIGKUNDE

Disc spring EIA male mould part

Author: B. Van Raemdonck | Date: 28/05/2017 | A4

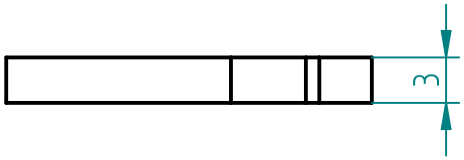

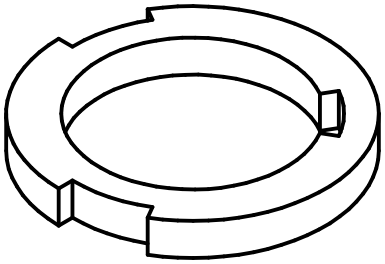

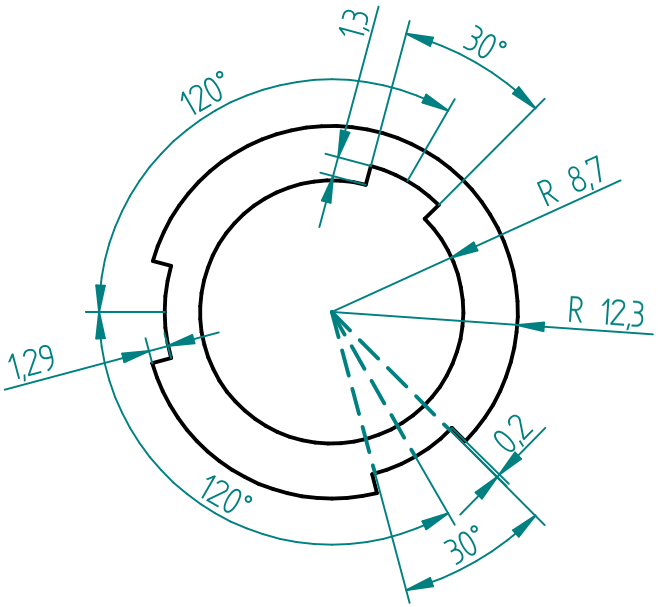

General roughness	General tolerance	Material:	Drawing No.	
	+0.1 mm −0.1 mm +0.5° −0.5°	Vero PureWhite	2	
Scale	Projection	Machine:	File No.	Amount
2:1		Objet30 Prime	1	1

KATHOLIEKE UNIVERSITEIT LEUVEN
DEPARTEMENT WERKTUIGKUNDE

Disc spring EIA mould spacer 3 mm

Author: B. Van Raemdonck | Date: 28/05/2017 | A4

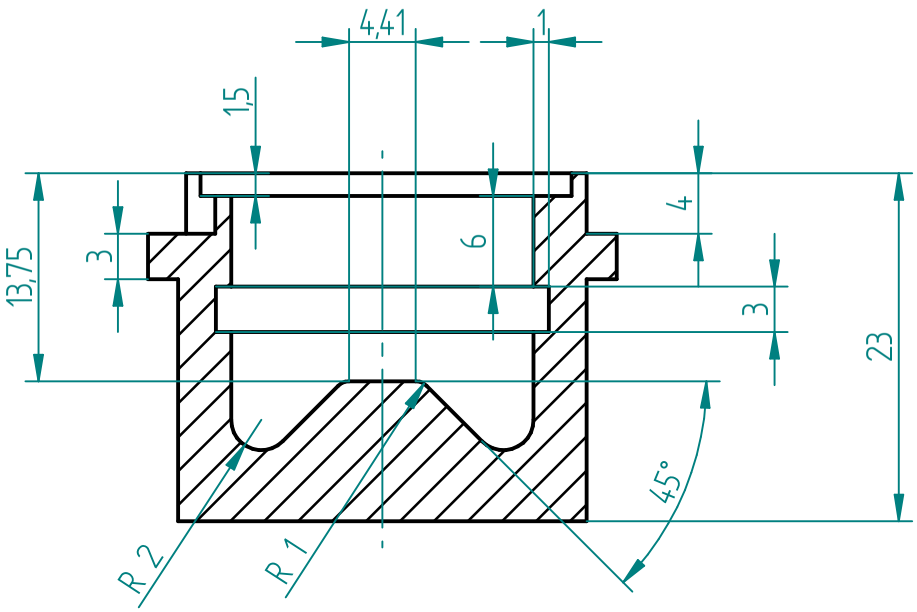

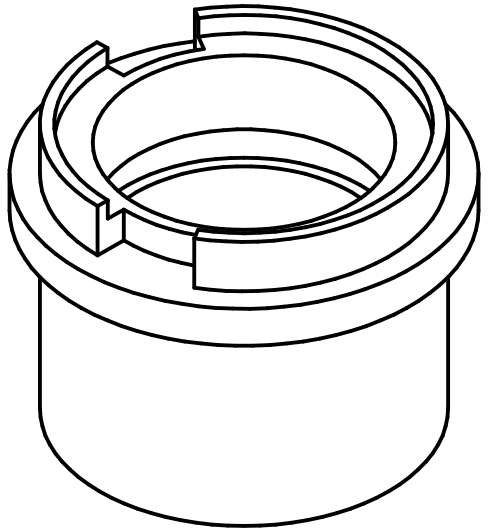

SECTION A–A

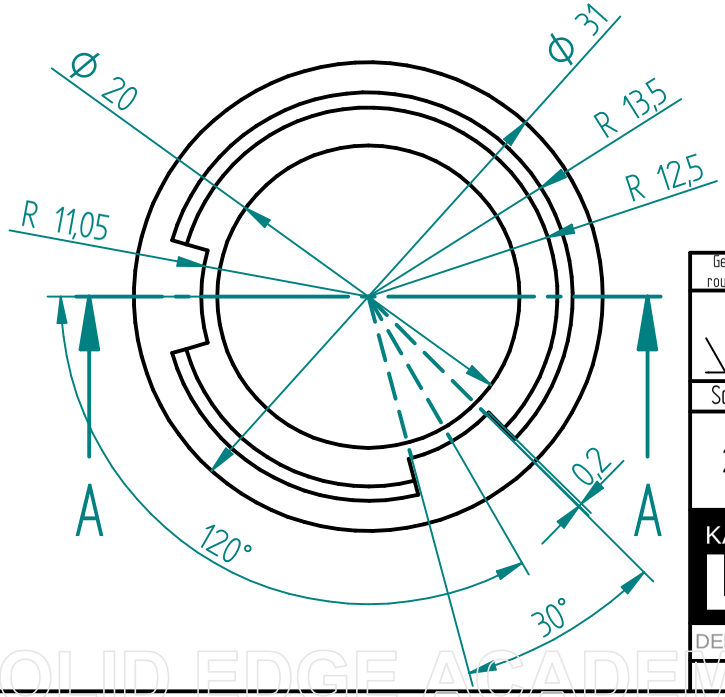

General roughness	General tolerance	Material:	Drawing No.
	+0.1 mm −0.1 mm +0.5° −0.5°	Vero PureWhite	3
Scale	Projection	Machine:	File No. / Amount
2:1		Objet30 Prime	1 / 1

KATHOLIEKE UNIVERSITEIT LEUVEN
DEPARTEMENT WERKTUIGKUNDE

Disc spring EIA female mould part

Author: B. Van Raemdonck | Date: 28/05/2017 | A4

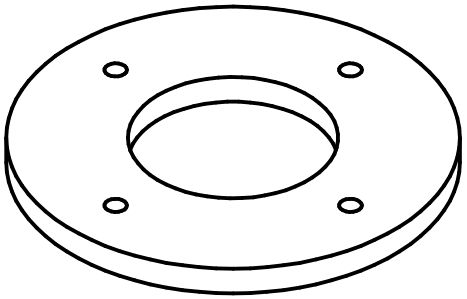

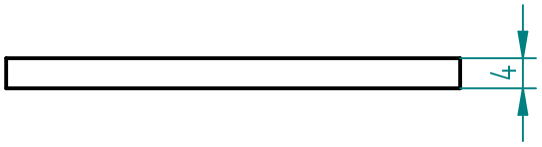

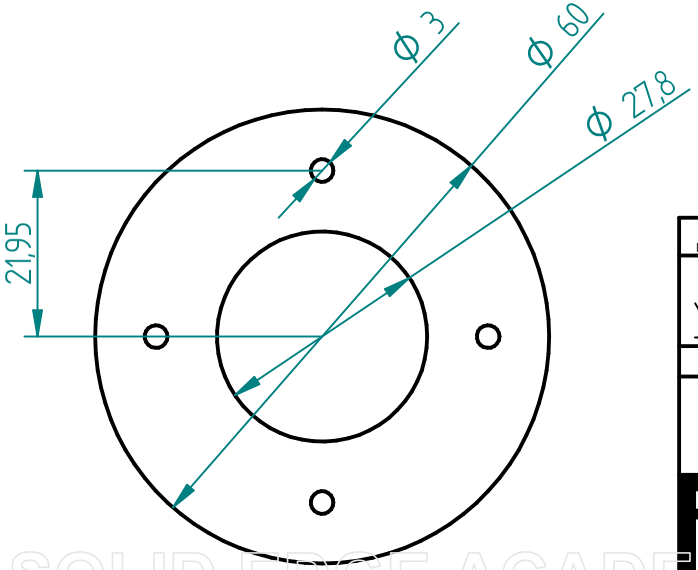

General roughness	General tolerance	Material:	Drawing No.	
	+0.1 mm −0.1 mm	PMMA plate	4	
Scale	Projection	Machine:	File No.	Amount
1:1		Trotec Speedy 100R	1	2

KATHOLIEKE UNIVERSITEIT LEUVEN
DEPARTEMENT WERKTUIGKUNDE

Disc spring EIA mould clamping ring

Author: B. Van Raemdonck	Date: 28/05/2017	A4

C.2 Technical drawings of the disc spring EIA clamping system

Section 5.2.1 describes the clamping system used to secure the disc spring EIA prototypes to a supply line. The following pages contain the technical drawings for the parts constituting that clamping system:

- page 73: base plate
- page 74: jaw plate
- page 75: compression ring
- page 76: locking plate

Standard M3 × 35 bolts with corresponding washers and nuts keep those parts together in the presence of high pressures. In the experiments performed in this study with the disc spring EIAs with membrane thicknesses of 0.65 mm and 1.00 mm, the bolts and locking plate were omitted because of the limited maximum pressure.

Finally, the designs in the technical drawings are updated versions of those used in the experimental study. The first difference is that in the updated version the outer radius of the jaw plates and the inner radius of the compression ring are smaller than the outer radius of the base plate. That prevents the compression ring from sliding or tilting past the jaw plates on assembling it, as is the case when they have the same radius as the base plate. The updated jaw plates also feature rounded inner corners to prevent damaging the actuator on assembly of the clamping system. Finally, the holes for the bolts in the jaw plate are larger than the shaft of the bolt to prevent the bolts from directing a part of the load of the compression ring away from the interface with the membrane. The other relative dimensions between the different parts remain the same as those of the design used in the experiments.

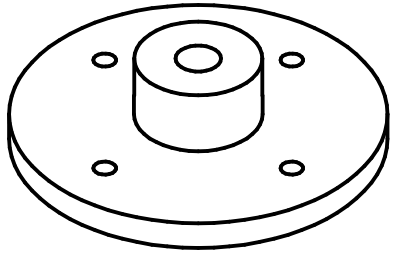

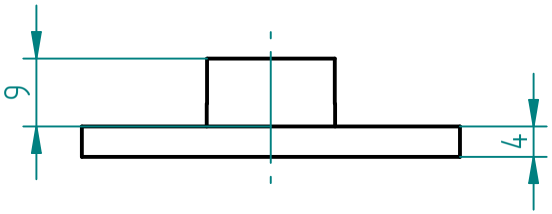

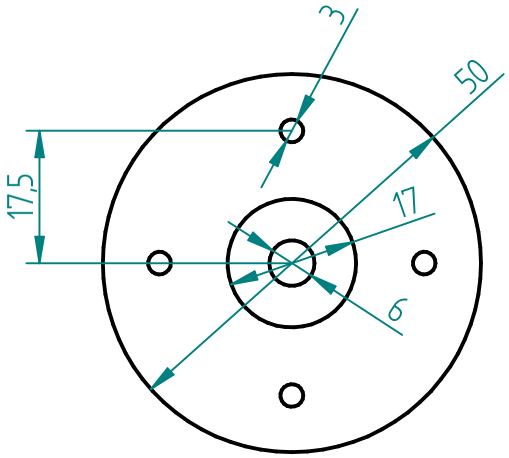

General roughness	General tolerance	Material:	Drawing No.	
	+0.1 mm -0.1 mm	PMMA plates	5	
Scale	Projection	Machine:	File No.	Amount
1:1		Trotec Speedy 100R	1	1

KATHOLIEKE UNIVERSITEIT LEUVEN
DEPARTEMENT WERKTUIGKUNDE

Disc spring EIA clamping base plate

Author: B. Van Raemdonck	Date: 28/05/2017	A4

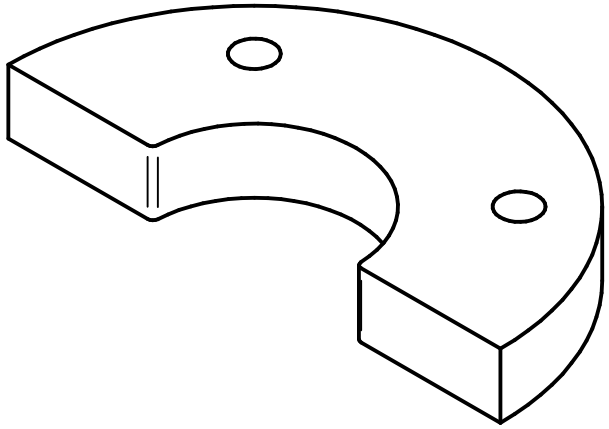

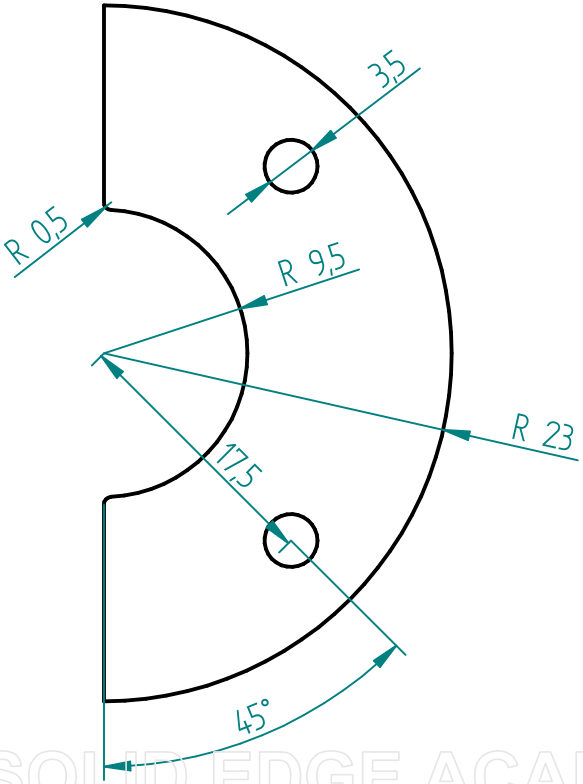

General roughness	General tolerance	Material:	Drawing No.
	+0.1 mm -0.1 mm	PMMA plate	6
Scale	Projection	Machine:	File No. / Amount
2:1		Trotec Speedy 100R	1 / 2

KATHOLIEKE UNIVERSITEIT LEUVEN
DEPARTEMENT WERKTUIGKUNDE

Disc spring EIA clamping jaw plate

Author: B. Van Raemdonck | Date: 28/05/2017 | A4

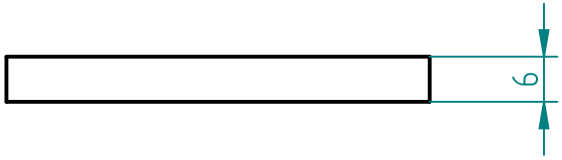

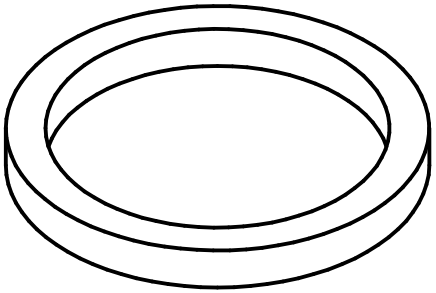

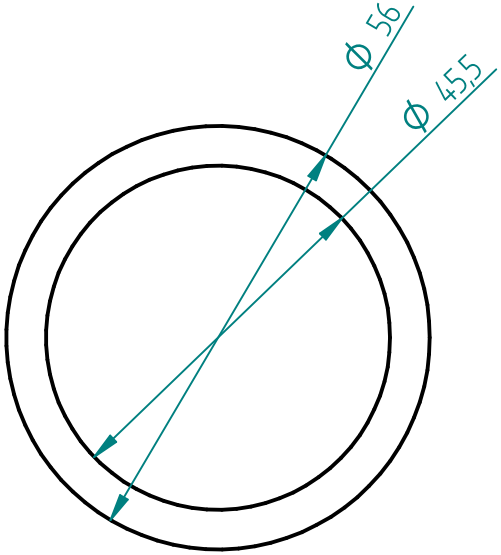

General roughness	General tolerance	Material:	Drawing No.	
	+0.1 mm -0.1 mm	PMMA plate	7	
Scale	Projection	Machine:	File No.	Amount
1:1		Trotec Speedy 100R	1	1

KATHOLIEKE UNIVERSITEIT LEUVEN
DEPARTEMENT WERKTUIGKUNDE

Disc spring EIA clamping compression ring

Author: B. Van Raemdonck | Date: 28/05/2017 | A4

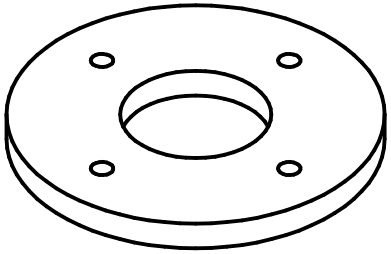

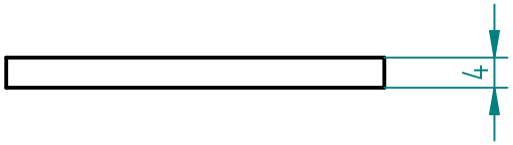

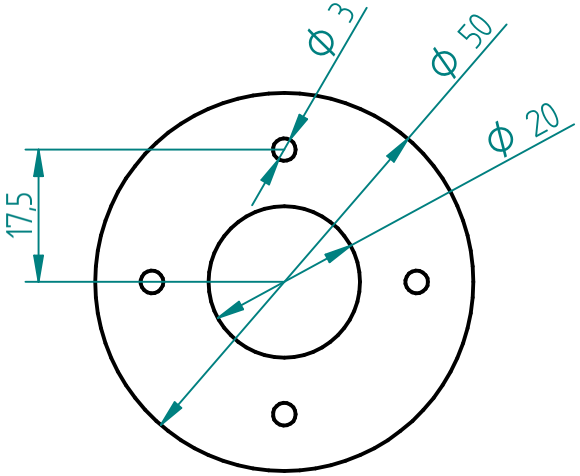

General roughness	General tolerance	Material:	Drawing No.	
√	+0.1 mm −0.1 mm	PMMA plate	8	
Scale	Projection	Machine:	File No.	Amount
1:1		Trotec Speedy 100R	1	1

KATHOLIEKE UNIVERSITEIT LEUVEN
DEPARTEMENT WERKTUIGKUNDE

Disc spring EIA clamping locking plate

Author: B. Van Raemdonck | Date: 28/05/2017 | A4

Bibliography

[1] L. Hines, K. Petersen, G. Z. Lum, and M. Sitti, "Soft Actuators for Small-Scale Robotics," *Advanced Materials*, vol. 29, Apr 4 2017.

[2] D. Rus and M. T. Tolley, "Design, fabrication and control of soft robots," *Nature*, vol. 521, pp. 467–475, May 28 2015.

[3] S. Kim, C. Laschi, and B. Trimmer, "Soft robotics: a bioinspired evolution in robotics," *Trends In Biotechnology*, vol. 31, pp. 23–30, May 2013.

[4] R. Deimel, O. Brock, and Ieee, "A Compliant Hand Based on a Novel Pneumatic Actuator," in *IEEE International Conference on Robotics and Automation (ICRA)*, IEEE International Conference on Robotics and Automation ICRA, pp. 2047–2053, 2013.

[5] R. F. Shepherd, F. Ilievski, W. Choi, S. A. Morin, A. A. Stokes, A. D. Mazzeo, X. Chen, M. Wang, and G. M. Whitesides, "Multigait soft robot," *Proceedings of the National Academy of Sciences of the United States of America*, vol. 108, no. 51, pp. 20400–20403, 2011.

[6] J. Kim, *Microscale Soft Robotics: Motivations, Progress, and Outlook*. SpringerBriefs in Applied Sciences and Technology, Springer International Publishing, 2017.

[7] D. Glozman, N. Hassidov, M. Senesh, and M. Shoham, "A Self-Propelled Inflatable Earthworm-Like Endoscope Actuated by Single Supply Line," *Ieee Transactions on Biomedical Engineering*, vol. 57, no. 6, pp. 1264–1272, 2010.

[8] P. Polygerinos, S. Lyne, Z. Wang, L. F. Nicolini, B. Mosadegh, G. M. Whitesides, and C. J. Walsh, "Towards a Soft Pneumatic Glove for Hand Rehabilitation," in *IEEE/RSJ International Conference on Intelligent Robots and Systems (IROS)*, IEEE International Conference on Intelligent Robots and Systems, pp. 1512–1517, 2013.

[9] B. Mosadegh, P. Polygerinos, C. Keplinger, S. Wennstedt, R. F. Shepherd, U. Gupta, J. Shim, K. Bertoldi, C. J. Walsh, and G. M. Whitesides, "Pneumatic Networks for Soft Robotics that Actuate Rapidly," *Advanced Functional Materials*, vol. 24, no. 15, pp. 2163–2170, 2014.

[10] F. Connolly, P. Polygerinos, C. J. Walsh, and K. Bertoldi, "Mechanical Programming of Soft Actuators by Varying Fiber Angle," *Soft Robotics*, vol. 2, no. 1, pp. 26–32, 2015.

[11] C. P. Chou and B. Hannaford, "Measurement and modeling of McKibben pneumatic artificial muscles," *Ieee Transactions on Robotics and Automation*, vol. 12, no. 1, pp. 90–102, 1996.

[12] J. T. B. Overvelde, T. Kloek, J. J. A. D'Haen, and K. Bertoldi, "Amplifying the response of soft actuators by harnessing snap-through instabilities," *Proceedings of the National Academy of Sciences of the United States of America*, vol. 112, no. 35, pp. 10863–10868, 2015.

[13] D. Yang, M. S. Verma, J. H. So, B. Mosadegh, C. Keplinger, B. Lee, F. Khashai, E. Lossner, Z. G. Suo, and G. M. Whitesides, "Buckling pneumatic linear actuators inspired by muscle," *Advanced Materials Technologies*, vol. 1, no. 3, 2016.

[14] B. Gorissen, C. Van Hoof, D. Reynaerts, and M. De Volder, "SU8 etch mask for patterning PDMS and its application to flexible fluidic microactuators," *Microsystems & Nanoengineering*, vol. 2, 2016.

[15] B. Gorissen, D. Reynaerts, S. Konishi, K. Yoshida, J. W. Kim, and M. De Volder, "Elastic Inflatable Actuators for Soft Robotic Applications," *Advanced Materials*, vol. 29, no. 43, 2017.

[16] R. Mangan and M. Destrade, "Gent models for the inflation of spherical balloons," *International Journal of Non-Linear Mechanics*, vol. 68, pp. 52–58, 2015.

[17] I. Müller and P. Strehlow, *Rubber and Rubber Balloons: Paradigms of Thermodynamics*. Lecture Notes in Physics, Springer Berlin Heidelberg, 2004.

[18] K. Bertoldi, P. M. Reis, S. Willshaw, and T. Mullin, "Negative poisson's ratio behavior induced by an elastic instability," *Advanced Materials*, vol. 22, no. 3, pp. 361–+, 2010.

[19] T. F. Li, C. Keplinger, R. Baumgartner, S. Bauer, W. Yang, and Z. G. Suo, "Giant voltage-induced deformation in dielectric elastomers near the verge of snap-through instability," *Journal of the Mechanics and Physics of Solids*, vol. 61, no. 2, pp. 611–628, 2013.

[20] L. Belding, B. Baytekin, H. T. Baytekin, P. Rothemund, M. S. Verma, A. Nemiroski, D. Sameoto, B. A. Grzybowski, and G. M. Whitesides, "Slit Tubes for Semisoft Pneumatic Actuators," *Advanced Materials*, vol. 30, Mar 1 2018.

[21] L. Meunier, G. Chagnon, D. Favier, L. Orgeas, and P. Vacher, "Mechanical experimental characterisation and numerical modelling of an unfilled silicone rubber," *Polymer Testing*, vol. 27, no. 6, pp. 765–777, 2008.

[22] M. Mooney, "A theory of large elastic deformation," *Journal of Applied Physics*, vol. 11, no. 9, pp. 582–592, 1940.

[23] R. Rivlin, "Large elastic deformations of isotropic materials. i. fundamental concepts," *Philosophical Transactions of the Royal Society of London A: Mathematical, Physical and Engineering Sciences*, vol. 240, no. 822, pp. 459–490, 1948.

[24] R. W. Ogden, "Large deformation isotropic elasticity - correlation of theory and experiment for incompressible rubberlike solids," *Proceedings of the Royal Society of London Series a-Mathematical and Physical Sciences*, vol. 326, no. 1567, pp. 565–584, 1972.

[25] A. N. Gent, "A new constitutive relation for rubber," *Rubber Chemistry and Technology*, vol. 69, no. 1, pp. 59–61, 1996.

[26] A. N. Gent, "Elastic instabilities in rubber," *International Journal of Non-Linear Mechanics*, vol. 40, no. 2-3, pp. 165–175, 2005.

[27] Y. Sun, S. Song, X. Q. Liang, and H. L. Ren, "A Miniature Soft Robotic Manipulator Based on Novel Fabrication Methods," *Ieee Robotics and Automation Letters*, vol. 1, no. 2, pp. 617–623, 2016.

[28] K. Suzumori, S. Endo, T. Kanda, N. Kato, H. Suzuki, and Ieee, "A bending pneumatic rubber actuator realizing soft-bodied manta swimming robot," in *IEEE International Conference on Robotics and Automation*, IEEE International Conference on Robotics and Automation ICRA, pp. 4975–+, 2007.

[29] G. Y. Mao, T. F. Li, Z. N. Zou, S. X. Qu, and M. X. Shi, "Prestretch effect on snap-through instability of short-length tubular elastomeric balloons under inflation," *International Journal of Solids and Structures*, vol. 51, no. 11-12, pp. 2109–2115, 2014.

[30] T. Wang, F. Xu, Y. Huo, and M. Potier-Ferry, "Snap-through instabilities of pressurized balloons: Pear-shaped bifurcation and localized bulging," *International Journal of Non-Linear Mechanics*, vol. 98, pp. 137–144, 2018.

[31] R. Hopf, L. Bernardi, J. Menze, M. Zundel, E. Mazza, and A. E. Ehret, "Experimental and theoretical analyses of the age-dependent large-strain behavior of Sylgard 184 (10:1) silicone elastomer," *Journal of the Mechanical Behavior of Biomedical Materials*, vol. 60, pp. 425–437, 2016.

[32] S. Cantournet, R. Desmorat, and J. Besson, "Mullins effect and cyclic stress softening of filled elastomers by internal sliding and friction thermodynamics model," *International Journal of Solids and Structures*, vol. 46, no. 11, pp. 2255 – 2264, 2009.

[33] E. L. Zheng, F. Jia, and X. L. Zhou, "Energy-based method for nonlinear characteristics analysis of belleville springs," *Thin-Walled Structures*, vol. 79, pp. 52–61, 2014.

[34] J. M. Auzin, "Squeezable pop-out action toy," May 1954. United States patent US2668394A.

[35] M. T. Hsu, "Deformable toy," Aug 2006. United States patent application US20080038988A1.

[36] E. B. van der Houwen, L. H. Kuiper, J. G. M. Burgerhof, B. van der Laan, and G. J. Verkerke, "Functional buckling behavior of silicone rubber shells for biomedical use," *Journal of the Mechanical Behavior of Biomedical Materials*, vol. 28, pp. 47–54, 2013.

[37] Smooth-On, "Dragon Skin®30 Product Information," 2018. https://www.smooth-on.com/products/dragon-skin-30/, accessed on 2018-04-16.

[38] J. L. Sparks, N. A. Vavalle, K. E. Kasting, B. Long, M. L. Tanaka, P. A. Sanger, K. Schnell, and T. A. Conner-Kerr, "Use of Silicone Materials to Simulate Tissue Biomechanics as Related to Deep Tissue Injury," *Advances in Skin & Wound Care*, vol. 28, no. 2, pp. 59–68, 2015.

[39] E. Riks, "Incremental approach to the solution of snapping and buckling problems," *International Journal of Solids and Structures*, vol. 15, no. 7, pp. 529–551, 1979.

[40] Dassault Systèmes, "Hyperelastic behavior of rubberlike materials," 2011. http://130.149.89.49:2080/v6.11/books/usb/default.htm?startat=pt05ch21s05abm07.html, accessed on 2018-05-06.

[41] G. Agarwal, N. Besuchet, B. Audergon, and J. Paik, "Stretchable Materials for Robust Soft Actuators towards Assistive Wearable Devices," *Scientific reports*, vol. 6, Sep 2016.

[42] stratasys, "Vero," 2016. http://www.stratasys.com/materials/search/vero, accessed on 2018-05-16.

[43] stratasys, "Objet30 Prime Specifications," 2016. http://www.stratasys.com/3d-printers/objet30-prime, accessed on 2018-05-16.

[44] Keller AG, "Piezoresistive Transmitters and Transducers." http://www.farnell.com/datasheets/17541.pdf?_ga=2.77217107.755514668.1526647930-685752999.1526647930, accessed on 2018-05-18.

[45] P. Rothemund, A. Ainla, L. Belding, D. J. Preston, S. Kurihara, Z. Suo, and G. M. Whitesides, "A soft, bistable valve for autonomous control of soft actuators," *Science Robotics*, vol. 3, no. 16, 2018.